NUREG/CR-1900
EGG-2060
Distribution Category: R3

MOLTEN FUEL-COOLANT INTERACTION OCCURRING DURING A SEVERE REACTIVITY INITIATED ACCIDENT EXPERIMENT

Mohamed S. El-Genk

Published March 1981

EG&G Idaho, Inc.
Idaho Falls, Idaho 83415

Prepared for the
U.S. Nuclear Regulatory Commission
Washington, D.C. 20555
Under DOE Contract No. DE-AC07-76IDO1570
FIN No. A6041

ABSTRACT

It is important to quantify the potential for, and to assess the consequences of an energetic molten fuel-coolant interaction (MFCI) during a hypothetical core meltdown accident. The results of a severe reactivity initiated accident in-pile experiment (designated RIA-ST-4) are presented and analyzed with respect to MFCI. Massive melting and extensive fragmentation of the molten debris (primarily a mixture of UO_2 fuel and zircaloy cladding) occurred during this experiment, and coolant pressures up to 35 MPa and coolant temperatures in excess of 940 K were achieved. The high coolant peak pressure was caused by a molten fuel-coolant interaction that may be viewed in light of the pressure detonation model. This interaction might have been triggered by a shock front developed in the flow shroud after fuel rod failure. The high coolant temperature achieved during the experiment was due to the formation of superheated steam in the shroud. The analysis revealed that the rate of energy transfer from the debris particles to the coolant during the MFCI could be much higher than that due to transient heat conduction, yet the thermal-to-mechanical energy conversion ratio is estimated to be about 0.3%.

Two fragmentation mechanisms of the molten debris particles are proposed, based on the results of the metallurgical examination and the scanning electron microscope analysis of the particles. For the first mechanism, it is hypothesized that pressure-induced stresses, caused by overheating liquid coolant droplets entrained in the molten debris, could rapidly rupture the frozen crust at the surface of the debris particles. Then, the molten debris (finely fragmented) would be ejected through the rupture area into the coolant. In the second mechanism, the fragmentation is thought to be caused by coolant jets that may develop during the collapse of void-like regions of film boiling on the surface of the debris particles. Phenomenological modeling of these two mechansims is presented, and the effects of the governing parameters are studied analytically.

SUMMARY

The behavior of light water reactor (LWR) fuels during off-normal and postulated accident conditions is being studied by the Thermal Fuels Behavior Program of EG&G Idaho, Inc., at the Idaho National Engineering Laboratory for the U.S. Nuclear Regulatory Commission. As a part of this program, a Reactivity Initiated Accident (RIA) Test Series has been performed in the Power Burst Facility (PBF) to determine the thresholds, modes, and consequences of fuel rod failure in terms of the energy deposition and the irradiation history of the fuel. Test conditions were indicative of those of the coolant in a commercial boiling water reactor during a hot startup (that is; coolant pressure of 6.45 MPa, coolant temperature of 538 K, and coolant flow rate of 0.085 L/s). Prior to performing the first experiment of the RIA Test Series, a scoping test (designated RIA-ST-4) was conducted to quantify any pressure pulses that might surge in the PBF in-pile test tube as a result of a severe fuel rod failure.

During the RIA-ST-4 experiment, a single, unirradiated, 20 wt% ^{235}U enriched, UO_2 fuel rod, contained within a zircaloy flow shroud, was subjected to a single, 76-ms power burst. The test rod failed approximately 32 ms after the initiation of the burst when the energy deposition (radially averaged at the axial flux peak location) was about 1550 J/g UO_2 (an increase in fuel enthalpy of ~1465 J/g). Although this energy deposition is well above what is possible during a postulated control rod(s) ejection or drop accident in commercial LWRs, and the system characteristics in the experiment (geometry and constraints) were not typical of those in an LWR core, the results of this experiment are of particular interest to the ongoing effort to understand the basic phenomena involved in molten fuel-coolant interactions (MFCI) occurring at high coolant pressure (6.45 MPa) and temperature (538 K). The purpose of this report is to present and analyze the results of the RIA-ST-4 experiment with respect to molten fuel-coolant interaction.

Extensive amounts of molten debris (primarily a mixture of UO_2 fuel and zircaloy cladding) were produced and expelled into the flow shroud and against the shroud wall upon fuel rod failure. A total of about 386 g became attached to the inner surface of the shroud wall, forming a solid layer with a uniform thickness of about 0.7 mm along the wall. The rest of the molten debris (~155 g) fragmented into small particles with an average diameter of ~1300 μm. The initial contact between the molten debris particles and the coolant could have initiated stable film boiling around the particles because the interface temperature was well above the thermodynamic critical temperature of water. The rapid breakup and coarse mixing of molten debris particles with the coolant were assumed prior to the passage of a shock wave in the flow shroud after rod failure. Such a shock wave may have been caused by gas release from the RIA-ST-4 test rod upon failure, impact of molten debris on the shroud wall, rapid generation of vapor in the flow shroud, precipitous collapse of a vapor layer or bubbles in the coolant adjacent to the interaction zone, and/or the formation of hydrodynamic instabilities (due, for example, to jet formation as bubbles or void-like regions of film boiling collapse on the surface of the debris particles). The passage of the shock front through the dense dispersion in the shroud may have caused the destabilization and collapse of film boiling, triggering the fine fragmentation of the molten debris particles, thus initiating a coherent thermal interaction between the particles and the coolant.

Approximately 90 g of molten debris fragmented into fine particles less than 2000 μm in diameter. Metallographic examination and scanning electron microscope analyses showed that a majority of the particles had craters and ruptures in the surface crust. Some of the particles were essentially empty, frozen shells with numerous small voids present in the crust. This appearance was common for both large (2.3 to 3.2 mm diameter) and small (10 to 20 μm diameter) particles. Part of the surface crust of some particles gave the appearance of swiss cheese. The holes in the crust (~40 to 100 μm deep and 20 to 40μm diameter) were round with sharp edges and slightly conical shapes which could have been caused by coolant jets penetrating the surface of the particles. The jets might have developed during the collapse of void-like regions of film boiling on the surface of the debris particles.

Three mechanisms have apparently contributed to the fine fragmenation of the debris particles in the RIA-ST-4 experiment. First, the impact of

molten debris on the flow shroud wall and on the coolant. Secondly, the rupture of the frozen crust at the surface of the debris particles due to pressure-induced stresses in the crust caused by overheating liquid coolant droplet(s) entrained in the molten debris. The molten debris was ejected through the rupture area into the coolant as finely fragmented particles. Incipient fragmentation by this mechanism is calculated to occur within a very short time (a fraction to a few ns). Decreasing the diameter of the entrained coolant droplets or increasing the temperature of the molten debris reduces the rupture time of the surface crust. This suggests that a fragmentation "chain" process could have occurred about a million times during the rise time (2 ms) of the peak coolant pressure in the RIA-ST-4 experiment. In this process, the breakup of large particles may result in subsequent entrainment of coolant droplets in smaller particles produced in the breakup, and in turn, their fragmentation. In the third mechanism, the fragmenation is thought to be caused by coolant jets. Calculations show that perforating the crust at the surface of the molten debris particles by jets of coolant is possible in both molten UO_2-Na and molten UO_2-water systems.

It is concluded that the coolant peak pressure (35 MPa) recorded during the RIA-ST-4 experiment was caused by molten fuel-coolant interaction, not gas release from the test fuel rod upon failure or UO_2 vapor pressure. On one hand, the test rod internal pressure at failure could have achieved a value in excess of 39 MPa; however, the work potential (9 to 20 J) of the filling gas upon expansion back to the initial coolant pressure (6.45 MPa) is negligibly smaller than that calculated (3.3 to 3.4 kJ) from the pressure impulse (0.285 MPa•s) measured during the experiment. On the other hand, the maximum temperature of molten debris during the RIA-ST-4 experiment was about 4200 K, at which temperature the contribution ($\sim$1.0 MPa) to the recorded pressure by UO_2 vapor is very small.

The effects of the initial core coolant conditions on coolant pressurization during an MFCI are also analyzed and results are applied to coolant conditions during the RIA-ST-4 experiment. The analysis shows that the amount of energy transfer necessary to cause a given pressurization of an initially saturated liquid coolant is very much less than that required by a two-phase coolant. Given an initial steam quality, increasing the initial core coolant pressure increases the peak pressure induced due to a certain amount of energy transfer. However, when the core coolant is initially a saturated liquid, increasing the initial coolant pressure reduces the peak pressure associated with the same amount of energy transfer. This analysis indicated that the coolant temperature (in excess of 940 K) achieved during the RIA-ST-4 experiment was due to the formation of superheated steam in the flow shroud during the expansion of the working fluid back to the initial coolant pressure. The rate of energy transfer from the debris particles to the coolant following a vapor film collapse is calculated to be much higher than that due to transient conduction, yet the thermal-to-mechanical energy conversion ratio is estimated to be only about 0.3%.

ACKNOWLEDGMENTS

This author is grateful to Mr. R. P. Anderson and Dr. D. R. Armstrong (Argonne National Laboratory), Dr. M. L. Corrandini (Sandia Laboratory), Dr. A. W. Cronenberg (Engineering Science & Analysis), Dr. R. R. Hobbins, Mr. J. L. Liebenthal, and Mr. P. E. MacDonald (EG&G Idaho, Inc.) for their review of and comments on this report. Special thanks to Mr. W. H. Love of the hot cell for his assistance during the metallographic examination of the debris and to Mr. D. V. Miley for the scanning electron microscope analysis of the debris particles.

CONTENTS

FIGURES

TABLES

MOLTEN FUEL-COOLANT INTERACTION OCCURRING DURING A SEVERE REACTIVITY INITIATED ACCIDENT EXPERIMENT

1. INTRODUCTION

The rapid mixing of a hot liquid with a cold, volatile one has produced, under certain conditions, violent and massive vapor generation accompanied by a destructive shock wave. This phenomenon is often referred to as "vapor explosion," "thermal explosion," or "thermal interaction," depending on the reference system. The term "molten fuel-coolant interaction" (MFCI) is widely used in nuclear reactor safety research to describe similar events, since in a nuclear reactor core the hot liquid is primarily molten fuel and the cold liquid is the core coolant (water in light water reactors or sodium in liquid-metal-cooled reactors).

Violent interactions[1-5] were reported in foundries (aluminum and steel in particular) and chemical and the natural gas transportation industries. Such incidents caused severe and massive structural damage in certain instances. Vapor explosions were also observed for various combinations of hot and cold liquids,[6-8] such as molten salt/water, molten oxides/water, molten silicates/water, aqueous solutions/water, and water/cryogenic fluids. Several incidents of energetic MFCI occurring in test reactor systems[9-11] have also been reported, some of which were severely destructive, as in the Boiling Water Reactor No. 1 (BORAX-I) and Special Power Excursion Reactor Test (SPERT) experiments and in the Stationary Low Power Reactor No. 1 (SL-1) incident.

The potential for and the consequences of an energetic molten fuel-coolant interaction in today's commercial light water reactors (LWRs) during a hypothetical core meltdown accident in which large amounts of molten fuel are produced is of concern. The wide interest in understanding the basic phenomena involved in a molten fuel-coolant interaction has generated considerable research activity. Despite this research, the possibility of an MFCI occurring in nuclear reactors (liquid metal or water cooled reactors) has not been ruled out. And, the specific interaction of molten UO_2 fuel with water under typical accident conditions in an LWR (relatively high coolant pressure and temperature) has been studied very little.

As a part of the Thermal Fuels Behavior Program of EG&G Idaho, Inc., a Reactivity Initiated Accident (RIA) Test Series has been performed in the Power Burst Facility (PBF) at the Idaho National Engineering Laboratory to determine the thresholds, modes, and consequences of fuel rod failure in terms of the energy deposition and the irradiation history of the fuel. Test conditions were indicative of those of the coolant in a commercial boiling water reactor during a hot startup (that is, coolant pressure of 6.45 MPa, coolant temperature of 538 K, and coolant flow rate of 0.085 L/s). Prior to performing the first experiment of the RIA Test Series, a scoping test (designated RIA-ST-4), which is the subject of this investigation, was conducted to quantify the magnitude of any pressure pulses that might surge in the PBF in-pile test tube as a result of a severe fuel rod failure.

A single, unirradiated, 20 wt% ^{235}U enriched UO_2 fuel rod contained within a zircaloy flow shroud was subjected to a 76-ms power burst during the RIA-ST-4 experiment. The fuel rod failed 32 ms after the initiation of the burst at a total energy deposition (radially averaged at the axial flux peak location) of approximately 1550 J/g UO_2. This energy deposition is well above what is possible in a commercial LWR during a hypothetical control rod ejection or drop accident.

Extensive amounts of molten debris were produced and expelled into the flow shroud and against the shroud wall upon fuel rod failure. A coolant pressure up to 35 MPa and coolant temperature in excess of 940 K, together with fine fragmentation[12,13] of the molten debris, occurred during this experiment. Although the mode of rod failure[14] and the movement of the molten

debris[15] during the RIA-ST-4 experiment could be entirely different than expected during a hypothetical core meltdown accident in an LWR, the results are of interest in the current effort to understand the interaction mechanisms of molten core debris (primarily a mixture of UO_2 fuel and zircaloy cladding) with water at high pressure and temperature. In this report, the results of the RIA-ST-4 experiment are discussed and analyzed[14-16] with respect to molten fuel-coolant interaction. Results of metallographic examinations and scanning electron microscope analyses of the debris particles are presented, and the fragmentation characteristics of the particles are discussed.

In Section 2, a brief description of the RIA-ST-4 experiment is presented and the results are analyzed. In Section 3, the results of metallurgical examinations and scanning electron microscope analyses of the debris particles are presented. Phenomenological modeling of two possible fragmentation mechanisms of the molten debris particles in the RIA-ST-4 experiment is presented in Section 4. In Section 5, the effects of coolant conditions on core coolant pressurization during a postulated MFCI in an LWR are assessed and the results applied to the coolant conditions in the RIA-ST-4 experiment. Conclusions are presented in Section 6 and additional discussion is presented in the appendix.

2. EXPERIMENT DESCRIPTION, CONDUCT, AND RESULTS

The RIA-ST-4 experiment[14-16] was conducted as a safety experiment of the Power Burst Facility (PBF) at the Idaho National Engineering Laboratory to quantify the magnitude of any pressure pulses that might surge in the in-pile test tube as a result of a severe fuel rod failure. The PBF consists of an open tank reactor vessel, driver core (1.3 m in diameter and 0.914 m high), canal for transfer and temporary storage of PBF fuel and test fuel assemblies, central flux trap region (0.21 m in diameter) in which the in-pile test tube is located, and a pressurized water coolant flow loop. The PBF reactor is controlled by eight steady state rods and four additional transient rods for reactivity control during power burst operation.

Test fuel, either as a single rod(s) or in a small cluster, is contained in the in-pile tube (IPT). The IPT is a thick-walled, Inconel 718, high-strength pressure tube designed to accommodate pressure pulses up to 51.7 MPa (7500 psi) above the pressure in the water coolant flow loop (the maximum steady state pressure in the loop is 15.6 MPa). The cooling water to the test rod(s) is provided by the water flow loop at controllable pressure, temperature, and flow rates representative of those in commercial LWRs. A schematic axial cross section of the PBF in-pile tube is shown in Figure 1.

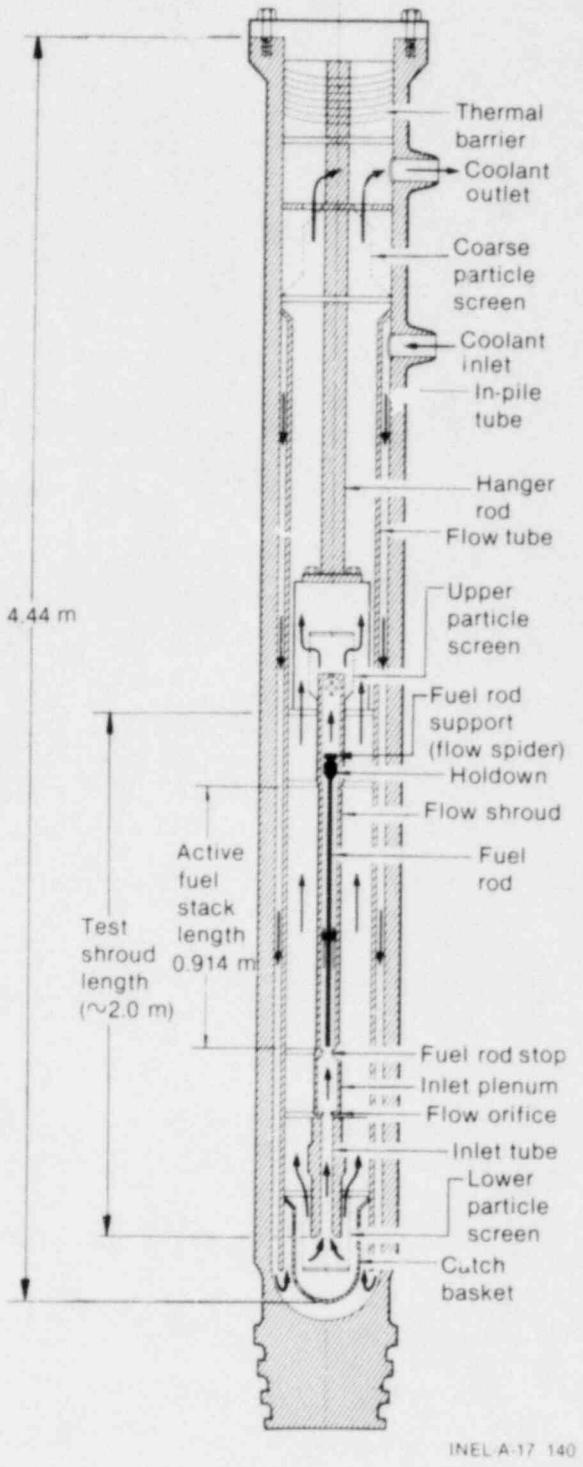

Figure 1. Schematic axial cross section of the PBF in-pile tube.

2.1 Experiment Description and Conduct

The RIA-ST-4 test train was instrumented for measurements of thermal neutron flux and coolant pressure, temperature, and flow rate. The test fuel rod was not instrumented. A schematic diagram of the test train, in which the approximate locations of some of the instruments are indicated, is shown in Figure 2. As shown in the figure, a small hole (3.175-mm diameter) was made in the shroud wall at the axial flux peak location to attach a pressure tube connected to a pressure transducer (17-MPa Bell & Howell) to measure the coolant pressure inside the shroud. This transducer was not mounted directly on the outer surface of the shroud wall because of the

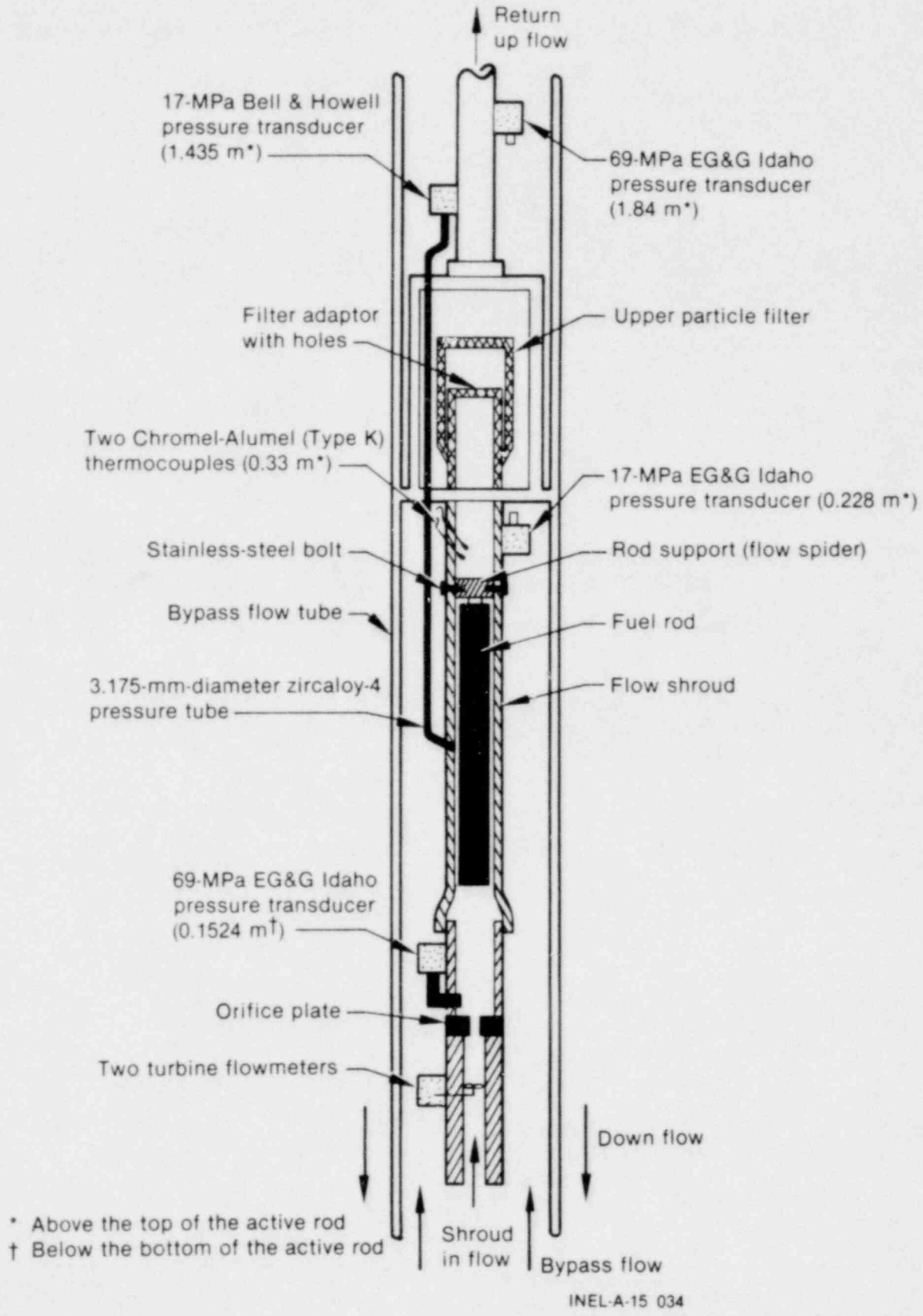

Figure 2. Schematic diagram of the RIA-ST-4 test train.

space restrictions in the bypass flow tube and the fact that the stainless steel casing of the transducer would cause undesired neutron flux depression at the axial flux peak location. Figure 3 presents a radial cross-sectional view of the test train assembly configuration. Instrumentation and results of the RIA-ST-4 experiment are detailed elsewhere.[14,16]

During the RIA-ST-4 experiment, the test fuel rod (cold internal pressure of about 3.79 MPa at room temperature of 293 K) was subjected to a single, 76-ms power burst. The reactor reached a peak power of 15.9 GW within 30 ms after initiation of the burst (the reactor period was approximately 3.85 ms). The burst was largely self-terminating because the fuel of the PBF driver core is designed with Doppler reactivity feedback capable of terminating bursts without a primary dependence on mechanical shutdown systems. Mechanical shutdown of the PBF reactor was initiated 90 ms after transient initiation.

The test fuel rod failed approximately 2.6 ms (apparent failure time) after peak power when the total energy deposition, radially averaged at the axial flux peak location, was about 1550 J/g UO_2 (fuel enthalpy of 1465 J/g). The total energy deposition during the burst totaled about 2930 J/g UO_2 (fuel enthalpy of about 2220 J/g). Although this energy deposition is much higher than is possible in a commercial LWR during a postulated RIA, this PBF safety experiment provided important information with respect to molten debris relocation and freezing on cold walls,[15] and the potential for an energetic thermal interaction (vapor explosion) occurring between molten debris (primarily molten UO_2) and water at high pressure and temperature.[12,13]

2.2 Experiment Results

The generation of coherent pressure pulses up to 35 MPa in the RIA-ST-4 experiment flow shroud, approximately 32.6 ms after initiation of the power burst, indicated test fuel rod failure.[a] However, the coolant pressure in the bypass flow tube only increased about 2 MPa during the experiment due to the gamma radiation heating of the bypass coolant during the power burst.[b] The coolant temperature recorded at the exit of the flow shroud (0.33 m above the top of the test fuel rod) reached values in excess of 940 K, which is much higher than the thermodynamic critical temperature of water (~647 K). Extensive amounts of molten UO_2 and zircaloy cladding were produced and ejected into the flow shroud and against the shroud wall following test rod failure. A molten debris layer having a thickness of approximately 0.7 mm was deposited along the inner surface of the test shroud, which continued to be cooled at its outer surface by coolant bypass flow. Severe fragmentation of the molten debris occurred, as evidenced by the particles (average diameter of ~1300 μm) collected from within the flow shroud and the particle filters. The results of the experiment are discussed in some detail in the following subsections.

2.2.1 Measurements of Coolant Pressure. The reactor power and coolant pressure recorded during the RIA-ST-4 experiment are presented in Figure 4. The 69-MPa EG&G Idaho pressure transducer installed at the inlet of the shroud (see Figure 2) gave the best indication of the shroud pressure after rod failure. Coolant pressure up to about 35 MPa (pressure increase of ~28.5 MPa) was recorded about 2 ms after the

a. Apparent failure time; see the following subsection for details.

b. During the RIA-ST-4 experiment, flow reversal associated with gamma heating of the liquid coolant in the flow shroud was not recorded due to the facts that (a) the test fuel rod had failed early during the power burst before flow excursion from the shroud could have occurred and (b) the measurement of the shroud coolant flow was provided by two unidirectional turbine flow-meters installed at the inlet of the shroud. Instead, rather severe flow anomalies were recorded at the same time that the pressure in the shroud began to increase at rod failure. In a recent reactivity initiated accident, nine-rod bundle test (designated RIA 1-4 and completed in April 1980), flow reversal was monitored by two bidirectional turbine flowmeters mounted at the inlet of the shroud. Both meters measured a flow reversal of -1.6 L/s following the power burst when the shroud coolant pressure reached 8.4 MPa (~1.95 MPa above the initial coolant pressure), followed by a flow stagnation for about 500 ms. Then, gradual flow increase back to the pretest flow rate (0.8 L/s) occurred as the coolant pressure decreased to the initial system pressure of 6.45 MPa. The purpose of Test RIA 1-4 was to provide information regarding loss-of-coolable fuel rod geometry following a postulated RIA event for a peak fuel enthalpy of 1170 J/g.

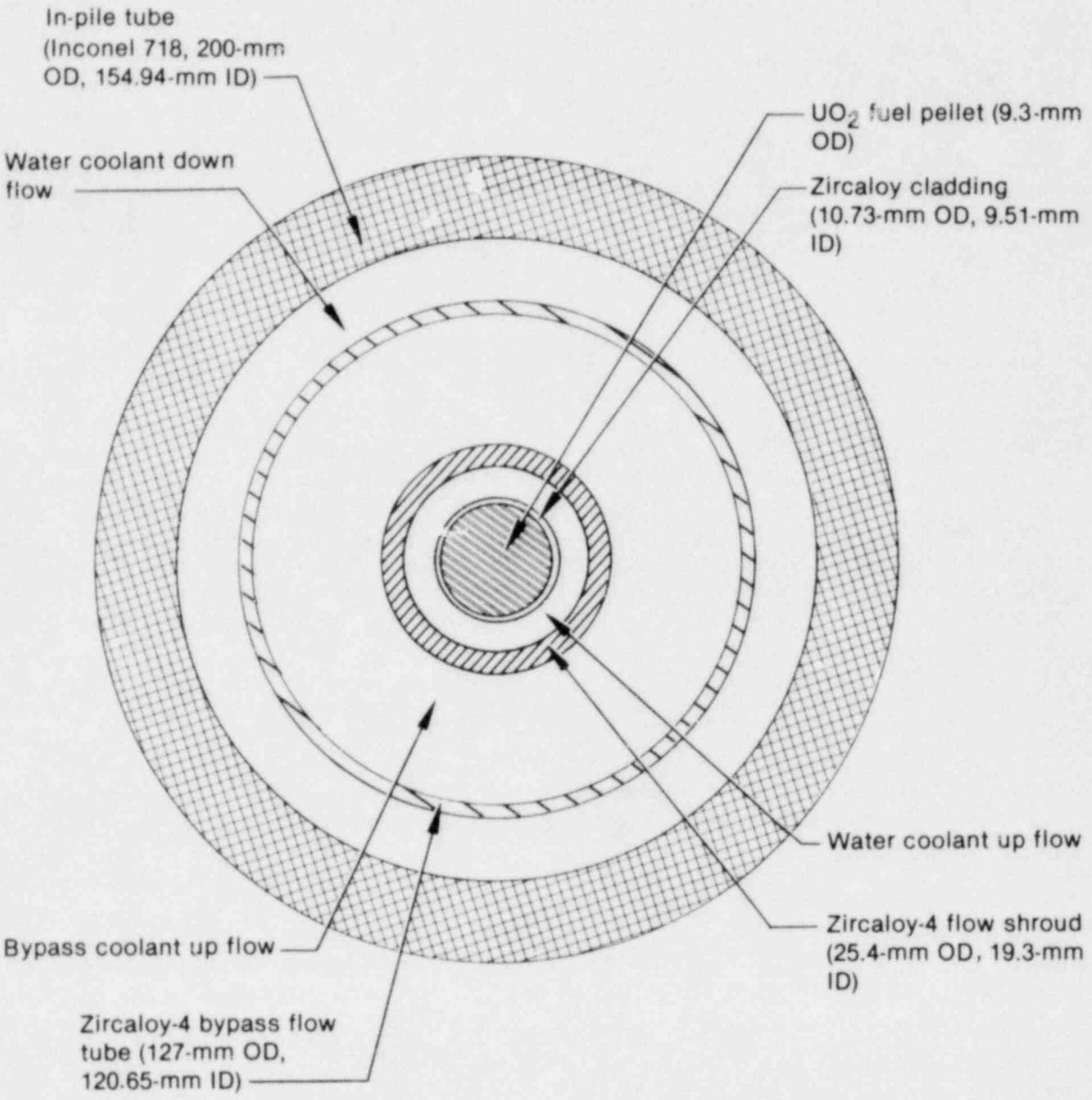

Figure 3. Radial cross-sectional view of test assembly configuration in the RIA-ST-4 experiment.

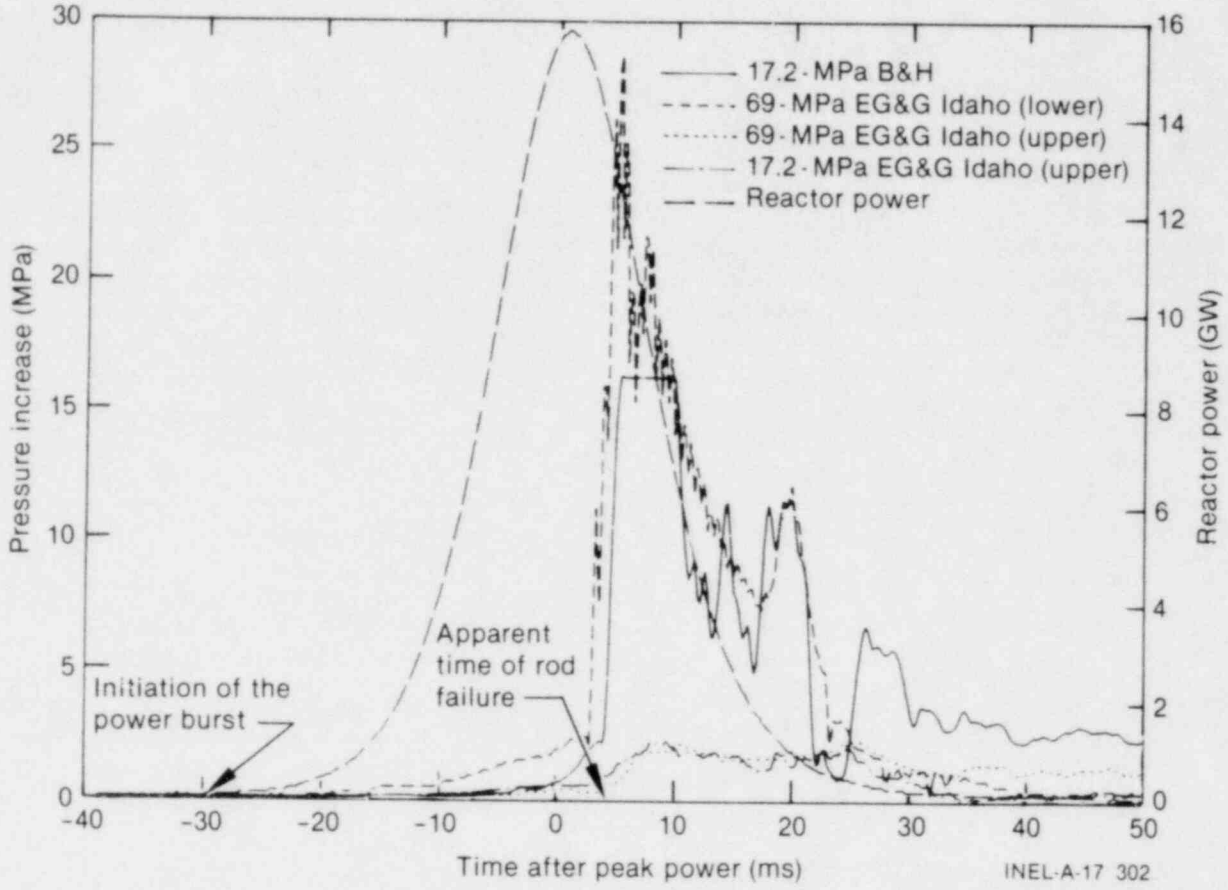

Figure 4. Measurements of reactor power and coolant pressure during the RIA-ST-4 experiment.

apparent time of rod failure (32.6 ms after the initiation of the burst). The recording of coolant pressure above the initial system pressure (6.45 MPa) continued over a period of about 30 ms past the time of rod failure.

Although the coolant pressure at the inlet of the shroud began to rise approximately 2.6 ms after reactor peak power (~30 ms after the initiation of the burst), indicating test fuel rod failure, the actual failure of the test rod would have occurred earlier. The difference in the time of failure is calculated by dividing the distance between the middle[a] of the test rod and the lower 69-MPa EG&G Idaho pressure transducer (~0.6 m) by the sonic velocity in water at 538 K (~1090 m/s). A delay time of approximately 0.6 ms is calculated between the actual time of rod failure and the indication of an abrupt pressure increase at the inlet of the shroud, revealing that the test fuel rod might actually have failed 2.0 ms after reactor peak power (~32.0 ms after the initiation of the power burst).

The 17-MPa Bell & Howell pressure transducer, installed to measure the shroud coolant pressure at the axial flux peak location, was expected to give an accurate indication of the maximum coolant pressure in the shroud (which might have been higher than the 35 MPa recorded at the inlet of the shroud). However, the transducer saturated at about 23 MPa (pressure increase of about 16.6 MPa), when the coolant pressure exceeded the maximum capacity of the transducer, after a smooth rise and a total rise time of about 1 ms.

As demonstrated in Figure 4, there is a delay in the incipient rise time of the shroud coolant pressure as recorded by the 17-MPa Bell & Howell transducer relative to that of the lower 69-MPa EG&G Idaho transdcer. This time delay, Δt, is expected because the two pressure transducers were mounted at unequal distances from the pressure source (that is, the axial flux peak location where rod failure would be expected to occur first). An estimate of Δt is obtained by the simple relation

a. Test rod failure is expected to occur first at the rod midplane, which corresponds to the axial flux peak location in the driver core.

$$\Delta t = (L_1 - L_2)/c \quad (1)$$

where L_1 and L_2 are the mounting distances of the 17-MPa Bell & Howell and the 69-MPa EG&G Idaho pressure transducers, measured from the middle[a] of the test shroud, respectively, and c is the sonic velocity in water at a temperature of 538 K (equal to that of the coolant at the inlet of the shroud). Values of L_1, L_2, and c are 2.3 m, 0.8125 m, and 1090 ms^{-1}, respectively, giving a total delay in the rise time between the two transducers of about 1.365 ms. As demonstrated in Figure 5, offsetting the time scale of the recorded coolant pressure by the Bell & Howell transducer 1.365 ms results in a perfect match with the 69-MPa EG&G Idaho transducer recording during the rise time. (This would have been the case if both transducers were mounted at equal distances from the initial failure location in the rod.) Such agreement between the coolant pressure measurements during the pressure rise time suggests that the RIA-ST-4 fuel rod failed at the axial flux peak location, and then the failure propagated in both axial directions along the rod.

2.2.2 Energy Deposition. At the time of rod failure (~32.0 ms after the initiation of the burst), the total radial average energy deposition at the axial flux peak location was approximately 1550 J/g UO_2. The corresponding fuel enthalpy was about 85 J/g less (1465 J/g UO_2) due to the heat transfer to the zircaloy cladding and to the coolant prior to failure. The average temperature of molten fuel at failure was estimated[15] to be between 3150 and 3400 K (about 40 to 300 K above the melting point of UO_2).

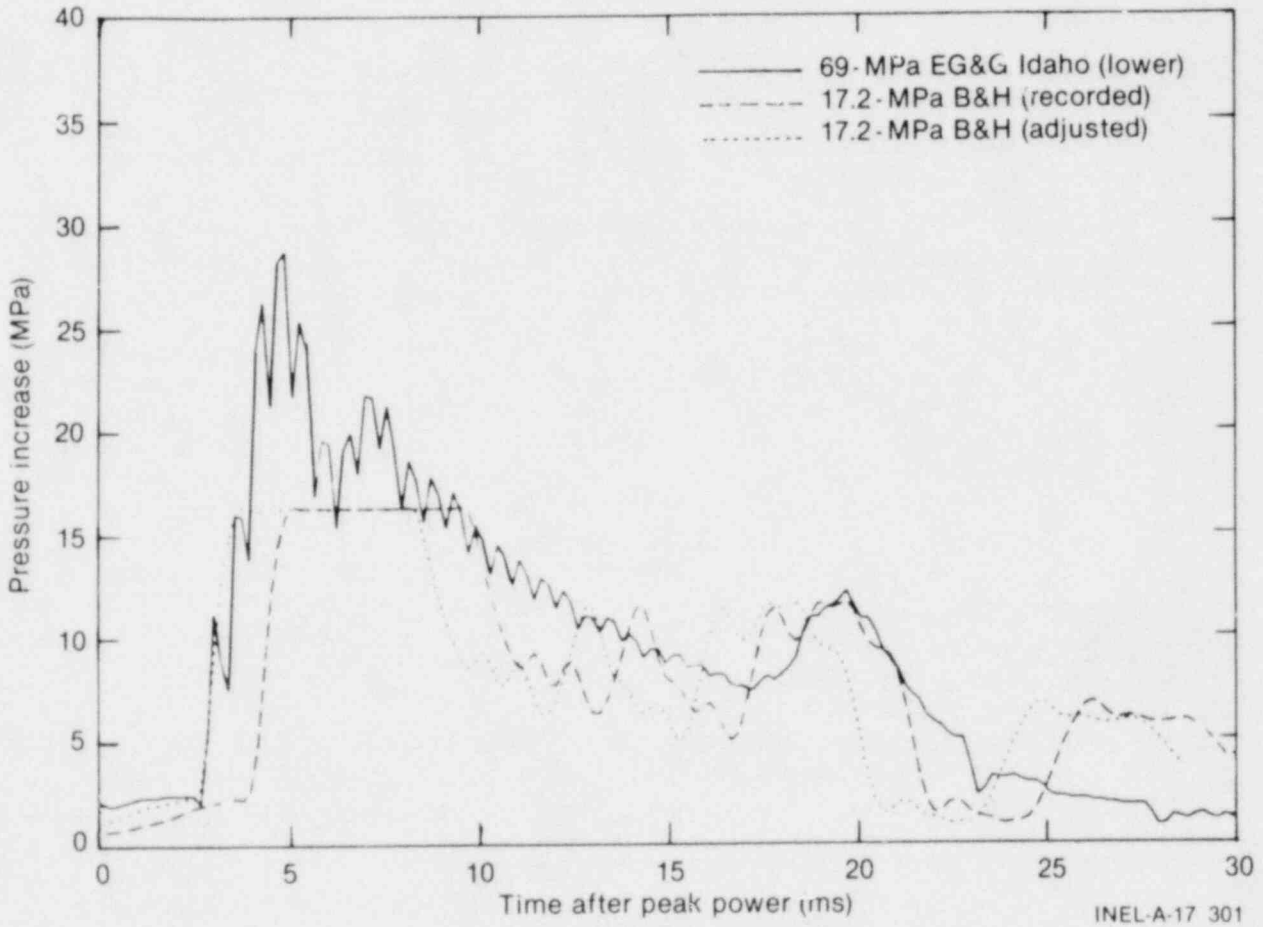

Figure 5. Recording of coolant pressure in the flow shroud.

a. Test rod failure is expected to occur first at the rod midplane, which corresponds to the axial flux peak location in the driver core.

The temperatures near the surface of the pellets during the RIA-ST-4 power burst were higher than near the center of the rod due to neutron self-shielding by the UO_2 pellets and the fact that the fuel rod temperature was initially uniform and equal to that of the coolant (538 K). The fuel peak temperature at the time of rod failure could have been about 4200 K,[14] at which temperature the maximum contribution to the recorded pressure by the UO_2 fuel vapor is negligibly small, about 1 MPa. By contrast, the pressure of the fill gas in the rod at failure could have been significant, as discussed in the next subsection.

2.2.3 Pressurization of the Test Rod During the Burst. The rapid radial expansion and melting of the fuel caused by the high energy deposition rate in the test rod during the RIA-ST-4 experiment (about 40 kJ/g•s) could have restricted the mass flow of the fill gas from the rod diametral gap to the upper gas plenum, resulting in some of the gas being trapped between the swollen pellets and the zircaloy cladding. It is assumed that this gas behaved perfectly and was pressurized at constant volume to an equilibrium temperature close to that of the melting point of UO_2 (~ 3100 K) before rod failure. Then, the rod internal pressure (cold rod pressure was 3.79 MPa at 293 K) could have achieved a value in excess of 39 MPa before rod failure. This high internal rod pressure may have caused premixing of the molten fuel particles with the coolant in the flow shroud. Also, the gas release from the rod upon failure might have contributed to the formation of a shock wave in the flow shroud.

It may be argued that the coolant peak pressure (~ 35 MPa) measured during the RIA-ST-4 experiment could be accounted for by the pressurization of the helium fill gas in the test rod. It is conservatively assumed that the entire volume of the helium gas (~ 2.8 cm^3) in the fuel rod expanded either isothermally or isotropically from 39 MPa to the initial coolant pressure of 6.45 MPa. During an isothermal expansion process, the work done by the expanding gas, given as

$$W = -P_1 V \ln\left(\frac{P_2}{P_1}\right) \qquad (2)$$

totals about 20 J, and where P_1 and P_2 are taken to be 6.45 and 39 MPa, respectively, and V is equal to 2.8 cm^3. On the other hand, the work done during an isotropic expansion of the fill gas

$$W = \frac{-V}{\gamma - 1}\left[P_2\left(\frac{P_1}{P_2}\right)^{\frac{1}{\gamma}} - P_1\right] \qquad (3)$$

totals about 9 J, and where γ is the ratio of specific heats (for helium, $\gamma = 1.667$). These estimates of the work potential are very much less than that calculated (3.3 to 3.4 kJ) from the impulse recorded (0.285 MPa•s) during the RIA-ST-4 experiment (see Figure 6 and Subsection 2.2.7). This suggests that the pressure pulses recorded during the RIA-ST-4 experiment could not have been caused by gas release from the test rod upon failure.

Close examination of the pressure trace of the lower 69-MPa EG&G Idaho pressure transducer (see Figures 4 and 5) suggests that the first pressure pulse (peak pressure increase ~ 16.6 MPa, width ~ 0.25 ms, and rise time ~ 0.4 ms) was caused by the release of hot pressurized gas from the test rod upon failure. This follows from the fact that the pulse had a relatively short rise time and small impulse (~ 0.0197 MPa•s, corresponding to a work potential of ~ 20 J), which would be expected due to the low density and mass of the released gas.

2.2.4 Molten Debris Relocation and Freezing on the Shroud Wall. Extensive amounts of molten UO_2 and zircaloy cladding were produced and ejected axially and radially within the flow shroud and against the shroud wall upon test rod failure.[15] A total of about 386 g of molten debris (primarily a mixture[a] of UO_2 and zircaloy), which represented approximately 51% of the total mass of UO_2 and zircaloy in the test fuel rod, deposited

a. Molten debris could have contained about 42 mole% UO_2 and 58 mole% zircaloy (corresponding to weight fractions of 78% UO_2 and 22% zircaloy, respectively), which are the same as those in the fuel rod. Therefore, the freezing temperature of the debris (~ 2640 K) would be expected to be much less than the UO_2 freezing point (~ 3100 K), but higher than that of the oxygen-stabilized alpha zircaloy (~ 2200 K).

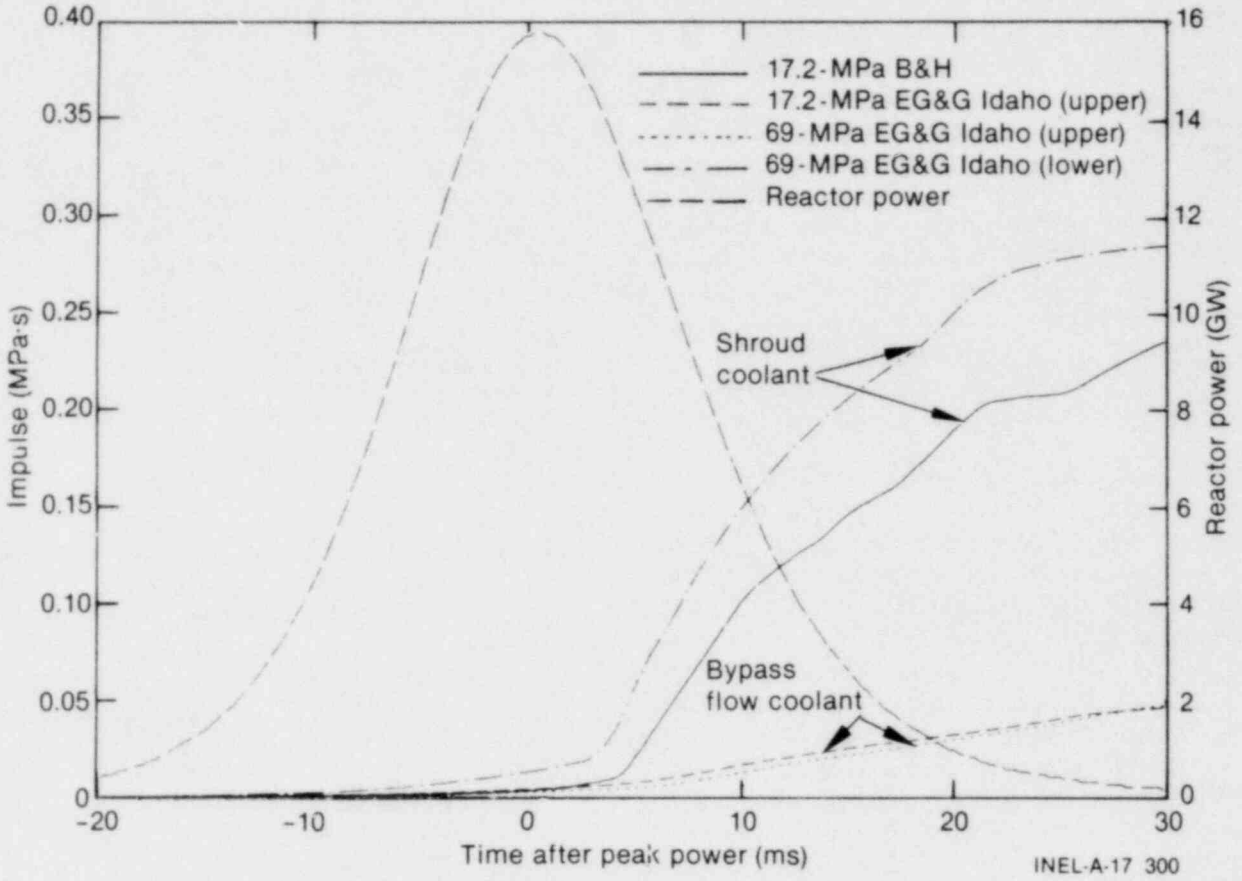

Figure 6. Measured pressure impulse in the shroud and bypass flow tube.

and froze on the inner surface of the shroud wall as a thin layer with a thickness of 0.7 mm. The shroud wall, however, did not melt upon being contacted by the molten debris.[14,15]

A physical model was developed in a recent study performed by El-Genk and Moore[15] to analyze the transient freezing of the molten debris in the RIA-ST-4 experiment and to assess the conditions for potential melting of the shroud wall upon contact with molten debris. Results of calculations indicated that transient freezing of the debris was governed by the radiative cooling at the debris layer surface in addition to the transient conduction through the shroud wall. The freezing process of the debris was strongly influenced by its internal heat generation (from the time of rod failure until the end of the power burst, ~45 ms) and zircaloy volume ratio.[a] It was concluded from the calculations that melting of the wall upon being contacted by molten debris in the RIA-ST-4 experiment should not have occurred, because of the small thickness of the wall, the continuous convective cooling along the wall outer surface, and the low initial temperatures of the wall (~538 K) and of the molten debris (~3500) at the time of contact. This conclusion agrees with the experimental results.

2.2.5 Deformation of the Test Shroud Wall. The zircaloy flow shroud did not rupture during the RIA-ST-4 experiment; however, the outside diameter of the shroud was enlarged from 25.4 mm to a maximum of about 27.66 mm (the wall had a thickness of 3.05 mm). This deformation (~8.9% strain) was apparently caused by the pressure impulse generated within the shroud, combined with the thermal strain induced in the

a. Molten debris could have contained about 42 mole% UO_2 and 58 mole% zircaloy (corresponding to weight fractions of 78% UO_2 and 22% zircaloy, respectively), which are the same as those in the fuel rod. Therefore, the freezing temperature of the debris (~2640 K) would be expected to be much less than the UO_2 freezing point (~3100 K), but higher than that of the oxygen-stabilized alpha zircaloy (~2200 K).

wall due to the deposition and freezing of molten debris on the shroud wall inner surface upon rod failure. The pressure impulses induced in the flow shroud (~0.285 MPa•s) and in the bypass flow tube (~0.051 MPa•s) upon rod failure are shown in Figure 6. The data plotted in Figure 6 were obtained by integrating the recorded pressure traces shown in Figure 4. The peak temperatures at the inner and outer surfaces of the wall were calculated[15] to have reached about 1900 and 1550 K, respectively (that is, a temperature differential of 350 K). Postexperiment measurements of the deformation of the flow shroud are presented in Figure 7.

2.2.6 Measurements of the Coolant Temperature. The only measurements of coolant temperature during the RIA-ST-4 experiment[14,16] were recorded at the exit of the flow shroud by two Chromel-Alumel (Type K) thermocouples located 0.33 m above the top of the test rod. No measurements of the coolant temperature were obtained at the inlet of the shroud because of thermocouple failure at this location before the initiation of the burst. Figure 8 presents the recorded coolant temperature at the exit of the flow shroud during the experiment. The arbitrary time zero in Figure 8 corresponds to the time of test rod failure. As shown, the temperature began to rise after rod failure (~32.0 ms after the initiation of the burst) and then the thermocouples saturated at 910 and 940 K, respectively, after a rise time of approximately 500 ms. The measured coolant temperature remained saturated for almost 5 s because the maximum setpoint of the electronics was 900 K. The measurements were restored as soon as the coolant temperature dropped below 900 K. The temperature declined slowly, approaching that of the initial coolant temperature in the shroud (~538 K) after an additional 3 s (~8.5 s after test rod failure).

The response of the thermocouples (as shown in Figure 8) is almost identical, suggesting that the recorded temperature was that of the coolant in the flow shroud and was not caused by a contact with the molten debris expelled upon rod failure. If the molten debris (~3500 K) had contacted the thermocouples, their stainless steel sheaths (melting point ~1700 K) would have melted, causing failure of the thermocouples or the formation of new junctions. In the former case, no temperatures would be recorded. However, in the latter case, the response of the thermocouples would not be identical unless both thermocouples were contacted with identical masses of molten debris, which is most unlikely. Furthermore, the thermocouples were located in the flow shroud about 0.33 m above the top of the test rod (see Figure 2), which makes the probability of contact by molten debris relatively small.

Measurements of coolant temperatures higher than the thermodynamic critical temperature of water (~647 K) reveal that superheated steam was present in the flow shroud for about 8.5 s after rod failure. This superheated steam may have been produced either during the pressurization process of the working fluid or upon the relief of the pressure pulses produced during the pressurization process (an assessment of the coolant conditions during RIA-ST-4 is presented in Section 3). The long saturation period of the coolant temperature instrumentation (~5 s) and the slow decline of the temperature are indications of the slow cooling process of the steam formed within the flow shroud upon rod failure. The cooling and consequent condensation of the water vapor in the flow shroud may have been suppressed for some time because of (a) the continuous heating by radiation[15] from the debris layer deposited on the inner surface of the shroud wall and (b) the ineffective cooling by transient conduction through the shroud wall because of the increased thermal resistance due to the frozen debris layer (mostly UO_2 fuel, which has a relatively low thermal conductivity).

2.2.7 Thermal-to-Mechanical Energy Conversion Ratio. The mechanical energy imparted to the system due to shroud coolant pressurization following test rod failure is approximately equal to the change in kinetic energy of to the shroud coolant, E_c. Considerations of momentum and energy transfer from the shock front to the coolant results in

1. Momentum Transfer

$$2 A_c I = M_c V_c \quad (4)$$

2. Energy Transfer

$$E_c = 1/2 M_c V_c^2 \quad (5)$$

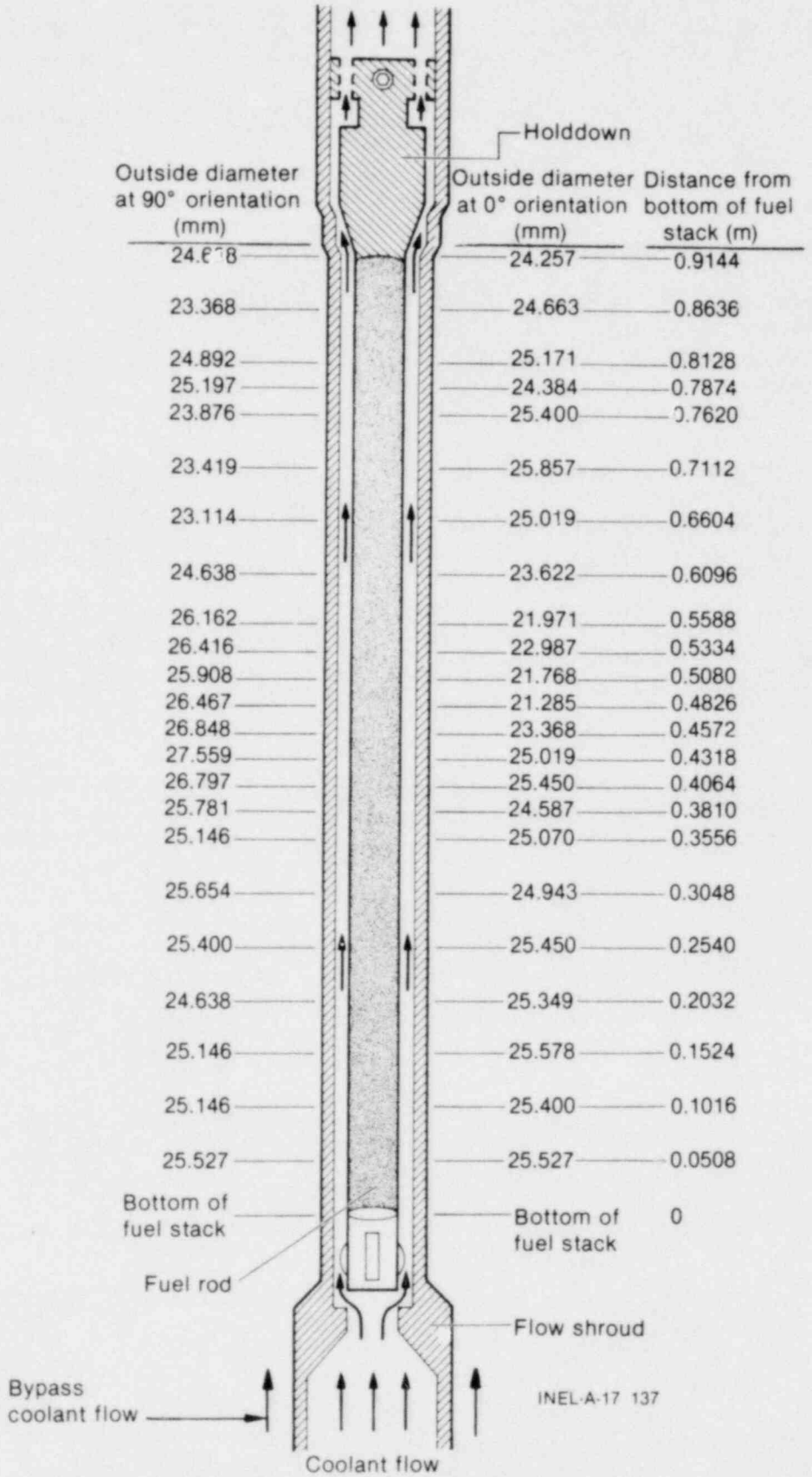

Figure 7. Posttest measurements of flow shroud deformation.

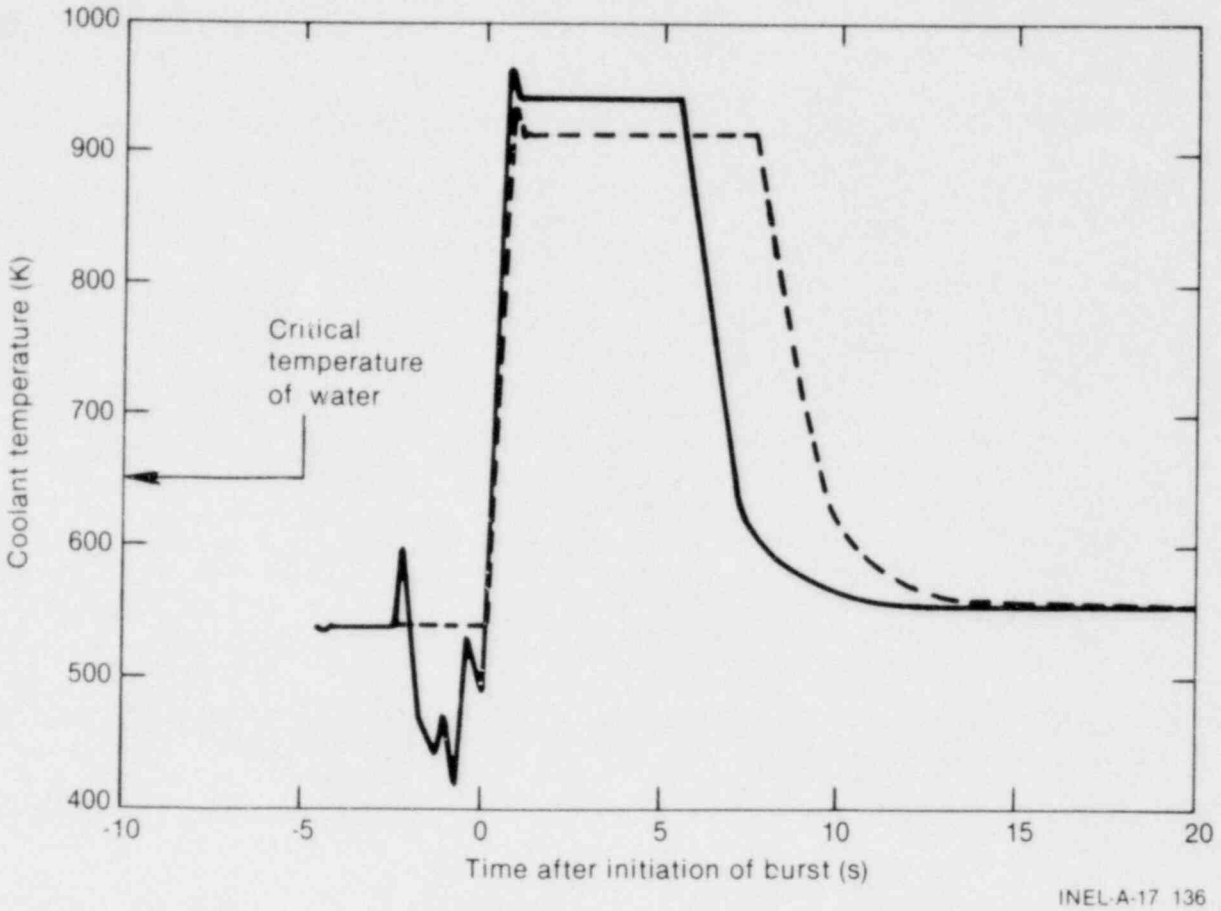

Figure 8. Coolant temperature recorded at the flow shroud exit during the RIA-ST-4 experiment.

where

A_c = cross-sectional flow area in active region of shroud where test rod is located

M_c = total mass of coolant that undergoes maximum acceleration in flow shroud

V_c = average expulsion velocity of coolant through entire length of shroud

I = measured pressure impulse (Figure 6).

It is assumed that two slugs of water of equal mass ($M_c/2$) were acted upon; the coolant above the axial flux peak location accelerated to the upper particle screen and that below the axial flux peak location accelerated to the lower particle screen at the inlet of the flow shroud (see Figure 1). The total coolant mass, M_c, is given by

$$M_c = \frac{\pi}{4}\left(D_i^2 - D_f^2\right) L\, \rho_c + V_s\, \rho_c \qquad (6)$$

where

ρ_c = coolant density

D_i = inner diameter (1.93 cm) of active region of shroud

D_f = diameter (1.075 cm) of test fuel rod

L = length of active region of shroud (92.7 cm)

V_s = coolant volume ($\sim 2458\ cm^3$) present in the remainder of the shroud above and below the test fuel rod region.

The total length of the flow shroud is about 2 m (see Figure 1).

As discussed previously, the thermocouples mounted ~0.33 m above the top of the fuel rod (see Figure 2) recorded coolant temperatures well above the thermodynamic critical temperature of water (647 K) for about 8.5 s after rod failure. Therefore, the entire length of the flow shroud (~2 m) is considered to have been voided completely during the expansion phase of the working fluid. The kinetic energy imparted to the coolant in the test loop and in the remainder of the in-pile tube is neglected because the coolant mass in the flow shroud is very small compared with the total coolant mass present in the system.

Eliminating V_c from Equations (4) and (5) gives the following simplified expression for E_c as

$$E_c = \frac{2}{M_c}(I\ A_c)^2 \qquad (7)$$

where I is equal to 0.285 MPa•s (Figure 6), and A_c is 2.0213 cm^2. In Equation (7), the kinetic energy transfer, E_c, to the coolant is proportional to the square of both the impulse, I, and the coolant flow area, A_c, and inversely proportional to the mass of the coolant, M_c, that undergoes maximum acceleration. The value of M_c depends on whether the coolant in the active length of the shroud (0.914 m long) was liquid or two-phase mixture at the time of rod failure. When the shroud coolant is liquid, the total mass of the coolant present in the flow shroud is about 2 kg (the coolant density is 755 kg/m^3, corresponding to the initial coolant temperature of 538 K). This estimate of M_c represents a maximum value of the coolant mass in the flow shroud, and in turn provides a lower bound of ~3.3 kJ for E_c [see Equation (7)].

Actually, the assessment of the coolant conditions in the active region of the flow shroud (see Section 5.3 for details) has indicated that the coolant in this region could have been a two-phase mixture at the time of rod failure. Assuming a steam quality (x) of 7%, the density of the coolant in the active region of the shroud becomes about 350 kg/m^3. However, the density of the coolant in the remainder of the shroud is considered to be equal to 755 kg/m^3. These considerations reduce the estimate of M_c to about 1.92 kg, resulting in an upper bound of ~3.4 kJ for E_c.

To calculate the thermal-to-mechanical energy conversion ratio[a] in the RIA-ST-4 experiment, the total energy insertion in the test rod at the time of failure, which is not exactly known, must be assessed. However, this energy would not be less than that necessary to melt the UO_2 fuel and the zircaloy cladding present in the test rod. Such an energy insertion, which totals about 951 kJ, is equal to the energy to melt the fuel, axially averaged over the length of the rod (~1272 J/g UO_2), times the UO_2 fuel mass present in the test rod (634 g), plus the energy required to melt the cladding (~1256 J/g zircaloy), times the mass of the cladding (~115 g). This gives an upper bound of 0.36% and a lower bound of 0.35% for the thermal-to-mechanical energy conversion ratio. These estimates could be lower, however, since the actual total energy deposition in the test rod would be higher than 1272 J/g due to the cosine axial flux distribution[b] and neutron self-shielding effects in the test rod. The cosine flux distribution results in a higher energy deposition at the axial flux peak location, and the neutron self-shielding produces higher energy depositions at the surface of the fuel pellets. These two effects could have increased the total energy deposition at the time of rod failure, thus reducing the thermal-to-mechanical energy conversion ratio.

As indicated earlier, the energy deposition in the RIA-ST-4 test rod at failure,[14,15] radially averaged at the axial flux peak location, was estimated to be about 1550 J/g UO_2. With this energy deposition, the energy insertion totals about ~1127 kJ and the thermal-to-mechanical energy conversion ratio becomes 0.29 to 0.3%. It is interesting to note that the largest thermal-to-mechanical energy conversion ratio determined

a. The thermal-to-mechanical energy conversion ratio is equal to the kinetic energy transfer to the coolant, E_c, divided by the total thermal energy deposition in the molten debris at the time of rod failure.

b. The axial average energy deposition is about 74% of that at the axial flux peak location.

for the CDC power excursion tests[17] was about 2.8% in Test 549 (during which pressure pulses up to 12 MPa were recorded upon test rod failure), compared with 35 MPa during the RIA-ST-4 experiment (see Table 1).

2.2.8 Discussion. The initial contact between the molten debris particles (at ~3200 K) and water (at ~600 K) causes the interface temperature (~2000 K) to be very much higher than the thermodynamic critical temperature of water (647 K). Thus, the formation of a stable vapor film around the debris particles upon contact with water is ensured. To produce the coolant peak pressure recorded during RIA-ST-4 (35 MPa) within the recorded rise time (2000 μs), energy must be transferred very rapidly from the molten debris particles to the coolant. This requires direct contact, efficient intermixing of the two liquids, and the formation of a large heat transfer area via the fine fragmentation of the molten debris particles.

To meet these requirements, the vapor film around the particles should collapse, which requires a powerful trigger since the initial coolant pressure at the time of rod failure was about 8.5 MPa (see Figure 4). Such a trigger (that is, peak pressure and impulse[18-27]) may have been developed due to several causes, such as the release of gas from the rod upon failure (Subsection 2.2.3), the impact of molten debris masses against the flow shroud wall, or the travel of the molten particles through the coolant at high velocities. Also, the precipitous collapse of a vapor layer or bubbles in the coolant adjacent to the interaction zone and the formation of hydrodynamic instabilities in the interaction zone (for example, due to jet formation as bubbles at the interface collapse) can give rise to pressure disturbances that may force liquid-liquid contact, and trigger the fine-scale fragmentation of the debris particles.

Although it is not clear at this point how the high internal test rod pressure at failure contributed to the triggering mechanism of the thermal interaction, this pressure was primarily responsible for the initial breakup and premixing of the molten debris particles with the coolant in the flow shroud. The interaction between the molten debris particles and the coolant may have been triggered locally at first, and then propagated as a shock front was developed and traveled through the remainder of the shroud. If a shock wave(s) was developed due to the release of fill gas from the rod upon failure, it may be argued that this wave would travel through the entire shroud before coarse premixing of the molten particles with the coolant occurs and, therefore, it could not contribute to the trigger of the fine-scale fragmentation of the debris particles. The rebuttal is detailed in the following paragraphs.

Upon rod failure, the molten debris can be ejected into the test shroud and against the shroud wall with an approximate velocity

$$V \simeq \sqrt{2\,\Delta P/\rho_f} \qquad (8)$$

where ΔP is the pressure difference driving the molten debris out of the failed rod, and ρ_f is the density of the molten debris (~8700 kg/m^3). The pressure difference is taken to be about 30 MPa (see Subsection 2.2.3) because the coolant pressure was about 8.5 MPa at the time of failure (see Figure 4). Thus, the ejection velocity of the debris could have been about 83 m/s. The molten debris traveled the distance between the surface of the test rod (~1.075 cm in diameter) and the inner surface of the shroud (1.93-cm inner diameter), that is, 0.855 cm, before impinging the zircaloy shroud wall. This takes no more than 104 μs. The impingement of molten debris onto the shroud wall results in a very high Weber number,[a] on the order of one million (see Section 3.2 for details), which is certainly capable of breaking up the molten debris mass into smaller particles. These particles and those expelled from the test rod upon failure would intermix with the shroud coolant. The impact on the shroud wall could produce a local high coolant pressure, which may have contributed to the trigger of the interaction. Figure 9 presents an illustration of the test rod failure and the initial breakup and premixing of the molten debris particles with the coolant in the shroud. As shown in Figure 9(c), some of the molten debris became attached to the inner surface of the shroud wall, forming the thin layer observed during the posttest examination of the shroud.[15]

a. The potential for hydrodynamic breakup of a molten substance can be expressed in terms of the ratio of inertial-to-surface tension forces, commonly called the Weber number. Breaking of a molten droplet occurs when the hydrodynamic forces exerted on the droplet overcome surface tension at the contact surface with another substance, which could be the cold liquid or a solid wall.

Table 1. Testing conditions and experimemtal results of the RIA-ST-4 experiment and some of the CDC power excursion tests

		Power Burst Facility (PBF)	Capsule Driver Core (CDC) Facility[6]				
		RIA-ST-4	479	491	507	536	549
1.	**Test Fuel**						
	Type	PWR fuel rod	GEX-PL	GEX-PL	SPXM-PL	SPXM-PL	SPXM-PL
	Material	UO_2	UO_2	UO_2	UO_2	UO_2	UO_2
	Burnup	Unirradiated	Unirradiated	Unirradiated	Unirradiated	Unirradiated	Unirradiated
	Cladding	Zircaloy-4	Zircaloy-2	Zircaloy-2	Zircaloy-2	Zircaloy-2	Zircaloy-2
	Active rod length (m)	0.914	0.128	0.612	0.127	0.127	0.127
	Pellet diameter (mm)	9.3	6.82	6.97	5.59	5.59	5.59
	Cladding outside diameter (mm)	10.73	7.87	7.94	6.35	6.35	6.35
	Cladding thickness (mm)	0.61	0.491	0.483	0.356	0.356	0.356
	Enrichment (wt% ^{235}U)	20	7.0	7.0	10.5	10.5	10.5
	Cold rod internal pressure (MPa)	3.79	0.1	0.1	0.1	0.1	0.1
	Total rod weight (g UO_2)	634	48	240	32	32	32
	Total cladding weight (g zircaloy)	115	9.5	45	5.5	5.5	5.5
2.	**Test Shroud or Capsule**						
	Material	Zircaloy-4	304 stainless steel	304 stainless steel	304 stainless steel	304 stainless steel	304 stainless steel
	Wall thickness (mm)	3.05	1.65	1.65	1.65	1.65	1.65
	Inner diameter (mm)	19.3	72.9	72.9	72.9	72.9	72.9
	Volume empty (cm^3)	~270	6500	6500	6500	6500	6500
	Water volume[a] (cm^3)	~180	5500	5500	5500	5500	5500
	Acoustic relief Time (ms)	The loop was liquid full	~1.1	~1.1	~1.1	~1.1	~1.1
3.	**Coolant Conditions**						
	Cooling condition	Forced convection	Free convection	Free convection	Free convection	Free convection	Free convection
	Coolant pressure (MPa)	6.45	0.1	0.1	0.1	0.1	0.1
	Coolant temperature (K)	538	~290	~290	~290	~290	~290
	Coolant flow Rate (L/s)	0.085	Stagnant water	Stagnant water	Stagnant water	Stagnant water	Stagnant water

Table 1. (continued)

4. Test Results	Power Burst Facility (PBF)	Capsule Driver Core (CDC) Facility[6]				
	RIA-ST-4	479	491	507	536	549
Total energy deposition[b] (J/g UO_2)	2930	1730	1800	2050	2600	2740
Total energy deposition[b] at failure[c] (J/g UO_2)	1550	1570	1380	1670	1760	1500
Maximum coolant pressure recorded (MPa)	35	4.96[d]	4.93[d]	1.25[d]	2.62[d]	12.07[d]
Rise time of the recorded pressure pulses (ms)	2.0	—	—	0.45	0.43	0.43
Total weight of debris particles (g)	155	55.4[e]	150	31.6	37.2[e]	37.9[e]
Mean particle diameter (μm)	1300	780	400	500	200	110

a. The CDC test capsule was filled with water to within 25 cm of the top; air at atmospheric pressure was contained in the top space of the capsule.

b. Radially averaged at the axial flux peak location.

c. Upon test rod failure, extensive amounts of molten fuel and cladding were dispersed and intermixed with the coolant in the vicinity of failed fuel rod.

d. During the CDC tests, pressure measurements were made by transducers located at the bottom of capsule, where doubling of the pressure magnitude might have occurred. Actual pressure in the interaction zone could be about half the recorded value.

e. The weight of the collected particles from these tests is more than the weight of the UO_2 in the test rod. The extra weight is due to molten cladding and structural materials from the test rod.

cles
h coolant

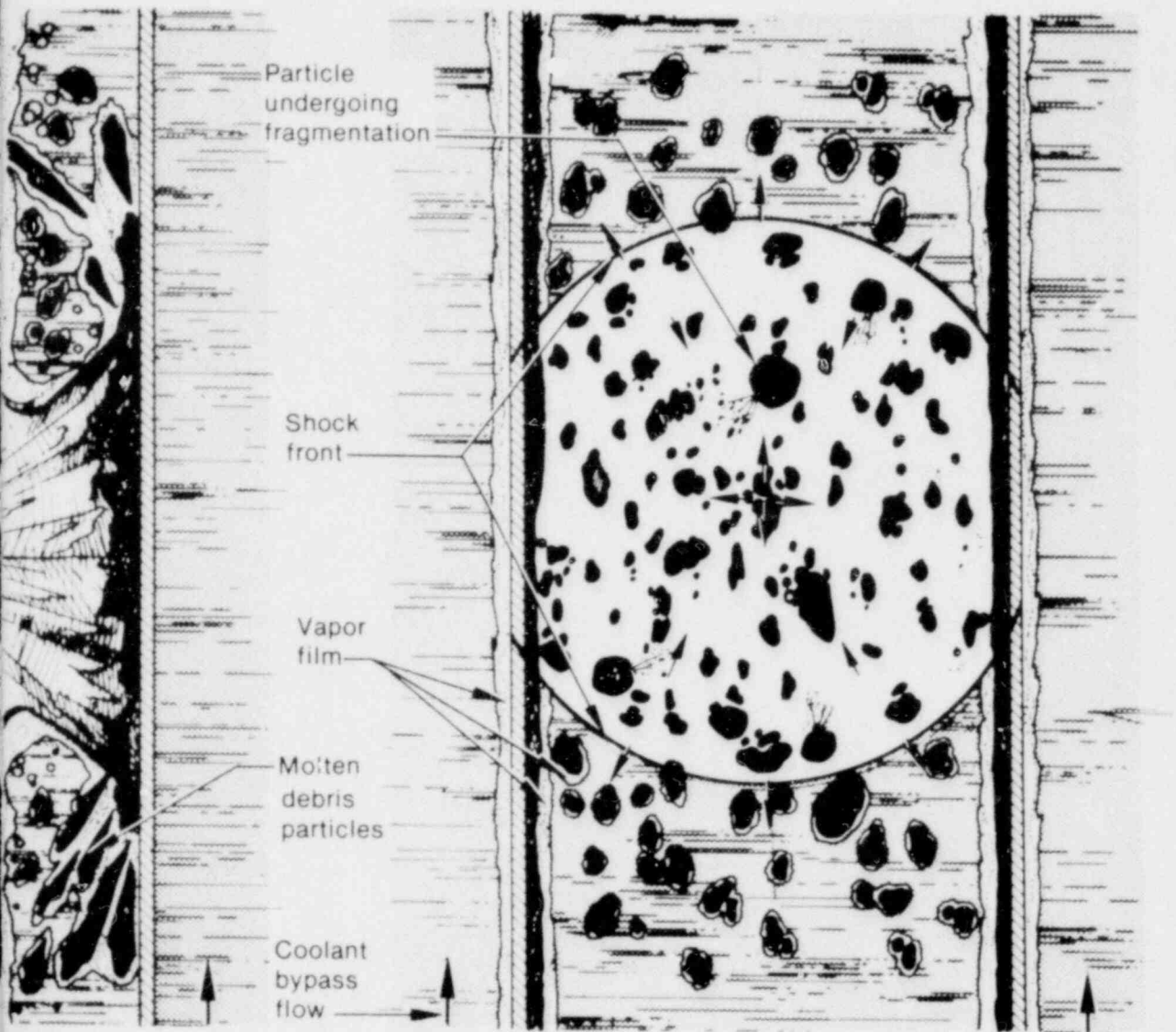

(c) Fine fragmentation of molten debris

INEL-B-17 152

ten debris during the RIA-ST-4 experiment.

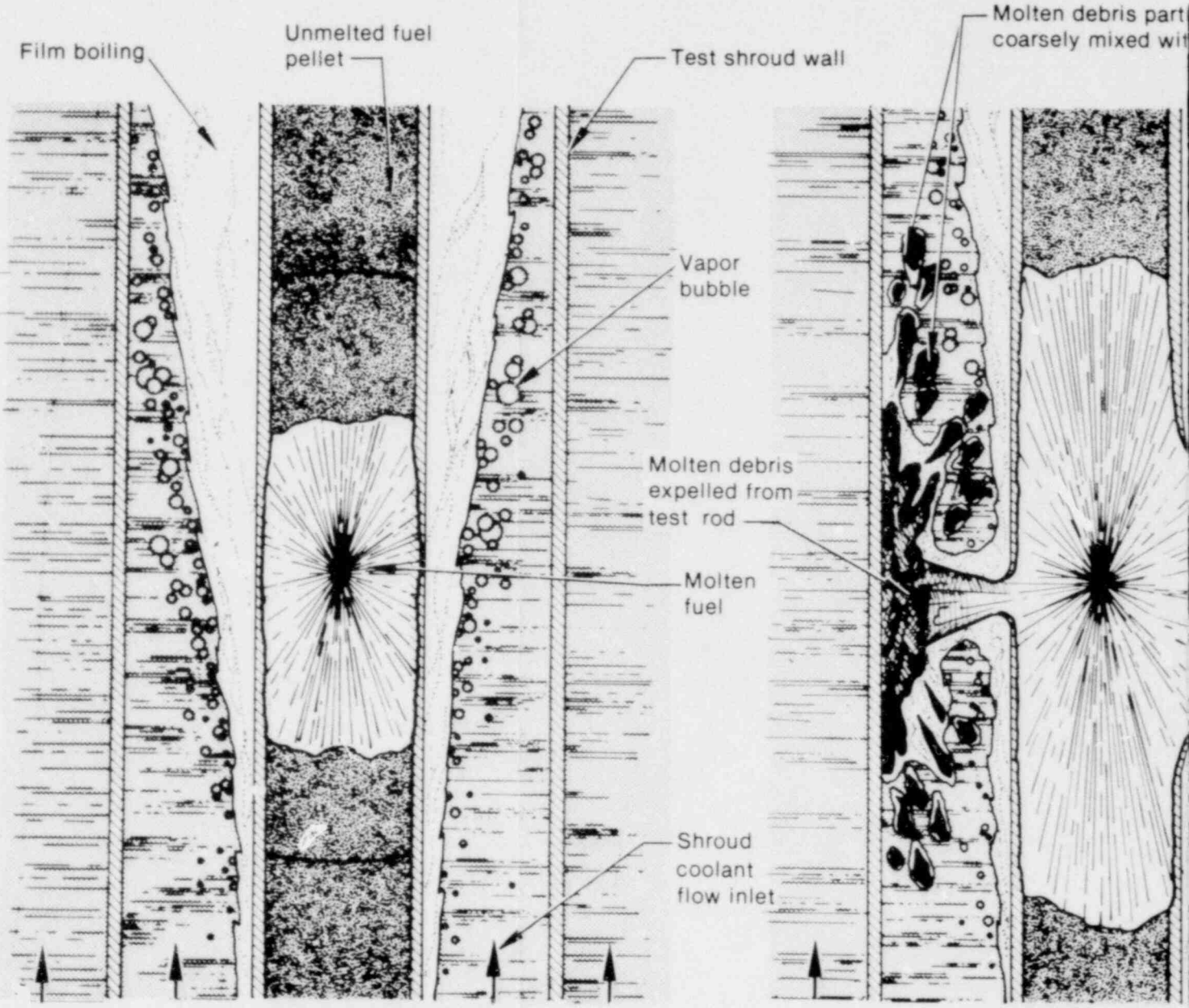

Figure 9. Illustration of fuel rod failure and fragmentation of mo

3. FRAGMENTATION CHARACTERISTICS OF THE MOLTEN DEBRIS

Severe fragmentation of molten debris occurred upon contact with the coolant in the shroud at the time of rod failure. This is evidenced by the particles collected from within the flow shroud and the particle filters in the test train. The typical appearance of the particles (shown in Figure 10) is spherical or round with relatively smooth surfaces, indicating that fragmentation occurred when the debris was molten. About 155 g of molten debris (primarily a mixture of UO_2 fuel and zircaloy cladding), or 20% of the total fuel and cladding mass in the test rod, were fragmented. Approximately 58 wt% of this amount (~90 g) fragmented into fine particles less than 2000 μm in diameter.

3.1 Distribution of Debris Particles

Particle collections obtained during the RIA-ST-4 experiment are listed in Table 2 and histogrammed in Figure 11. These particles are compared in Figure 12 with those obtained during high power excursion tests performed in the Capsule Driver Core (CDC) facility[a] at the Idaho National Engineering Laboratory.[17,28] Facilities, test fuel characteristics, and results of both the RIA-ST-4 and the CDC experiments are listed in Table 1. The particle distributions plotted in Figure 12 show that the average particle size from the CDC tests varied from 110 to 800 μm, versus an average particle size of about 1300 μm from the RIA-ST-4 experiment. Although the average particle size from the RIA-ST-4 experiment is significantly greater than that from the CDC tests, the RIA-ST-4 pressure pulses were much higher than those recorded during the CDC tests. For example, the total mass of the debris particles (150 g) from Test CDC-491 is almost equal to that from the RIA-ST-4 experiment (155 g); however, the average particle diameter and the coolant peak pressure recorded were 400 μm and 4.93 MPa (as compared to 1300 μm and 35 MPa in the RIA-ST-4 experiment).

The average particle sizes from the CDC tests[17,28] were independent of the total weight of the fragmented particles and of the characteristics of the test fuel rod. This suggests that the destabilization and collapse of film boiling around the particles might have been more difficult in the PBF experiment (initial coolant pressure ~6.45 MPa and high system contraints) than in the CDC tests (initial coolant pressure ~0.1 MPa). Therefore, the fragmentation process during the RIA-ST-4 experiment did not proceed to as great a degree, resulting in a more coarse fragmentation of the debris.

The acoustic relief time of the RIA-ST-4 test train was relatively long (a few milliseconds), because the loop was totally filled with water. The acoustic relief time during the CDC power excursion tests[17] was about 1.1 ms (the test capsule was filled with water to within 25 cm from the top). These times are longer than the measured rise times of the pressure pulses in the PBF experiment (~2 ms) and in the CDC tests (~0.43 to 0.45 ms), respectively, indicating that the interactions between molten fuel particles and coolant in those experiments were rapid and coherent. During the RIA-ST-4 experiment, however, the coolant phase at the time of contact with molten debris (that is, liquid or a two-phase mixture), the initial coolant pressure,[29] the geometrical constraint imposed by the shroud wall, the inertial constraint by the coolant, and the relatively high acoustic constraint[30-32] of the PBF loop (the loop was totally water filled) could have all contributed to the recorded high pressurization of the coolant. The effects of coolant conditions (that is, initial coolant phase and pressure) on coolant peak pressurization during an MFCI in LWRs are assessed in Section 5.

---

a. The data from the CDC program were obtained by placing a single rod or a small cluster of fuel rods in a closed capsule containing water at atmospheric pressure and room temperature. In those tests the water availability for mixing with failed fuel rods was unrestricted by a shroud. By contrast, the test rod in the RIA-ST-4 experiment was shrouded and cooled by forced convection. Prior to each CDC test the capsule was partially filled with water to within 25 cm from the top. The top space contained air at atmospheric pressure. Measurements of the cladding surface temperature, capsule pressure, and water column velocity were obtained during each test.

For a shock wave that travels at the sonic velocity (~1090 m/s in water at 538 K), 420 μs are required for it to travel from the midplane (corresponding to the axial flux peak location where rod failure is expected to occur first) to either end of the active length of the flow shroud (~50 cm). This means that the shock wave would travel about 11 cm in either direction before the initial breakup and premixing of the molten debris with the shroud coolant could have occurred (~104 μs after failure). It should be noted that the travel distance of the shock wave might be less than 11 cm, because a nonuniform burst of the test rod at failure could have delayed the development of a shock front. Therefore, the molten debris produced from the remainder of the test rod (~70 cm or 75% of the active flow shroud) easily might have been premixed with the coolant in the shroud prior to the arrival of the shock front. The passage of a shock wave (due to gas release and/or other causes) through the dense dispersion in the flow shroud might have caused the destabilization and collapse of the vapor film formed around the debris particles, triggering the fine fragmentation of the particles and initiating coherent thermal interaction between the debris particles and the coolant. Additional discussion of the aspects of molten fuel-coolant interaction is presented in Appendix A. In particular, the spontaneous nucleation and the pressure detonation models are discussed relative to the results of the RIA-ST-4 experiment.

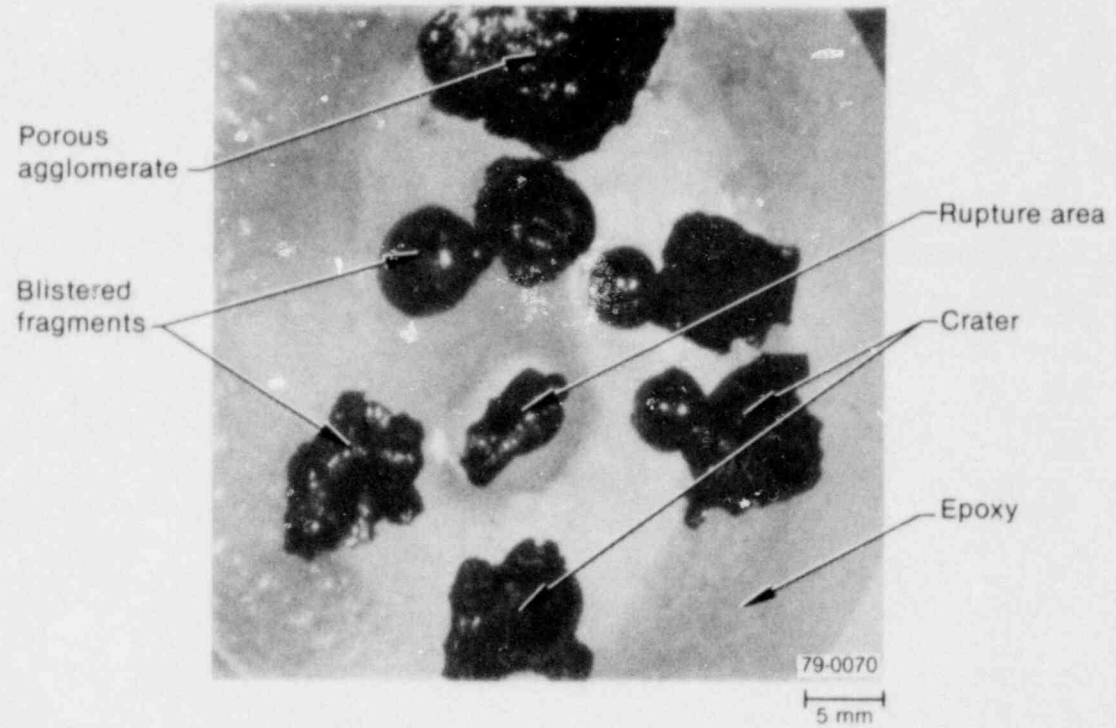

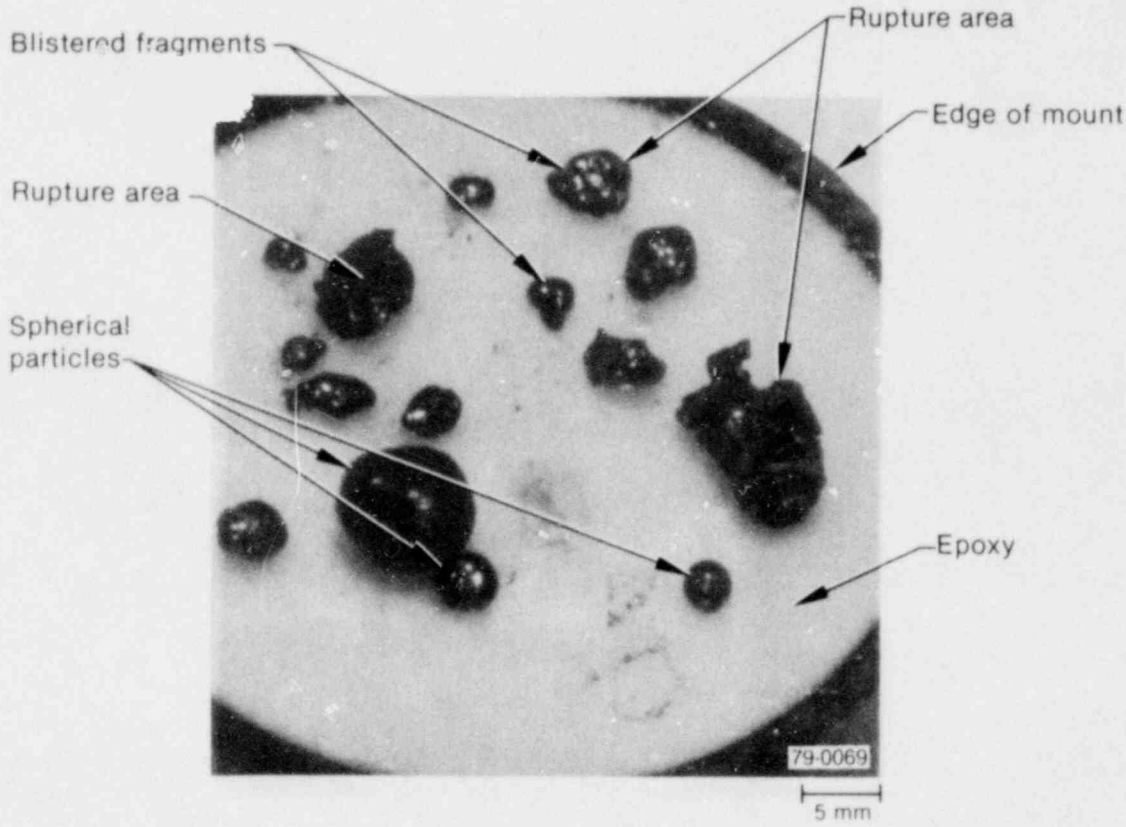

Figure 10. Collection of debris particles from the RIA-ST-4 experiment.

Table 2. Particle distribution from the RIA-ST-4 experiment

Range of Particle Size (μm)	Average Particle[a] Diameter (μm)	Weight[b] (g)	Weight Percent	Cumulative Percent
<38	—	0.2896	0.19	0.19
38 to 45	41	0.3956	0.25	0.44
45 to 63	54	1.4176	0.91	1.35
63 to 75	69	1.610	1.04	2.39
75 to 106	90	2.9041	1.87	4.26
106 to 150	128	7.1984	4.64	8.90
150 to 212	181	2.3133	1.49	10.39
212 to 355	283	6.0730	3.91	14.30
355 to 500	427	5.9915	3.86	18.16
500 to 850	675	14.4668	9.32	27.48
850 to 1180	1015	18.1768	11.71	39.19
1180 to 1700	1440	15.9812	10.30	49.49
1700 to 2000	1850	13.0328	8.40	57.89
2000 to 5600	3800	54.0412	34.83	92.72
>5600	—	11.2792	7.27	99.99

a. The arithmetic mean value of the particle size range.

b. Total particle weight ~ 155.1711 g.

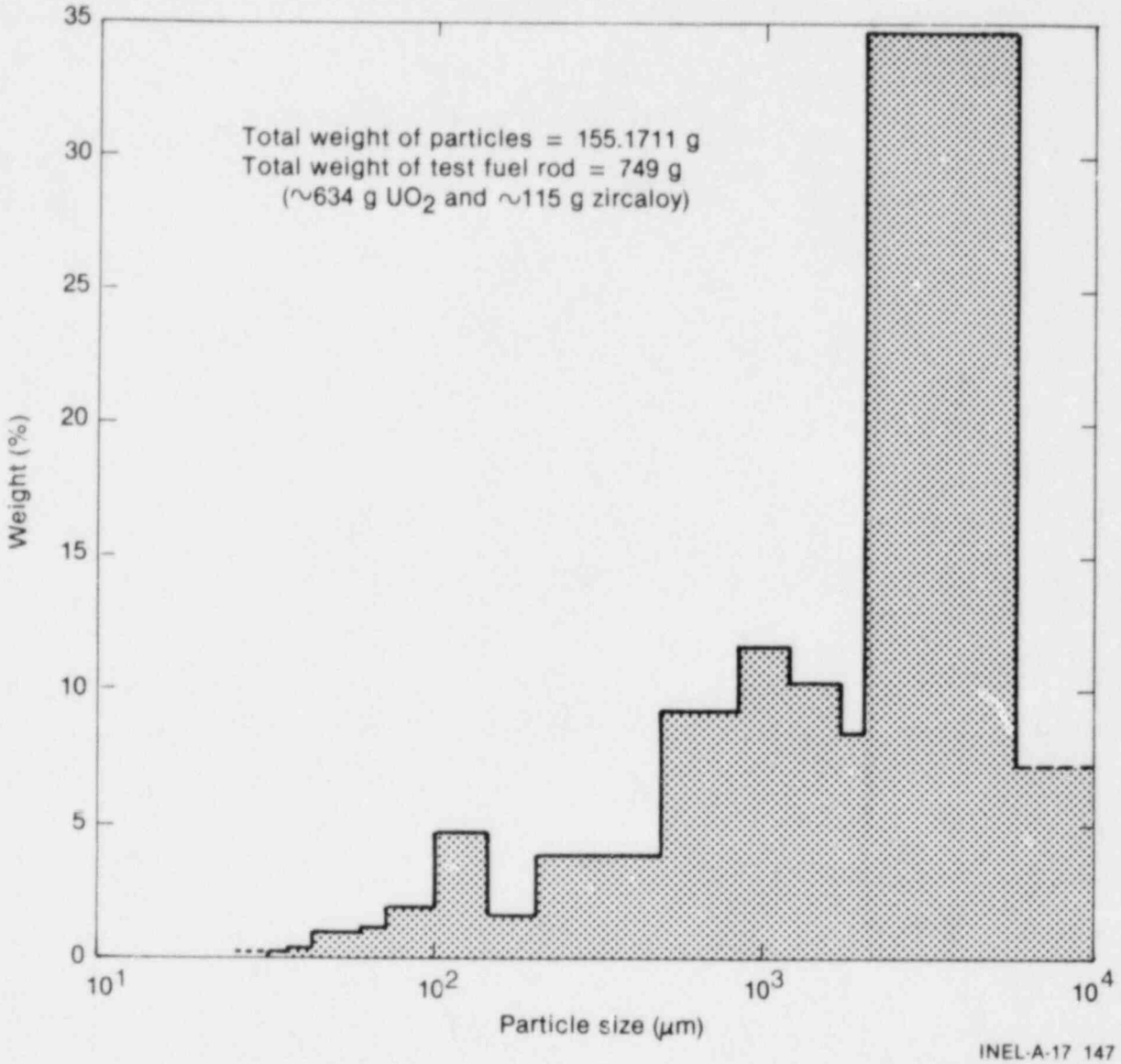

Figure 11. Histogram of the debris particles produced during the RIA-ST-4 experiment.

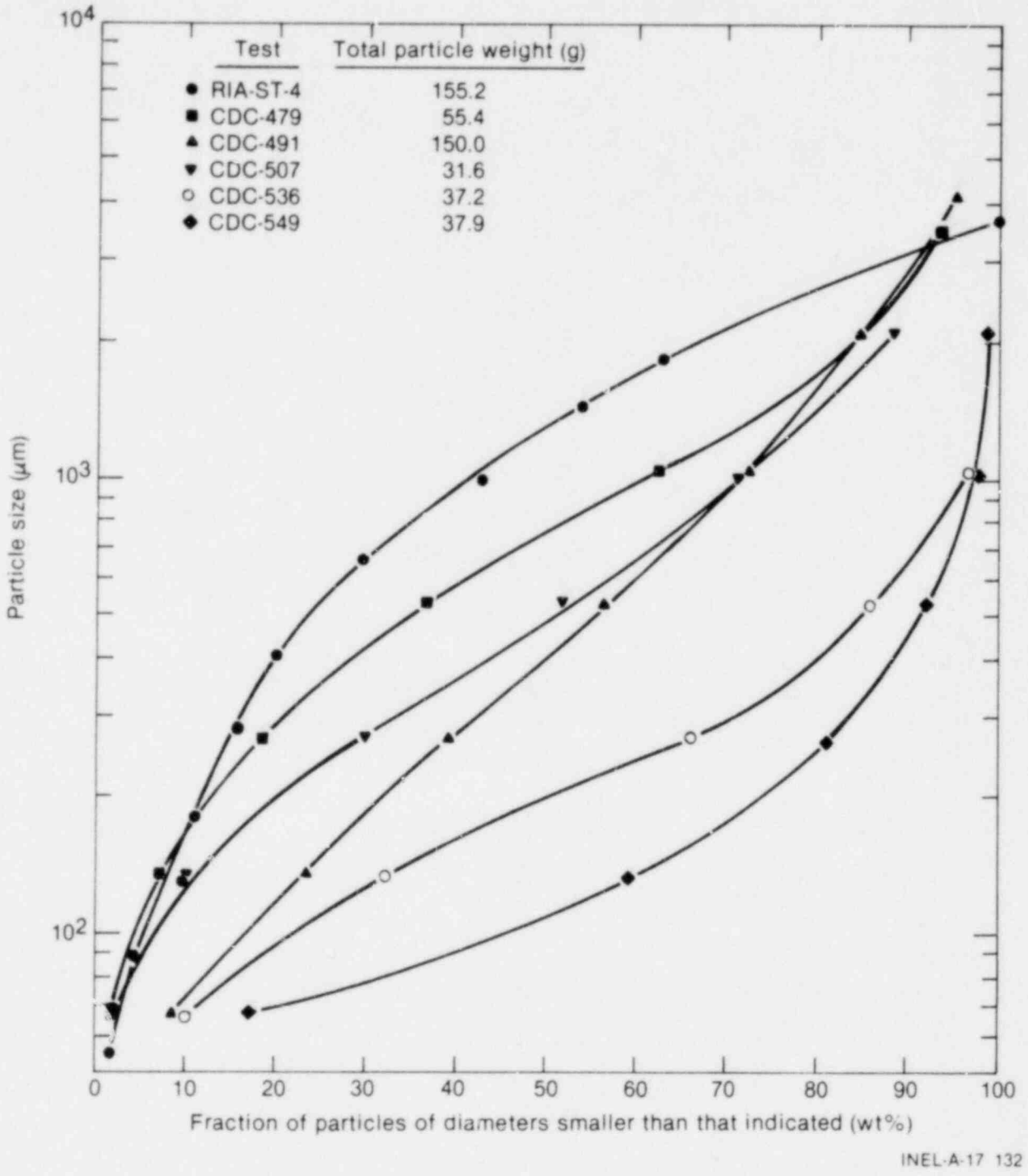

Figure 12. Comparison of particle distribution in RIA-ST-4 experiment with that during CDC power excursion tests.

3.2 Fragmentation Due to Impact Disintegration

Impact disintegration of the molten debris occurs when the hydrodynamic inertial force exerted on the molten mass overcomes the surface tension force at the impact surface. As demonstrated in Figure 9, impact disintegration of molten masses expelled from the test rod at failure could have occurred upon impingement onto the inner surface of the zircaloy shroud wall and onto the surface of the coolant. The severity of disintegration is directly proportional to the value of the Weber number, We, which is the ratio of the inertial to surface tension forces

$$We = (\rho_f V^2)/(\sigma_s/D) \qquad (9)$$

where

ρ_f = density of the impinging material (~ 8700 kg/m^3)

D,V = diameter and ejection velocity of molten debris masses

σ_s = interfacial surface tension between molten debris and water.

It is assumed that σ_s is the difference between the molten UO_2-air interfacial tension (a value of 0.45 N/m was recommended for molten UO_2)[33] and the air-water interfacial tension (~ 0.03 N/m).

Assuming that the average diameter of molten debris masses, D, ejected from the test rod at failure was about the diameter of the test rod before failure (~ 1 cm), the Weber number could have been about one million, which corresponds to an ejection velocity of about 83 m/s. This estimate of the Weber number is certainly capable of causing severe fragmentation of the molten debris, which is discussed in the following paragraphs.

The kinetic energy of the molten debris masses prior to their breakup would be used, in part, to create the new surface of the fragmented particles. The rest of this energy would be acquired by the fragmented particles as kinetic energy. The average diameter of the fragmented particles, d_f, can be estimated by comparing the fraction, ϵ, of the kinetic energy contributed to the breakup with the work required to create a new surface.

$$\frac{1}{2}\epsilon \rho_f \left(\frac{\pi D^3}{6}\right) V^2 = \pi \left(n_f d_f^2 - D^2\right) \sigma_s \qquad (10)$$

where n_f is equal to $(D/d_f)^3$ and,

$$d_f = \frac{D}{1 + (\epsilon V^2 D/12 \sigma_s)} . \qquad (11a)$$

Substituting Equation (8) into the above equation gives

$$d_f = \frac{D}{1 + (\epsilon \Delta P D/6 \sigma_s)} \qquad (11b)$$

where d_f is independent of the density of the ejected molten debris mass, but dependent on its diameter.

When the ejection velocity of the molten mass is very high, which may have been the case in the RIA-ST-4 experiment because of the high pressure in the test fuel rod at failure [that is, $\Delta P >> (6\sigma_s/\epsilon D)$], Equation (11b) is simplified as

$$d_f = \frac{6 \sigma_s}{\epsilon \Delta P} \qquad (12)$$

where d_f, in this case, is proportional to the surface tension between the impinging material and the surface of impact and is inversely proportional to the fraction of the kinetic energy used in the breakup and the driving pressure difference ΔP. The average diameter of the fragmented particles is independent of the size of the molten mass before breakup [Equation (12)]. For ϵ equal to only 1% and ΔP equal to 5 MPa, the average size of the fragmented particles, d_f, is about 50 μm. Such an estimate of d_f is very much less than the average diameter (~ 1300 μm) of the debris particles from the RIA-ST-4 experiment. This suggests that the impact disintegration of the molten debris could have partially contributed to the fine fragmentation of the debris particles.

The metallurgical examination and the scanning electron microscope analysis of the debris particles provided evidence of two possible additional mechanisms of fragmentation: (a) the rupture of

the frozen crust at the surface of the particles due to pressure-induced stresses in the crust caused by overheating liquid coolant droplets entrained by the molten debris, and (b) the penetration of the crustal surface of the particles by coolant jets. The results of the investigation relative to these two mechanisms are discussed in the following subsections and a phenomenological analysis is presented in Section 4.

3.3 Fragmentation Due to Rupturing the Surface Crust

The metallurgical examination and the scanning electron microscope analysis of the debris particles[13] indicated that a majority of the particles have craters or ruptures in the sides through which the inside of the particles was discharged, leaving empty, frozen debris shells. Radial cross sections of three particles (~2.3 to 3.2 mm in diameter) are shown in Figure 13. Note that the insides of the particles are empty and the frozen shells (~50 to 600 μm thick) are full of voids of different sizes (> 4 μm). These voids, as well as the large central void, may have formed because of the entrainment of liquid coolant droplets (a few μm in diameter) by the molten debris during the initial mixing of the molten debris particles with the coolant, as discussed in Section 4. Figure 14 presents illustrative sketches of the entrainment[a] of liquid coolant droplets in the molten debris particles. The rapid energy transfer to the entrained coolant droplet causes rapid pressurization inside the particles and induces stresses in the frozen crust at the surface. Eventually the crust ruptures when the induced stresses exceed the ultimate tensile strength of the crust, ejecting the finely fragmented molten debris inventory through the rupture areas and into the coolant stream. The surface crust forms upon quenching of the molten debris particles by the coolant following the collapse of film boiling around the particles. Figure 15 presents illustrative sketches of the fragmentation of molten debris particles by rupturing of the surface crust.

Photos of debris particles taken through the scanning electron microscope are presented in Figures 16 and 17. The large, smooth opening in the side of the particle shown in Figure 16(a) suggests that the opening occurred when the inside of the particle was molten. Fragmentation of large (2.3- to 3.2-mm diameter) as well as small (10- to 40-μm diameter) debris particles apparently occurred by this mechanism during the RIA-ST-4 experiment. Figure 17 shows collections of small particles that ruptured at the surface, attached to the surface of larger particles. The figure also shows several blisters in the surface of the large particle.

The rupture of the surface crust and the voiding phenomena of the particles observed from the RIA-ST-4 experiment agree with the results of high power excursion tests[34-37] performed in the Japan Nuclear Safety Research Reactor (NSRR). Coolant pressurization up to about 12 MPa was recorded during these tests. Figure 18 presents radial cross sections of two of the particles obtained from one of the NSRR tests and shows the formation of one or more major voids in the particles. Notice, however, that the voids formed in the frozen shell were fewer and larger than those observed from the RIA-ST-4 experiment.

3.4 Fragmentation Due to Coolant Jets

The rapid, asymmetric collapse of void-like regions of film boiling on the surface of the debris particles by a shock front could have caused the development of coolant jets at the liquid-vapor interface.[24,25,38] High velocity coolant jets may form with a collapse pressure in excess of 0.5 MPa.[b] The penetration velocity, U, of the jets into the surface crust (this crust might form instantaneously upon quenching of the particle surface following vapor film collapse) is solely controlled by the density of the jet, ρ_j, the density of the crust, ρ_s, and the approach velocity of the jet, V.[41]

$$U = \frac{V}{1 + (\rho_s/\rho_j)^{1/2}} \qquad (13)$$

where the velocity of the jet before impinging the surface crust[38] is

a. Entrainment of coolant droplets in the molten debris is assumed to occur very rapidly, so that evaporation of the coolant does not occur during the entrainment process.

b. The jet is a high velocity jet if $\Delta P >> 0.118\ \sigma_s$, where σ_s is the fracture stress of solid UO_2 (~45 MPa at 2600 K[39,40]). See Section 4 for details.

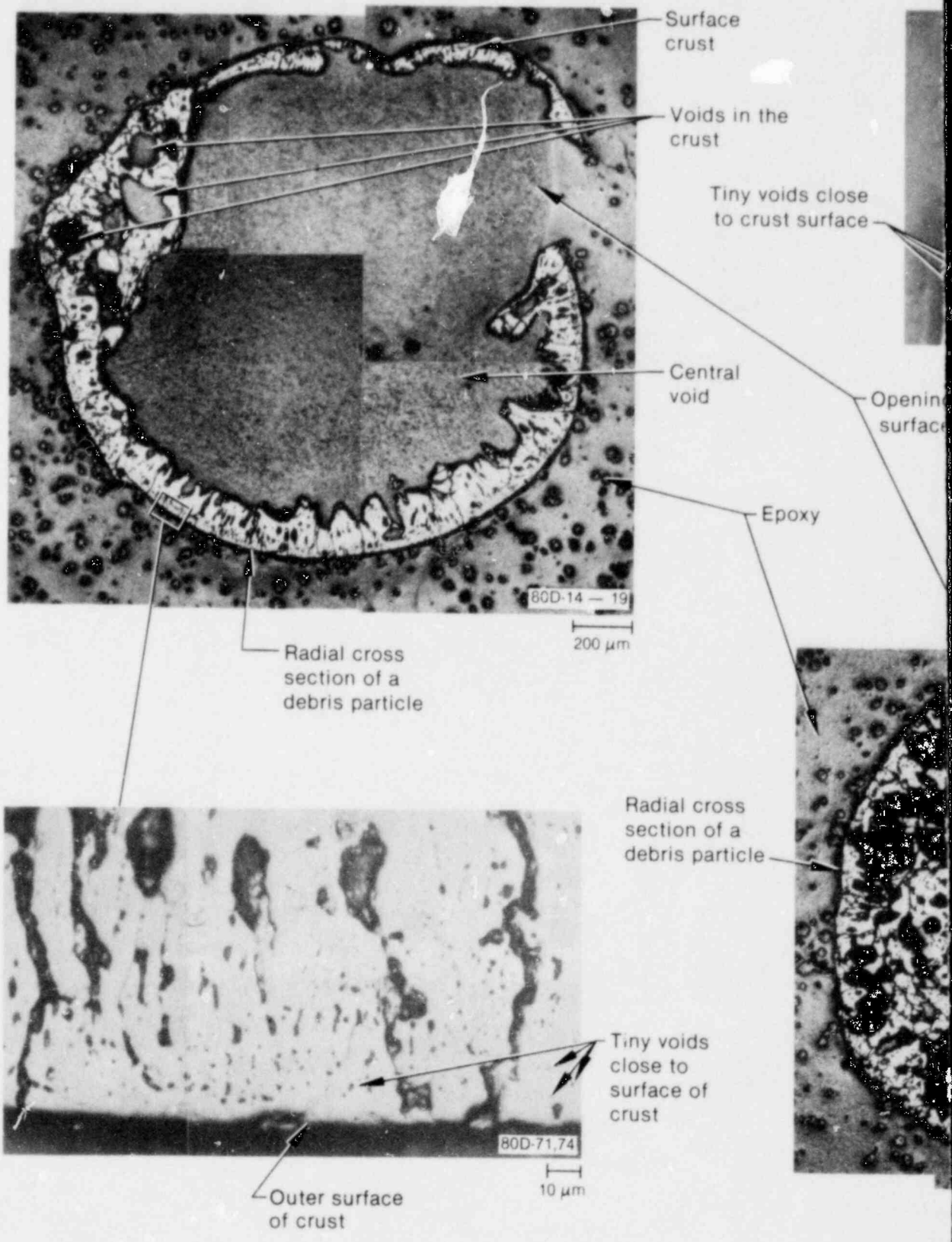

Figure 13. Radial cross-sectional view of

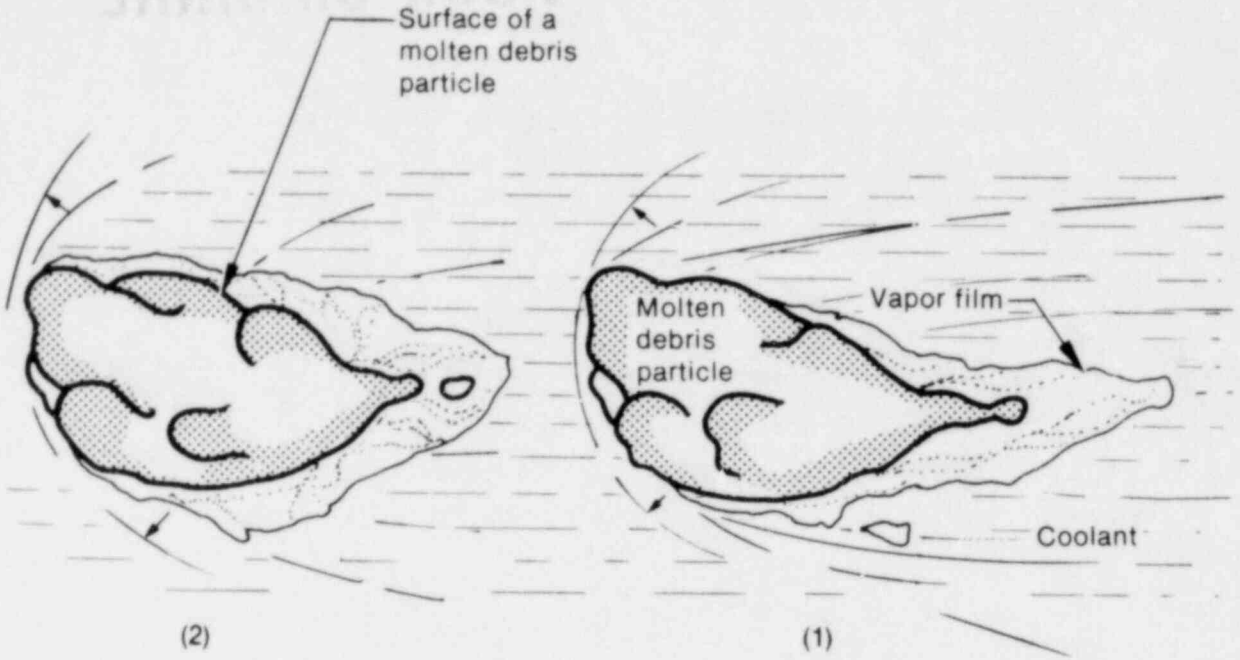

(a) A molten debris particle accelerating through the coolant

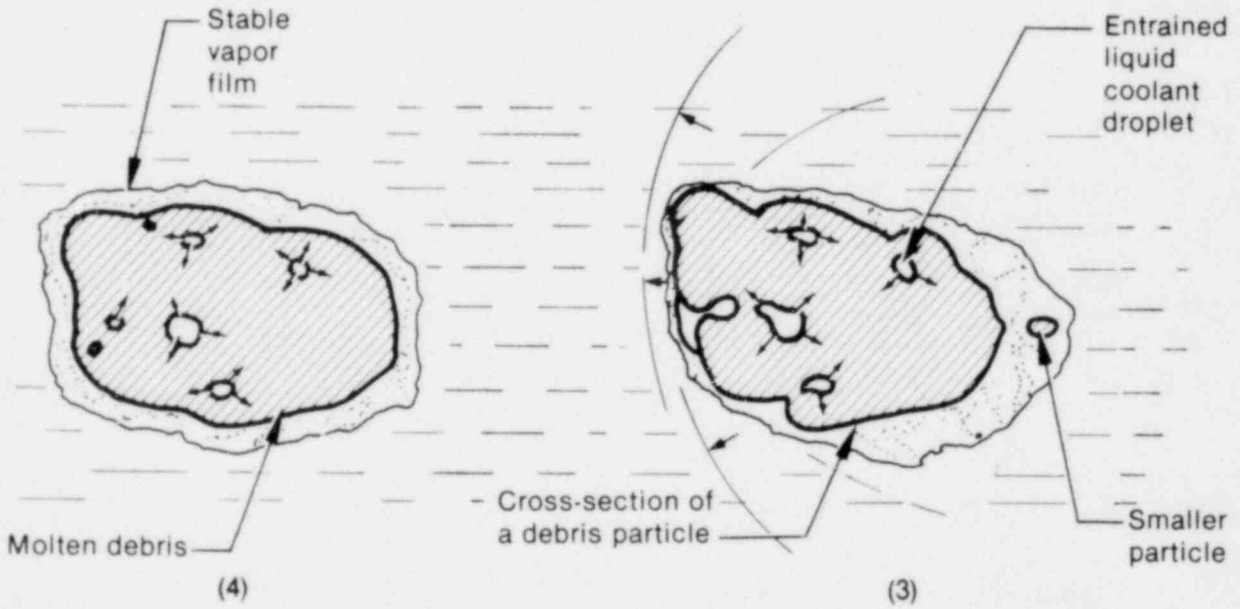

(b) Liquid coolant entrained by a molten debris particle

INEL-A-17 150

Figure 14. Illustration of liquid coolant entrainment in a molten debris particle.

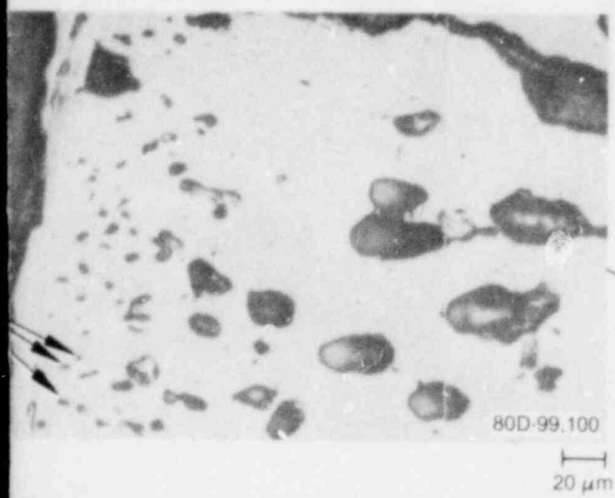

g in the
e crust

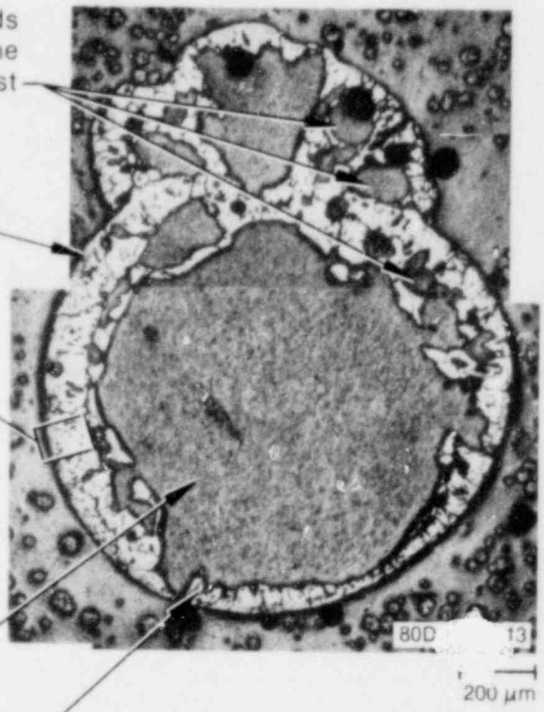

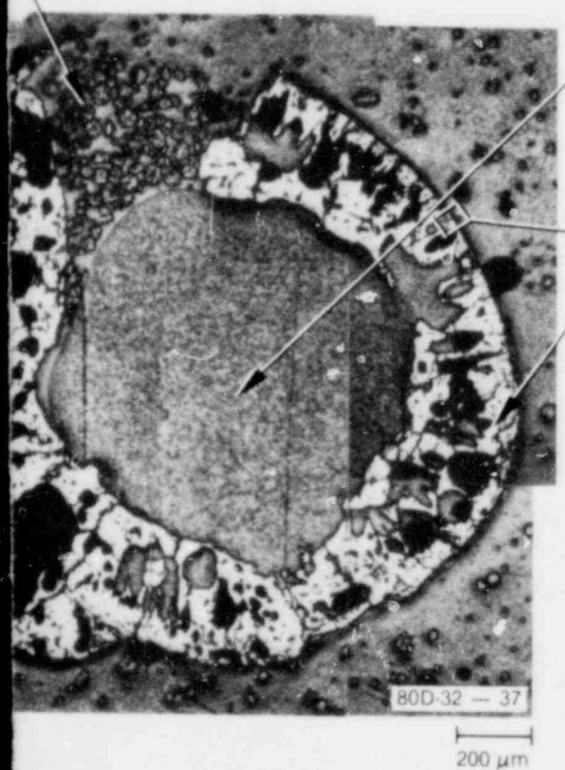

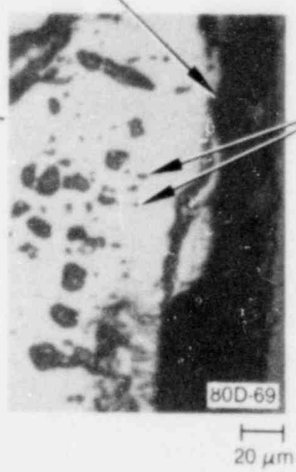

debris particles produced during the RIA-ST-4 experiment.

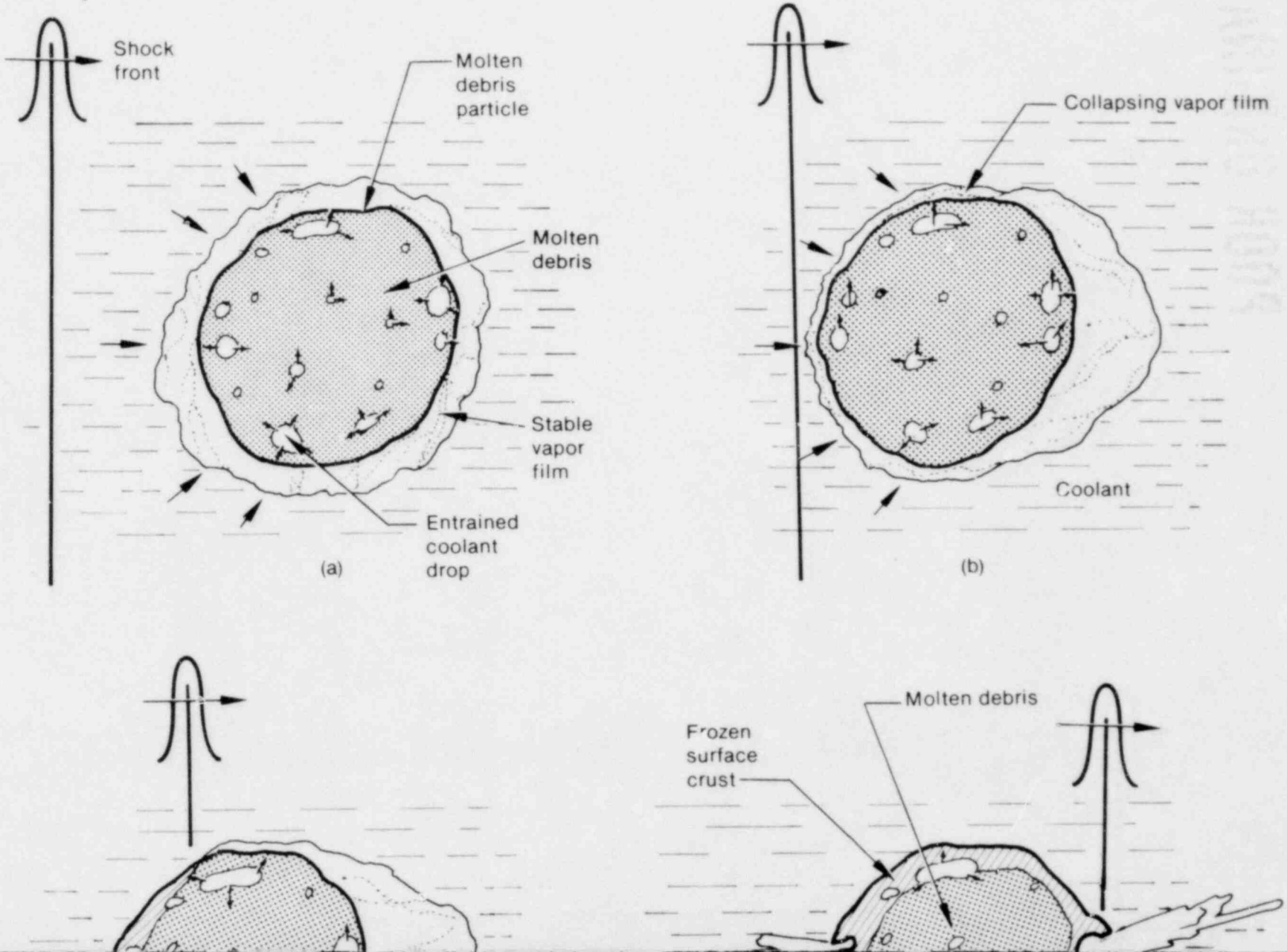
Shock front
Molten debris particle
Molten debris
Stable vapor film
Entrained coolant drop
(a)
Collapsing vapor film
Coolant
(b)
Molten debris
Frozen surface crust

[1] Crust surface

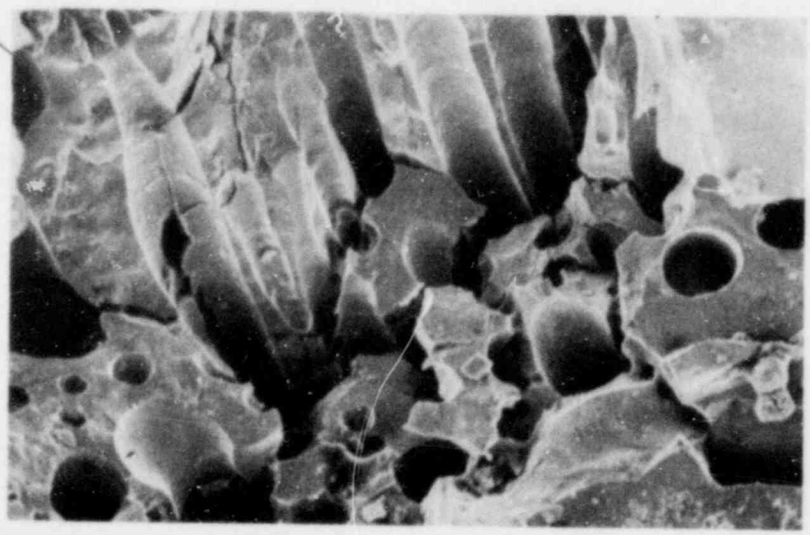

[2] Oblique view of particle crust

20 μm

(c) Traces of coolant jets penetrating the particle surface upon vapor film collapse

A-ST-4 experiment.

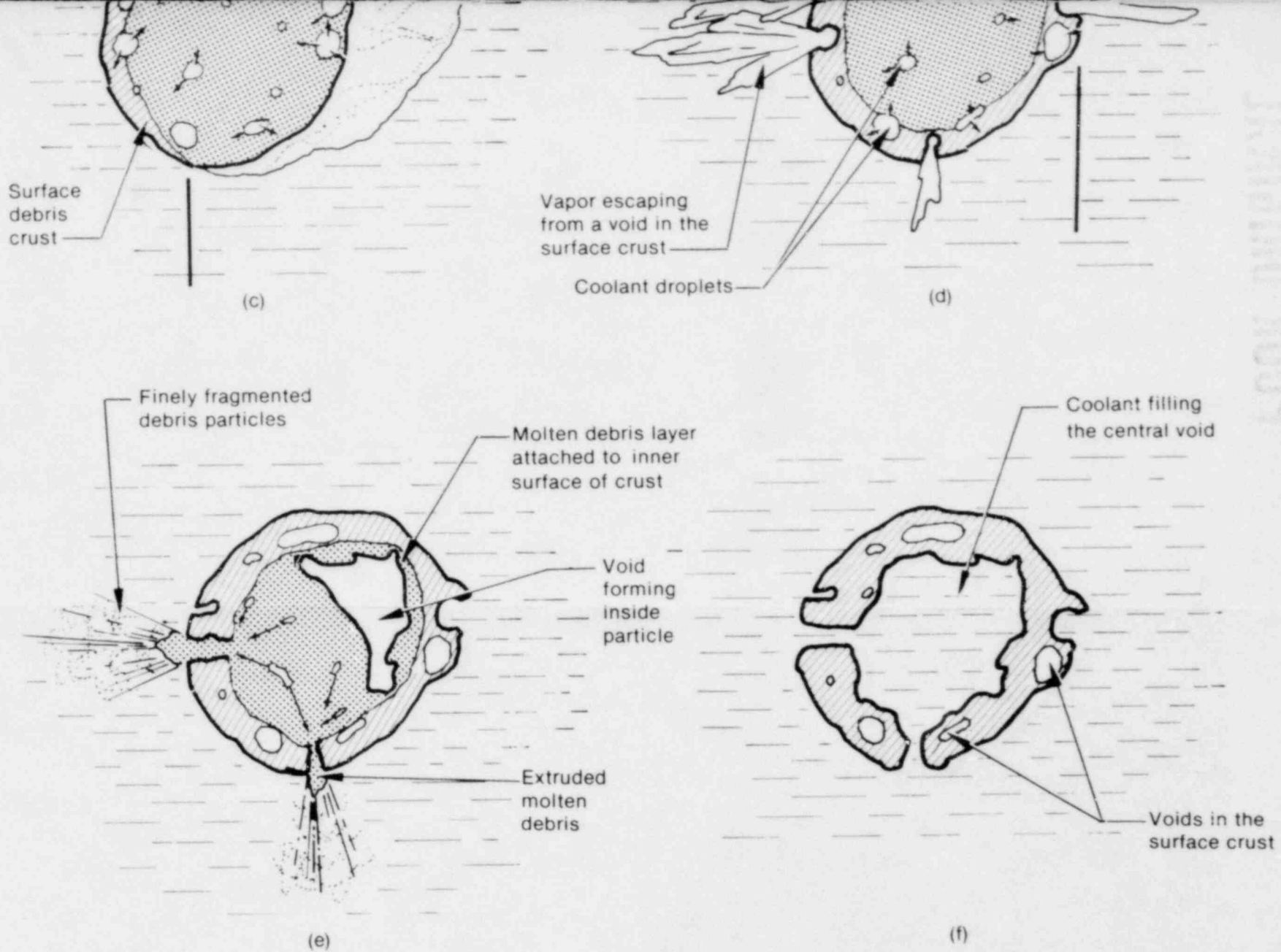

Figure 15. Illustration of debris particle fragmentation due to rupturing of the surface crust.

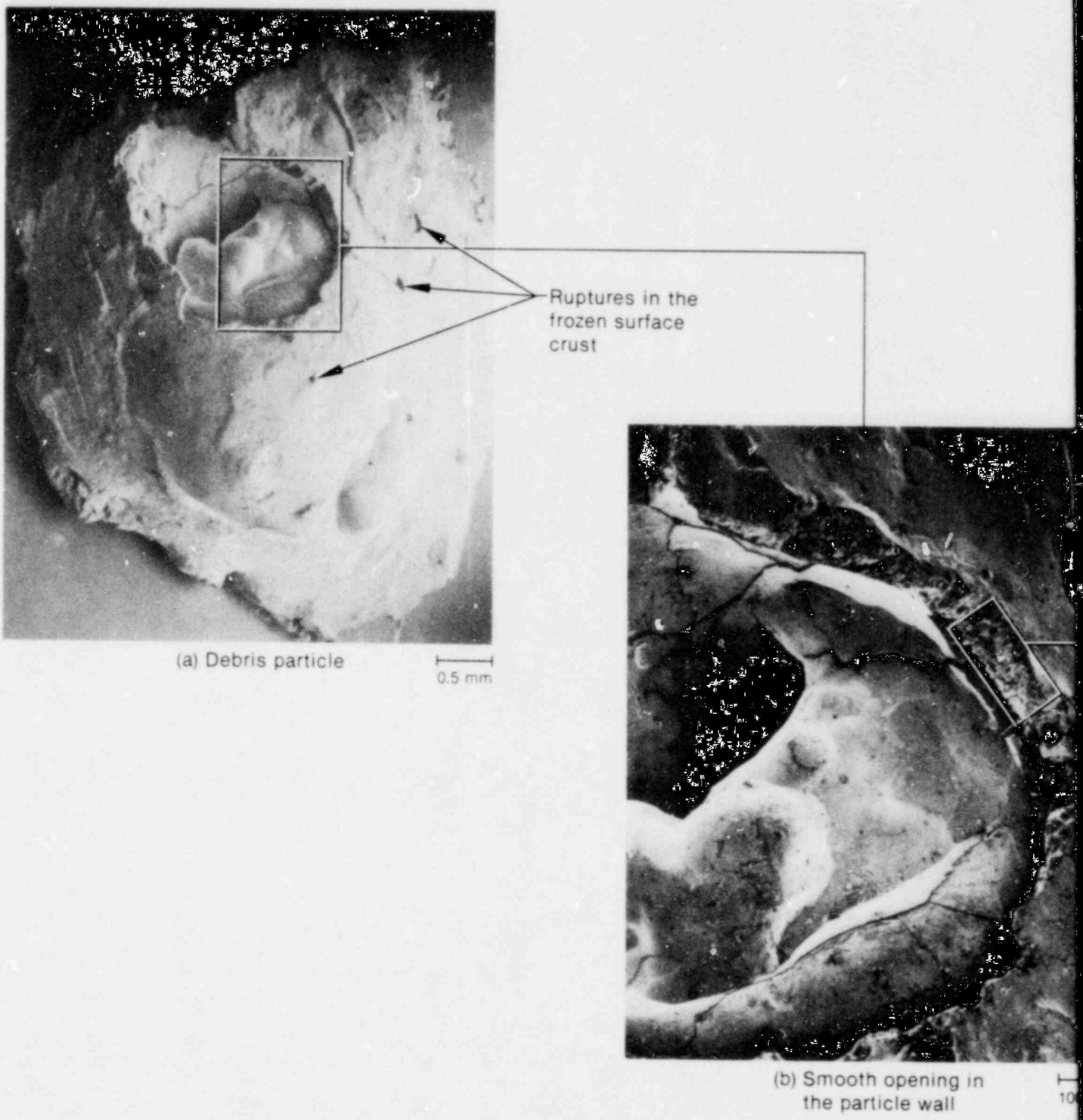

Figure 16. Scanning electron photomicrographs of a debris particle from the R

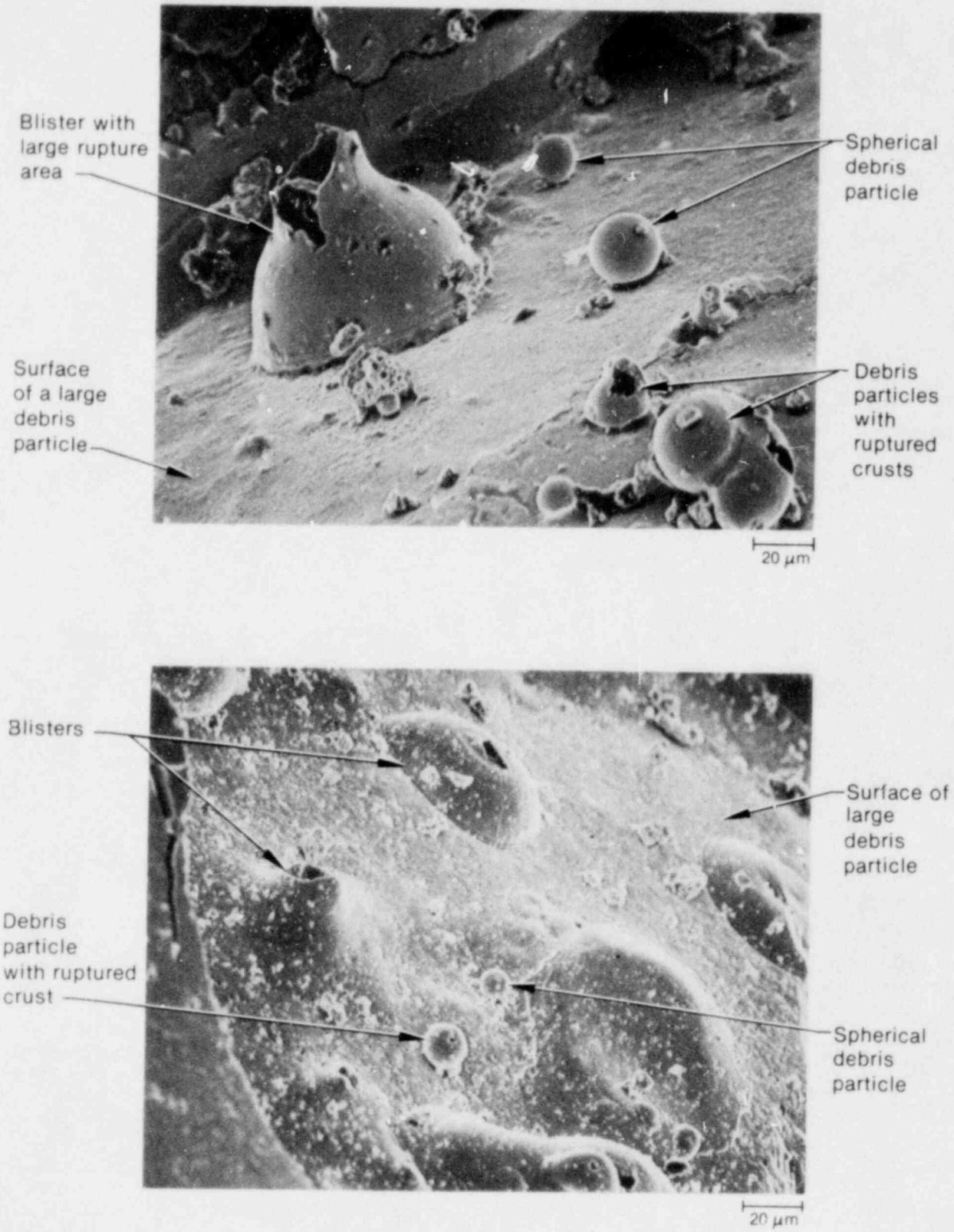

Figure 17. Scanning electron photomicrographs of the surface of debris particles from the RIA-ST-4 experiment.

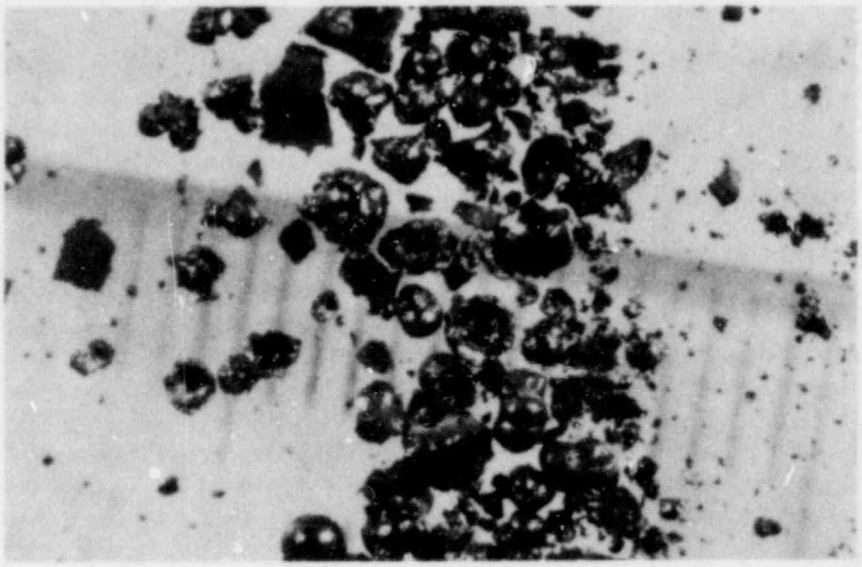

(a) Collection of debris particles

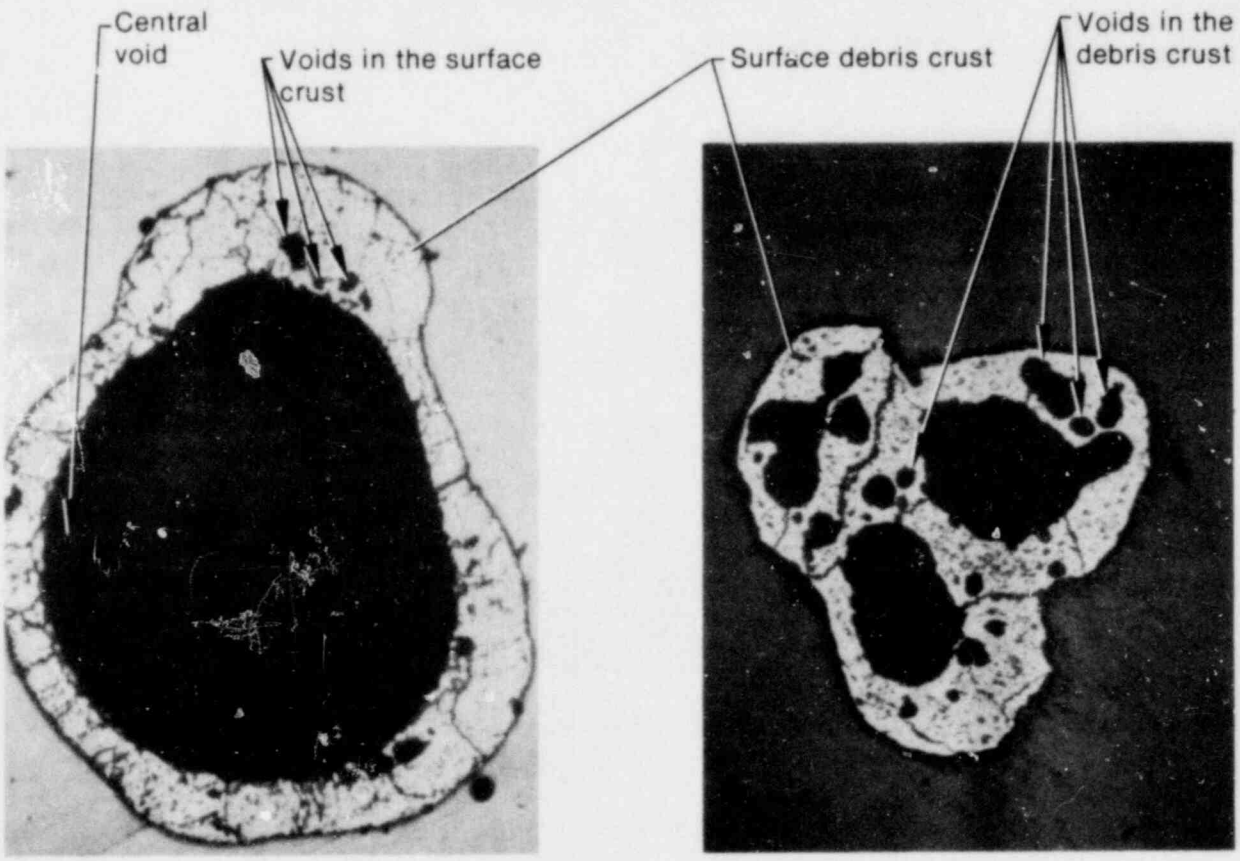

(b) Radial cross-sectional views of two debris particles

Figure 18. Debris particles from a power excursion test conducted at the Japan Atomic Energy Research Institute. (Photos courtesy of Shu Shiozawa, JAERI.)

$$V \simeq 13\,(\Delta P/\rho_j)^{1/2}\,. \qquad (14)$$

Equations (13) and (14) give values of about 86 and 1000 m/s for the penetration and the approach velocity of the jet, respectively. The measured depth of the holes shown in Figure 16(c) (a scanning electron photomicrograph taken at the surface of a debris particle) is in the range of 40 to 100 μm. Such penetration of the liquid jets into the surface crust could have occurred within 0.46 to 1.1 μs, which is a very short time in comparison with both the total travel time of the shock wave through the shroud ($\sim$420 μs) and the rise time of the recorded pressure pulses ($\sim$2000 μs).

As shown in Figures 16(c) and 19, a portion of the particle surfaces gave the appearance of swiss cheese. The holes in the crust are round, with sharp edges, and are slightly narrower at the bottom and wider at the surface. This conical appearance matches that of liquid jets observed experimentally by Bowden,[42] by Benjamin and Ellis,[43] and others in their cavitation studies. The observed jets had a conical shape, with a small diameter at the tip of the jet and a larger diameter at the base attached to the collapsing interface. In these experiments, high speed liquid jets, often formed during bubble collapse near walls, caused significant damage to solid surfaces. Evidence for fragmentation by coolant jets has also been obtained by Board et al.,[24] and Buchanan and Dulforce[25] in their out-of-pile dropout experiments. The possible role of such jets in producing surface disintegration and rapid energy transfer in metal-water thermal explosions has been discussed by Jakeman and Potter.[23]

It might be argued, however, that the holes shown in Figures 16(c) and 19 were caused by release of gas to the surface of the particles. In this case, the entrapped gas will tend to form spherical, or nearly spherical, bubbles due to surface tension forces. Then, the release of such gas from the surface of the particle upon quenching (which is a relatively slow process due to the compressibility of the gas) would have resulted in the formation of shallow, spherical depressions in the surface crust. This is at variance with the present experimental observations. Furthermore, the presence of gas in the molten debris is ruled out on the basis that the test rod was previously unirradiated and the irradiation time before rod failure was extremely short ($\sim$32 ms). Therefore, it may be concluded that the holes could not have been formed by the release of gas to the surface of the particles, but that they were induced by jets of coolant.

In summary, three mechanisms may have contributed to the fine fragmentation of the molten debris particles in the RIA-ST-4 experiment: (a) fragmentation due to the impact of the molten debris on the inner surface of the flow shroud wall and on the coolant, (b) rupture of the frozen crust at the surface of the particles due to pressure-induced stresses in the crust caused by overheating liquid coolant droplets entrained in the molten debris, and (c) penetration of the surface crust by coolant jets. Although the second mechanism could produce a massive number of relatively coarse fragments, the latter mechanism might produce relatively smaller quantities of fine debris particles because of the small dimensions of the jets (a few μm diameter). In addition, the penetration of coolant jet into the surface of the particles might effectively enhance the heat transfer at the surface of the particles. Board et al.,[24] have suggested that if coolant jets were to penetrate the molten material, rapid, fine-scale mixing would be inevitable and explosive energy transfer would necessarily follow. Other fragmentation mechanisms,[44-53] such as the acoustic cavitation[47] and the boundary layer stripping along the equator of the particles,[49-53] are not ruled out and require further investigation.

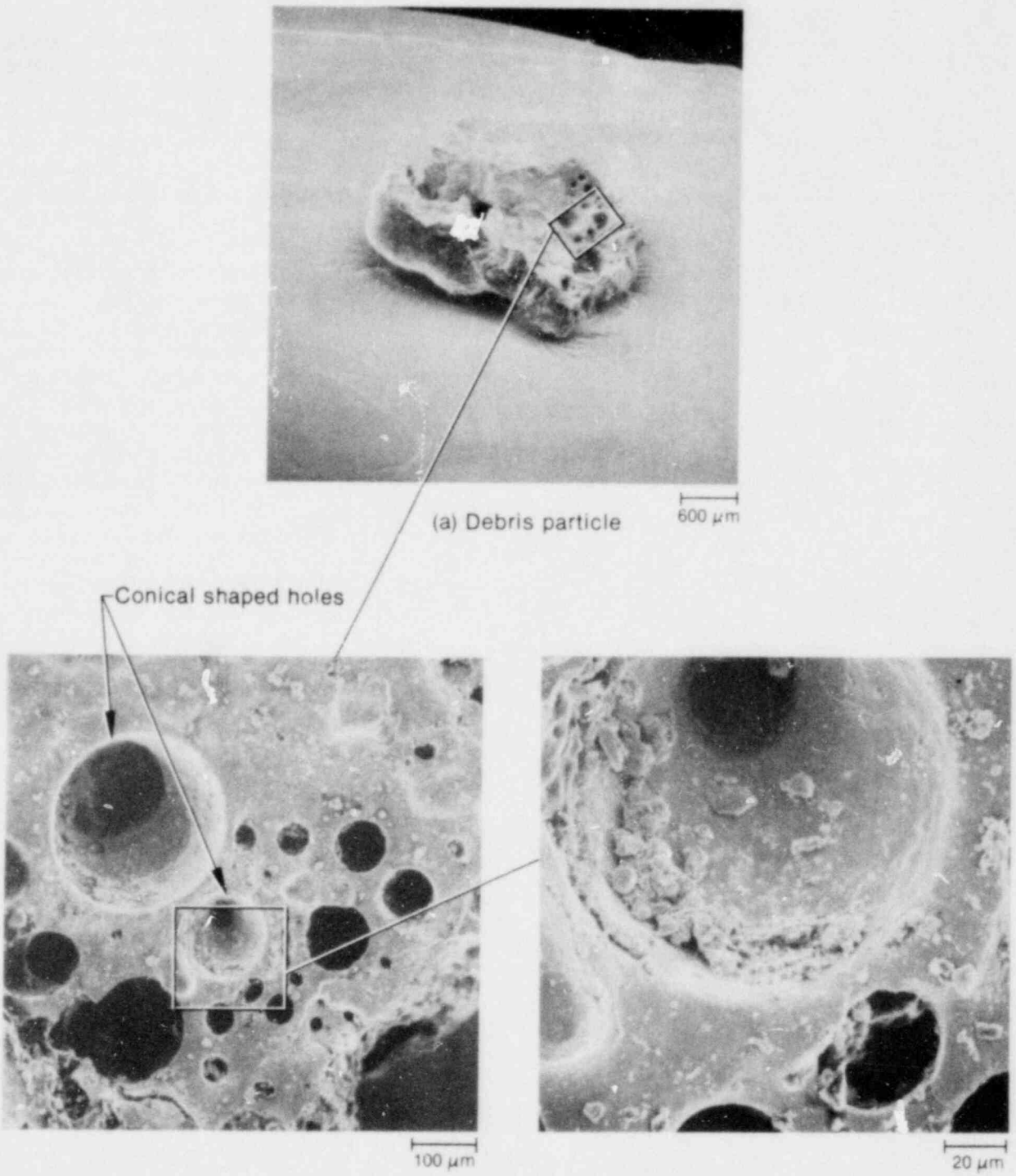

Figure 19. Scanning electron photomicrograph showing evidence of coolant jet penetration of the surface of a debris particle from the RIA-ST-4 experiment.

4. PHENOMENOLOGICAL ANALYSIS OF THE FRAGMENTATION OF MOLTEN DEBRIS

In this section, phenomenological models are presented for the fragmentation of molten debris due to (a) the rupture of the surface crust of the particles due to pressure-induced stresses caused by liquid coolant entrainment in the molten debris particles and (b) coolant jets striking the surface of the debris particles.

4.1 Fragmentation Due to Pressure-Induced Stresses

Should contact occur between molten core debris (primarily a mixture of UO_2 fuel and zircaloy cladding) and the coolant, the interface temperature might drop below the equilibrium freezing temperature (3100 K) and the homogeneous crystallization temperature[44] (2400 to 3100 K) of molten UO_2. Therefore, if a coolant droplet(s) is entrained in the molten debris, the induced pressurization inside the debris particles caused by overheating the droplet could rupture the crustal surface of the particle. Figures 14 and 15 present illustrative sketches of the fragmentation of debris particles by rupturing the surface crust. A schematic of the physical model is shown in Figure 20. A spherical droplet of liquid coolant, initially at temperature T_o, is assumed to be entrained at time zero (entrainment time) in a molten debris particle initially at a temperature T_b ($T_b >> T_o$).

In the present analysis, the following assumptions are considered:

1. The entrainment of liquid coolant in the molten debris occurs very rapidly, so that instantaneous evaporation of the coolant does not occur during the entrainment
2. The compressibility of the entrained liquid coolant and that of the molten debris are negligible (since the pressurization time is expected to be very small, a few nanoseconds)
3. The heat transfer from the molten debris to the entrained coolant droplet is governed by transient heat conduction
4. The entrained coolant droplet and the molten debris inside the particle are in intimate contact, and freezing of the debris is prohibited at the interface
5. Freezing at the surface of the molten debris particle begins immediately (time $t = 0$) following entrainment of the coolant droplets in the molten debris particle
6. The pressure acting on the inside of the surface crust is equal to that in the entrained coolant droplet.

The dimensions of the debris particle are very much larger than those of the liquid coolant droplet, so that the problem can be considered that of transient conduction to a liquid sphere surrounded by an infinite medium of another liquid.

The governing heat transfer equations in both the coolant droplet, $0 < r < R$, and the surrounding medium, $R < r < \infty$, are

$$\frac{\partial T_c}{\partial t} = \alpha_c \frac{1}{r^2} \frac{\partial}{\partial r}\left[r^2 \frac{\partial T_c}{\partial r}(r,t)\right] \tag{15}$$

and

$$\frac{\partial T_m}{dt} = \alpha_m \frac{1}{r^2} \frac{\partial}{\partial r}\left[r^2 \frac{\partial T_m}{\partial r}(r,t)\right] \tag{16}$$

respectively, where subscript c pertains to the coolant droplet and m to the molten debris. The boundary conditions are

$$\frac{\partial T_c}{\partial r}(0,t) = 0$$

$$T_c(R,t) = T_m(R,t)$$

$$T_m(\infty,t) = T_b$$

$$k_c \frac{\partial T_c}{\partial r}(R,t) = k_m \frac{\partial T_m}{\partial r}(R,t) \tag{17}$$

and the initial conditions are

$$T_c(r,0) = T_o$$

$$T_m(r,0) = T_b. \tag{18}$$

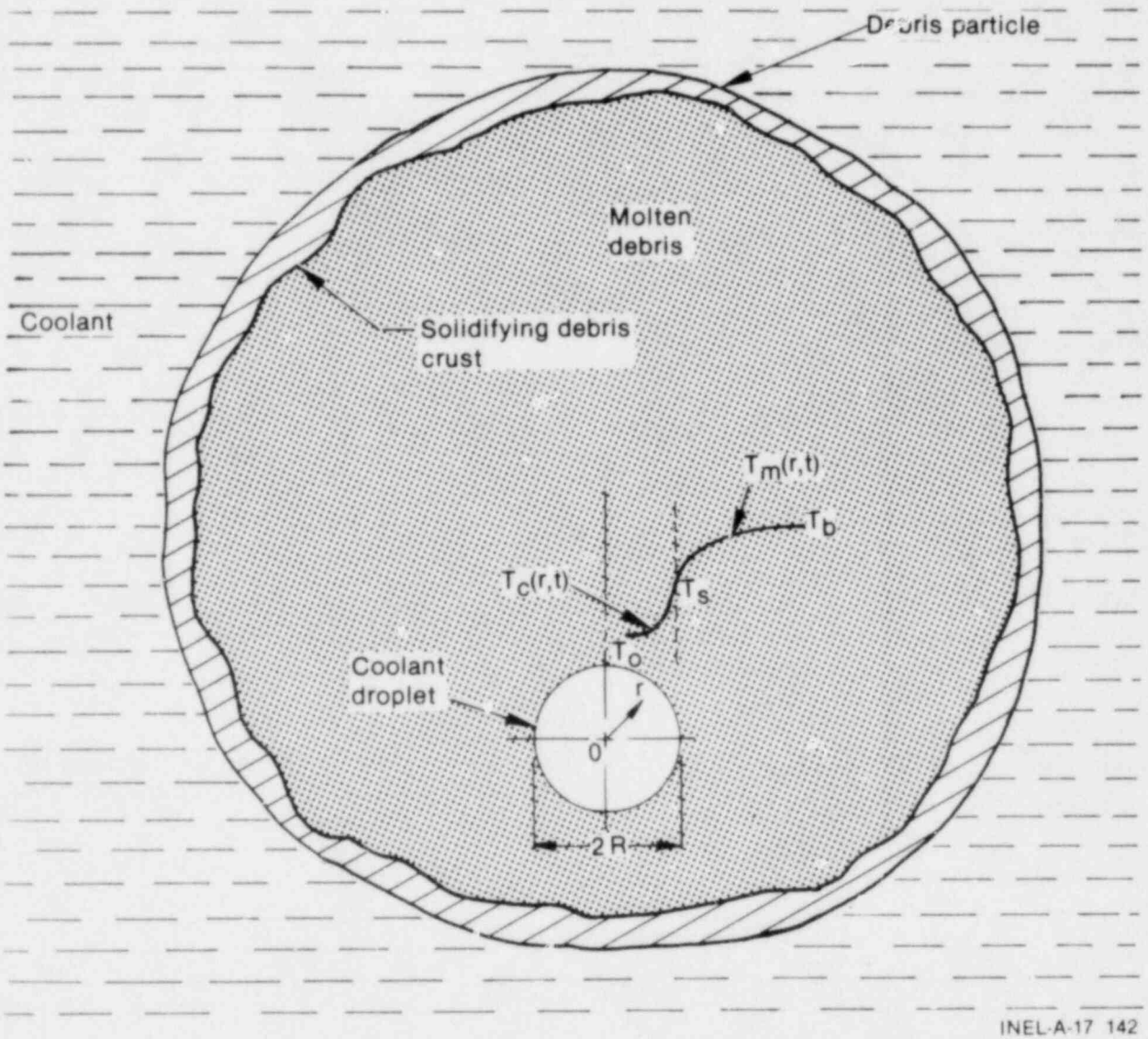

Figure 20. Physical model for fragmentation by pressurization due to overheating a liquid coolant droplet entrained in molten debris.

The solution to this problem has been introduced by F. Cooper[54] using Laplace transformation. For a time less than that required for the thermal boundary layer in the spherical coolant droplet to reach the center of the droplet, r = 0 (that is; $t << \tau_c$, the thermal diffusion time constants, where $\tau_c = R^2/\alpha_c$), the transient heat flux at the surface of the coolant droplet, r = R, is found to be as shown in Equation (19) at the bottom of the page.

Equation (19) can be used to calculate the overall heating rate of the entrained coolant droplet

$$\frac{dQ}{dt}(t) = 4\pi R^2 \, q\,(R,t) \, . \tag{20}$$

The equation of state of the liquid coolant can be written as

$$dv = -\beta_T \, v \, dP + \alpha_p \, v \, dT \tag{21}$$

where

v = specific volume of coolant

P = coolant pressure

T = coolant temperature.

Assuming a constant volume pressurization of the coolant droplet, Equation (21) reduces to

$$\frac{dT}{dt} = (\beta_T/\alpha_p)\frac{dP}{dt} \tag{22}$$

where β_T is the isothermal compressibility and α_p is the thermal expansion coefficient of the coolant. The change in the pressure of the heated coolant droplet, P, can be related to the changes of enthalpy, h, and the overall heating of the droplet, per unit mass, Q*, through the use of the first law of thermodynamics

$$\frac{dh}{dt} = \frac{dQ^*}{dt} + v\frac{dP}{dt} \, . \tag{23}$$

Equation (23) and the thermodynamic relation

$$dh = Cp \, dT + v\,(1 - T\,\alpha_p)\, dP \tag{24}$$

gives

$$Cp\frac{dT}{dt} = \frac{dQ^*}{dt} + T\,v\,\alpha_p\frac{dP}{dt} \tag{25}$$

where Cp is the specific heat of the coolant at constant pressure. Eliminating the left side of Equations (22) and (25), the following first-order differential equation of the transient pressure rise in the entrained coolant droplet is obtained:

$$\frac{dP}{dt} = \frac{-\alpha_p}{(M\,C_p\,\beta_T - T\,V_t\,\alpha^2_p)}\frac{dQ}{dt} \tag{26}$$

where V_t and M are the total volume and the total mass of the entrained liquid droplet. The minus sign in the right side of Equation (26) is introduced to account for the flow of energy from the debris to the coolant droplet, which is in the negative direction of the polar coordinate, r.

The first-order, differential Equations (20), (22), and (26) are solved simultaneously to calculate the instantaneous values of the pressure, P(t), and the temperature, T(t), in the entrained liquid coolant droplet, and the thermal energy, Q(t), transferred to the droplet from the surrounding molten debris. The time at which the pressure of the entrained coolant droplet reaches

$$q(R,t) = \frac{k_c\,k_m\,(T_m - T_c)}{R\,\Sigma}\left\{\sqrt{\tau_c} - \frac{k_m\,(\sqrt{\tau_c} + \sqrt{\tau_m})}{\beta\,\Sigma}\left[1 - e^{\beta^2 t}\,\mathrm{erfc}\,(\beta\sqrt{t})\right]\right\}$$

$$+ \frac{k_c\,k_m\,(T_m - T_c)}{\Sigma}\left\{\sqrt{\frac{\tau_c}{\pi\alpha_m t}} - \frac{k_m\,(\sqrt{\tau_c} + \sqrt{\tau_m})}{\beta\,\Sigma}\left[\frac{\beta}{\sqrt{\alpha_m}}\,e^{\beta^2 t}\,\mathrm{erfc}\,(\beta\sqrt{\tau})\right]\right\} \tag{19}$$

where $\tau_m = (R^2/\alpha_m)$, $\beta = (k_m - k_c)/\Sigma$, $\Sigma = (k_c\,\tau_c + k_m\,\tau_m)$, R is the radius of the coolant droplet, and k and α are the thermal conductivity and the thermal diffusivity, respectively.

the ultimate tensile strength of the solid debris (for solid UO_2 at 2600 K, a value of 45 MPa was recommended)[39,40] is considered to be the rupture time of the solidified crust at the surface of the molten debris particle.

Figure 21 presents a plot of the dimensionless pressure in the entrained coolant droplet (the pressure in the droplet divided by the initial coolant pressure) versus time. At the time t = 0 (initial time of entrainment), the initial coolant pressure was 8.5 MPa (see Figure 4) and the coolant temperature is taken to be equal to the saturation temperature (572 K). As shown in Figure 21, the size of the entrained coolant droplet strongly influences the transient pressurization inside the molten debris particles. With smaller droplet diameter, D_p, the pressure induced in the droplet increases faster with time. Also, increasing the intial temperature of the molten debris, T_b, increases the energy transfer, Q(t), to the entrained liquid, and thus induces faster pressurization inside the debris particle.

The rupture (or breakup) time of the crustal surface is plotted in Figure 22 in terms of the diameter of the entrained coolant droplet, D_p, and the initial temperature of the molten debris, T_b. In general, the rupture time (that is, the incipient fragmentation time of the debris particles) is in the order of a few nanoseconds, which is very much shorter than the fracture time calculated using shell theory.[44,55-60] Figure 22 shows that increasing the droplet diameter significantly increases the rupture time of the crust. For example, increasing the droplet diameter from 10 to 100 μm results in an almost fifteenfold increase of the time at which rupture of the solid shell occurs. Also, increasing the initial temperature of the molten debris slightly reduces the rupture time, as shown in Figure 22. These results are expected due to the fact that the rise rate of the pressure in the coolant droplet [Equation (26)] is inversely proportional to the volume of the droplet, V_t (that is, the diameter of the droplet raised to the third power), and it is directly proportional to the heat transfer rate from the debris to the coolant droplet [that is, the initial temperature of the debris; see Equations (19) and (20)].

The previous analysis suggests that the fragmentation of debris particles during an MFCI due to pressure-induced stresses caused by overheating

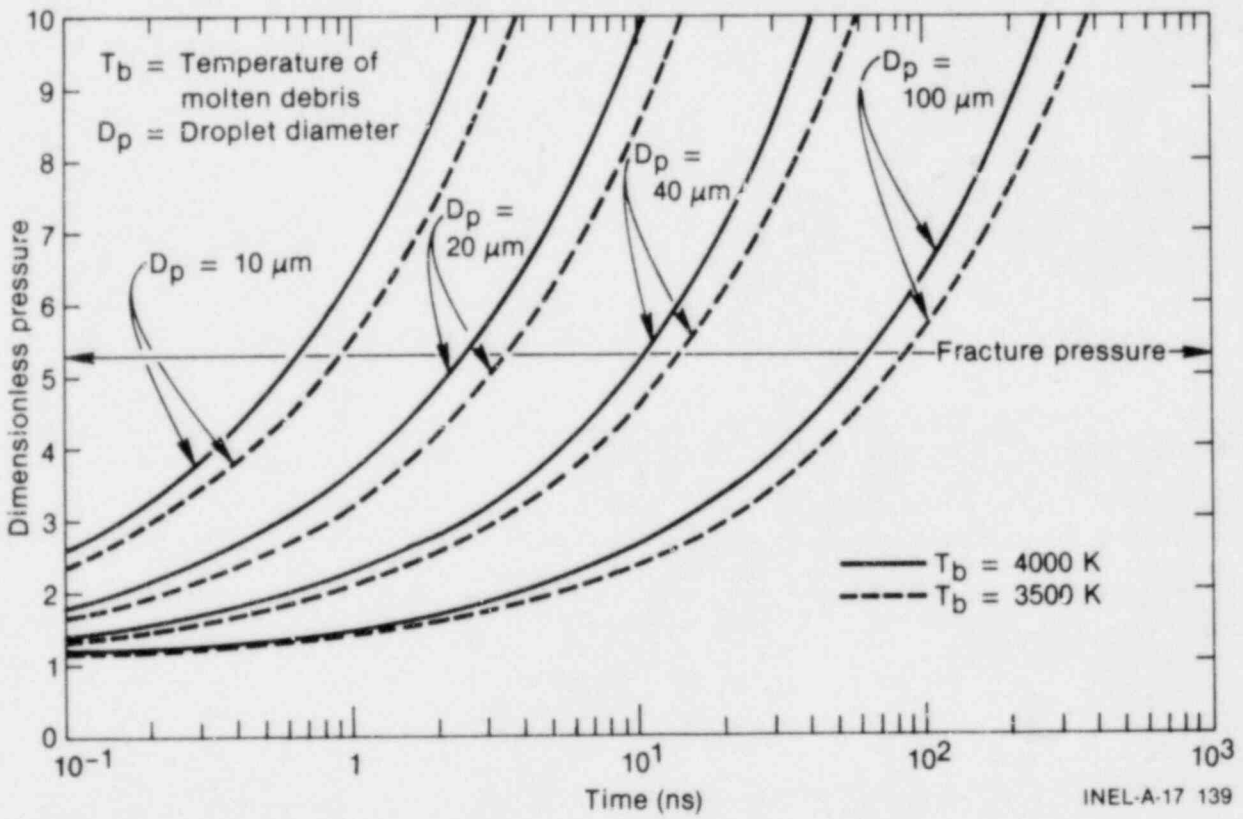

Figure 21. Effects of collapse pressure differential and diameter of liquid coolant droplet on the rupture time of the surface crust.

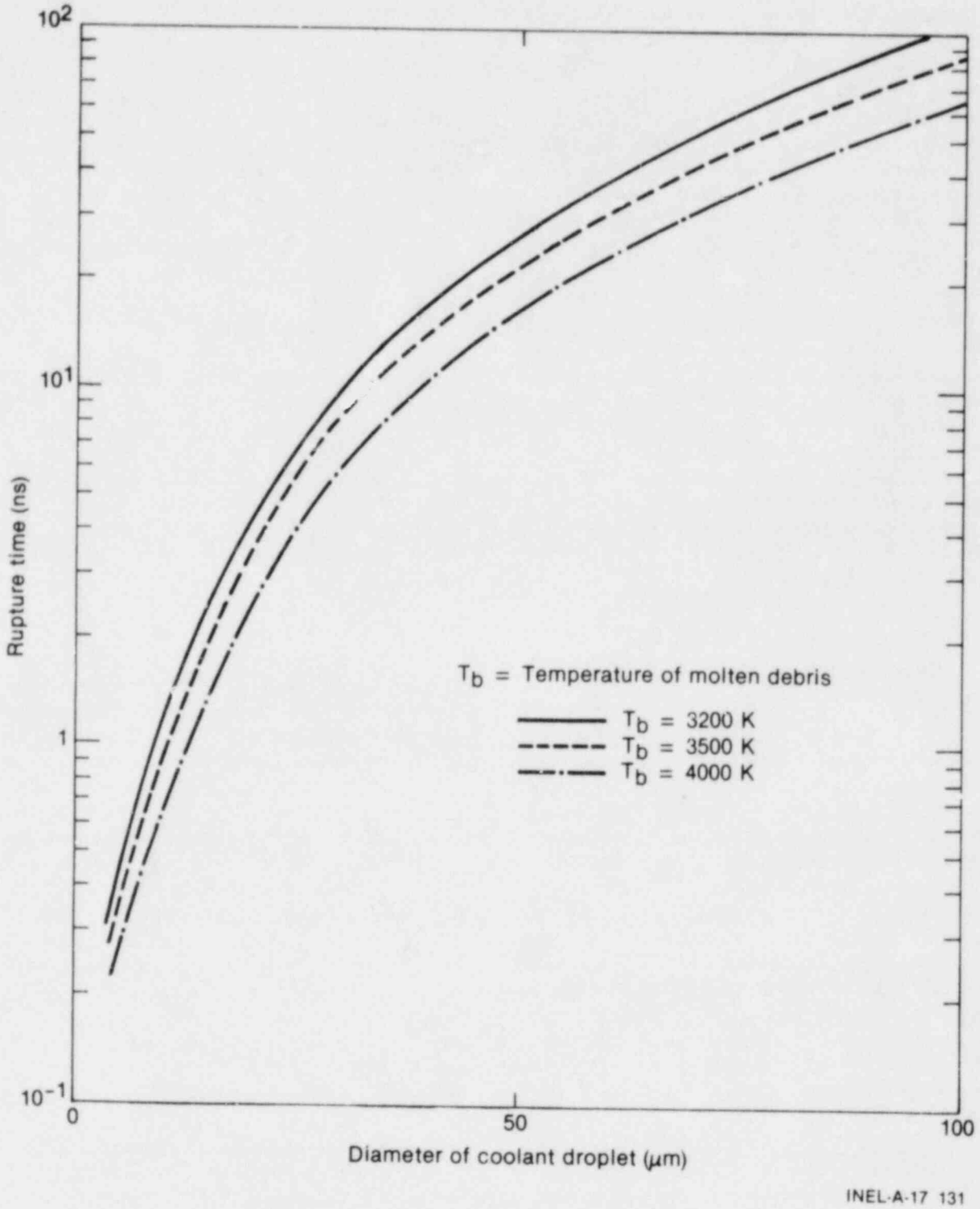

Figure 22. Rupture time as a function of molten debris temperature and diameter of the liquid coolant droplet.

entrained liquid droplets is a possible mechanism. This is assuming that the entrainment of the liquid coolant droplets occurs very fast, so that instantaneous flash evaporation of the droplets would not occur. Yet, the validity of this assumption needs further investigation. Calculations show that rupture of the solid shell at the surface of the debris particles occurs within a very short time, less than one thousandth of the breakup time predicted by the shell theory. The scanning electron microscope analysis of the particles in the RIA-ST-4 experiment (see Section 3) has indicated that rupture of the surface crust was dominant for both larger (~3.2-mm diameter) and smaller (10- to 40-μm diameter) particles. This suggests that the breakup of larger particles might have resulted in the entrainment of liquid coolant in the smaller particles produced in the breakup of the larger ones and, in turn, their fragmentation. Thus, a fragmentation "chain reaction" could have occurred. Theoretically, more than one million successive fragmentations could have occurred during the recorded rise time (~2 ms) of the coolant peak pressure (35 MPa) in the RIA-ST-4 experiment.

4.2 Fragmentation Due to Coolant Jets

S. G. Bankoff[61] has stated, "It appears that destabilization of film boiling proceeds in three stages: thinning of the vapor film, partial contact by tongues of liquid and spreading of the contact regions." In general, the rapid, asymmetric collapse of void-like regions of film boiling on the surface of the debris particles might cause the development of coolant jets at the liquid-vapor interface.[24,25,38,42] F. B. Bowden,[42] on the basis of his experimental observations, has indicated that "If a small cavity or bubble in a liquid is subject to impact or to shock, tiny Monroe jets may be formed on its concave surface." The velocity of the jet depends on the curvature of the liquid surface as well as the driving pressure.

The violent character of vapor cavities in a liquid, inasmuch as they can give rise to extremely high hydrodynamic pressures when they collapse, is very well known[43] from cavitation studies. Liquid jets formed by involution of collapsing bubbles near a wall were capable of causing significant damage to the solid surface.[62] Rattray[63] performed a perturbation study suggesting that the effect of a solid wall in disturbing the flow during the collapse of an initially spherical bubble could cause the formation of a liquid jet directed toward the wall. This theory was later confirmed experimentally[42,43] and theoretically.[38] Benjamin and Ellis[43] observed cavitation induced by the asymmetric collapse of vapor bubbles by means of high speed cinema photography. The bubbles were nearly spherical as they started to collapse, then they became elongated in the direction normal to the wall and, finally, they tended to flatten and form an inward moving jet on the side of the bubbles opposite the wall. Plesset and Chapman[38] have developed a numerical simulation for the collapse of an initially spherical vapor bubble near a solid wall. They have shown that the solid wall influences the bubble early in the collapse by reducing the upward motion of the lower portion of the bubble. This causes the bubble to elongate in the direction normal to the wall, which agrees with Rattray's suggestion. As the bubble acquires kinetic energy, the energy concentrates in the upper portion, which eventually flattens and forms a jet. Once the jet is formed, the speed of its tip remains fairly constant.

The diameter of the hole produced in a solid target by a liquid jet is considerably greater than, and is not directly related to, the diameter of the jet.[41] It is more closely related to the energy delivered by the jet per unit depth of penetration. For a steady, continuous jet, the penetrating velocity of the jet into a target is less than the approaching velocity of the jet, and the product of the velocity times the cross-sectional area must be the same at all points (principle of conservation of mass). This gradient in velocity along the jet length causes the cross-sectional area of the jet to increase as it penetrates the target material.[41] It has been found experimentally that the hole diameters in hard materials (e.g. steel) are smaller than in soft ones (e.g. lead), since more work has to be done to open a hole in the harder materials.

As illustrated in Figure 23, coolant jets may form during the collapse of a void-like region of film boiling, driven by a shock wave onto the surface of the molten particles. The induced liquid-liquid contact quenches the surface of the particles very rapidly and may initiate instantaneous freezing of the surface if the interface temperature is below the freezing temperature of the debris. If

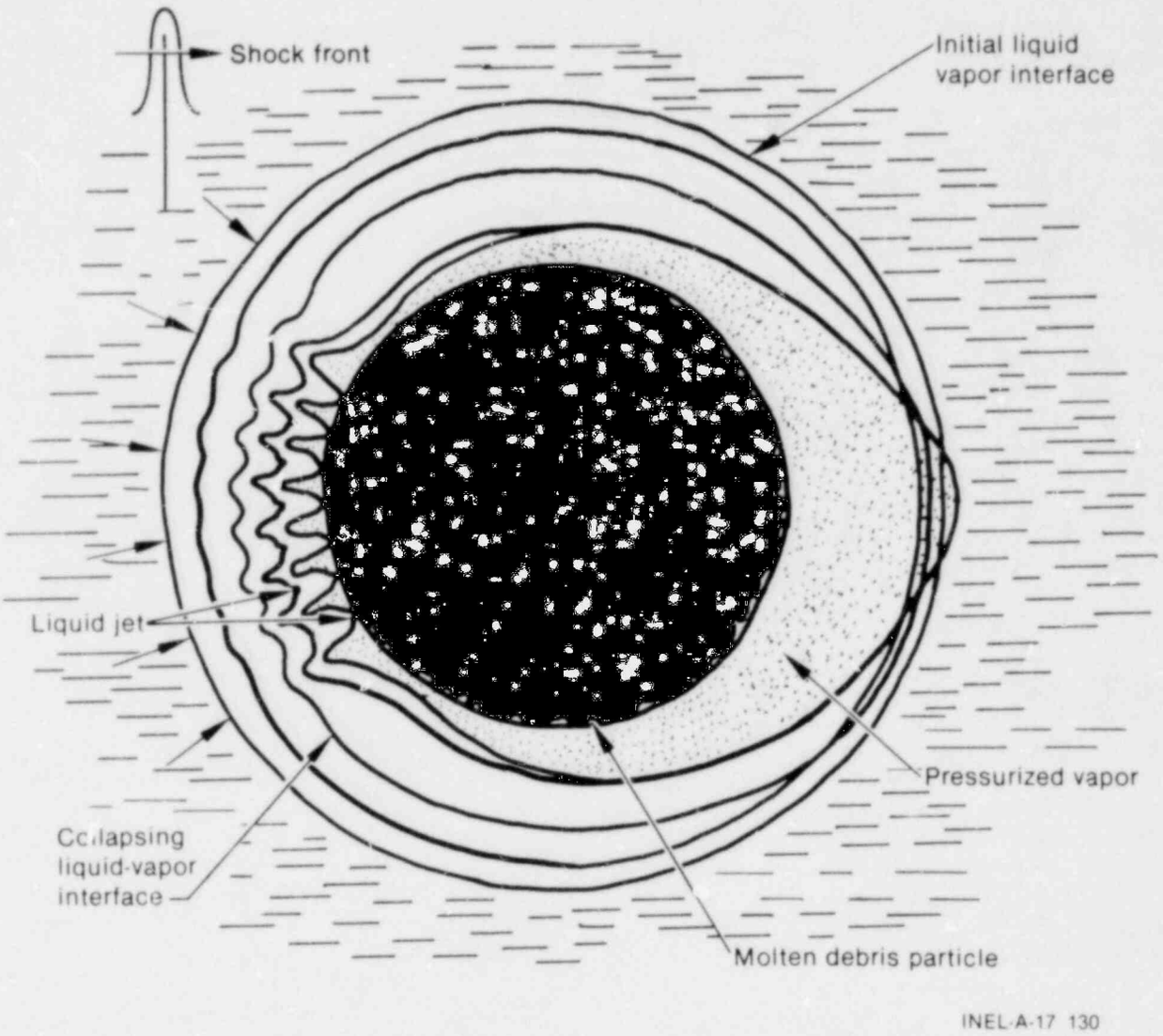

Figure 23. Illustration of coolant jet development during the collapse of a vapor film on the surface of a molten debris particle.

surface freezing occurs, it proceeds at a rate greater than the striking velocity of the coolant jets. Depending on the penetration velocity of the jets, partial penetration or perforation of the surface crust may occur (see Figure 24), causing fine, but not massive fragmentation of the surface. The penetration of coolant jets into the surface crust of the debris particles is much like that of a high speed jet of water from a fine hose nozzle penetrating a bank of soft mud. Target material is splashed out at high velocities, radially from the point of impact, in a finely fragmented form. The fragmentation of the debris particles by coolant jets is analyzed subsequently.

The resistance of a solid target to penetration by a liquid jet depends on the striking velocity of the jet, the strength of the jet and of the target, and the geometry of the target. In general, liquid jets can be classified as high velocity and low velocity jets, and for each the penetration characteristics are different. When the pressure exerted on the target by a liquid jet is very much greater than the yield stress, σ_s, of the target material, the jet is designated a high velocity jet

$$1/2\ \rho_j\ V^2 >> \sigma_s \qquad (27)$$

where ρ_j and V are the density and the approach velocity of the jet, respectively. In this case, the target inertia controls the depth of penetration. For a low velocity jet, however, it is the elastic properties of the target material that determine whether or not jet penetration takes place.

The theory of penetrating a solid target by high speed jets has been developed[41] based on the steady state classical hydrodynamics of perfect fluids, which is applicable because the strength of the target materials can be neglected at the high striking pressure encountered. The basic equation is a form of Bernoulli's equation

$$\gamma\ \rho_j\ (V - U)^2 = \rho_s\ U^2 \qquad (28)$$

where U is the time rate of change of the depth of penetration into the target (jet penetrating velocity) and ρ_s is the density of the target material; γ is called the "breakup" factor and depends on the form of the jet (that is, a continuous or a broken jet) and the distance between the point at which the jet is originated and the surface of the target (that is, the thickness of vapor film surrounding the debris particles). For a continous jet, a value of unity is recommended.[62,64] For broken jets, a value other than unity should be considered. For the purpose of the current application (that is, molten fuel fragmentation), γ is taken to be unity, since the jets that may develop during the local collapse of a void-like region of film boiling are expected to be short and continuous. Solving Equation (28) for U gives

$$U = \frac{V}{1 + (\rho_s/\rho_j)^{1/2}}.$$

Plesset and Chapman have found that the jet velocity, V, scales as

$$V \simeq 13\ (\Delta P/\rho_j)^{1/2}$$

where ΔP is the pressure differential causing the collapse of the vapor film, and the jet dimensions (length, ℓ, and radius, r) scale as the initial radius of the collapsing vapor bubble. The previous two equations are the same as Equations (13) and (14), respectively, in Section 3. For the collapse of a vapor film on the surface of a molten fuel particle, it seems reasonable to assume that the jet dimen sions would vary with the initial thickness of the vapor film, ξ. The thicker the vapor film, the greater would be the coolant jet dimensions, that is,

$$\ell = C_1\ \xi$$

$$r = C_2\ \xi \qquad (29)$$

where C_1 and C_2 are constants that can be found (to a first approximation) from Plesset and Chapman's[38] results as $C_1 = 0.4929$ and $C_2 = 0.1186$.

Through use of Equation (14), Equation (27) becomes

$$\Delta P >> 0.0118\ \sigma_s \qquad (30)$$

which indicates that for a high velocity jet to develop during the collapse of a vapor film that surrounds a molten UO_2 particle, ΔP must be much greater than ~0.5 MPa (ultimate tensile stress of solid UO_2 at 2600 K is 45 MPa).[39,40] The integration of Equation (13) with respect to time leads to the following expression for the depth of penetration[41]

$$d = \ell \left(\frac{\rho_j}{\rho_s}\right)^{1/2}. \qquad (31)$$

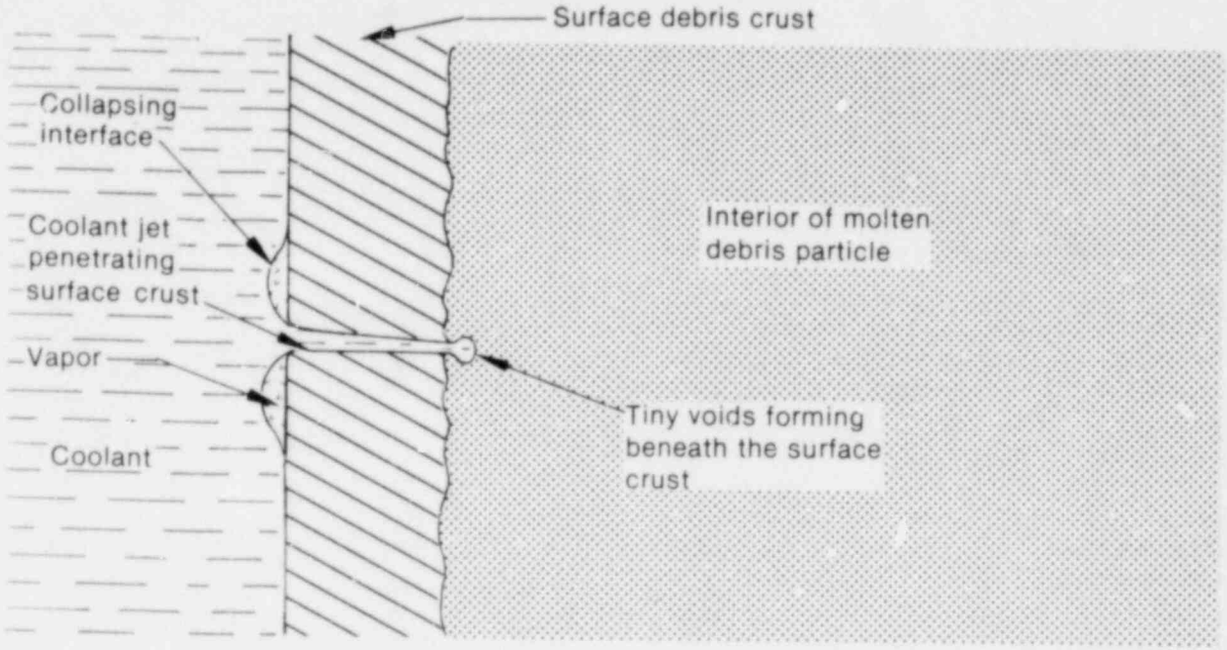

(a) Coolant jet perforating the surface crust

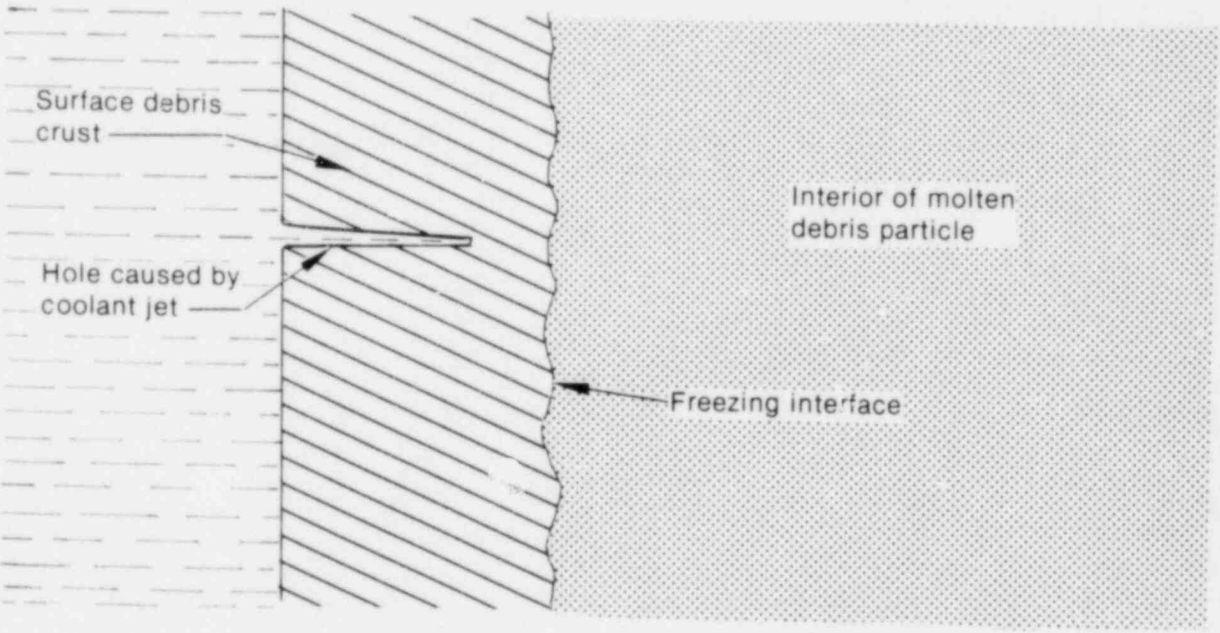

(b) Partial coolant jet penetration of the surface crust

INEL-A-17 149

Figure 24. Illustration of a coolant jet perforating and penetrating the solid crust at the surface of a molten debris particle.

Equation (31) shows that the depth of penetration, d, is independent of the velocity of the jets; it is proportional to the square root of the jet density and inversely proportional to the square root of the target density. From Equations (13) and (31) the penetration time of the jet is

$$t_j = \left(\frac{d}{U}\right) = \frac{\ell}{V}[1 + (\rho_j/\rho_s)^{1/2}]. \qquad (32)$$

Following the collapse of the vapor film onto the surface of a molten particle, two processes might be initiated simultaneously: freezing of the surface of the particle and penetration of the surface crust by coolant jets. Should the interface temperature drop below the fusion temperature of the fuel, freezing of the crust would commence and proceed at a very high rate, and it is the solid properties that would govern the penetration process of the jets. Figure 25 illustrates coolant jets penetrating a solid surface following the collapse of a vapor film. If the jet starts penetrating the surface crust at time zero, then the thickness of the surface crust, $\delta(t)$, and the velocity of freezing, $d\delta/dt$, are[65]

$$\delta(t) = 2\lambda\sqrt{\alpha_s t}$$

and

$$\frac{d\delta}{dt} = \lambda\sqrt{\frac{\alpha_s}{t}} \qquad (33)$$

where α_s is the thermal diffusivity of the frozen crust and λ is the freezing coefficient of molten debris. As illustrated in Figure 26, the freezing process is considered as a one-dimensional freezing problem in infinite geometry since the jet and surface crust dimensions are very much smaller than the radius of the molten debris particle.

The energy equation in the molten debris region ($\delta \le r \le \infty$) is

$$\frac{\partial T_m}{\partial t} + u_m\frac{\partial T_m}{\partial r} = \alpha_m\frac{\partial^2 T_m}{\partial r^2} \qquad (34)$$

where u_m is a velocity component that develops in the molten debris region at the change-of-phase front ($r = \delta(t)$) due to the change of debris density upon freezing. If the density change is negligible (that is, $u_m = 0$), Equation (34) reduces to the classical, one-dimensional transient heat conduction equation. The velocity component in Equation (34) is given as

$$u_m = -\epsilon\frac{d\delta}{dt}. \qquad (35)$$

In the frozen crust [$0 \le r < \delta(t)$] and in the coolant ($-\infty \le r \le 0$), assuming no coolant evaporation occurs at the interface, $x = 0$, the transient temperature field can be described by Fourier's equation

$$\frac{\partial T}{\partial r} = \alpha\frac{\partial^2 T}{\partial r^2}. \qquad (36)$$

The exact solution of Equations (34) through (36) is readily available[65] through the use of Equation (33), the temperature continuity boundary conditions

$$T_m(\infty,t) = T_b$$

$$T_s(0,t) = T_c(0,t)$$

$$T_m[\delta(t),t] = T_f$$

and

$$T_c(-\infty, t) = T_o \qquad (37)$$

and the heat flux continuity boundary conditions

$$k_m\frac{\partial T_m}{\partial r}(\delta,t) = k_s\frac{\partial T_s}{\partial r}(\delta,t) + \rho_s L_s\frac{d\delta}{dt} \qquad (38a)$$

and

$$k_s\frac{\partial T_s}{\partial r}(0,t) = k_c\frac{\partial T_c}{\partial r}(0,t). \qquad (38b)$$

The application of the heat flux continuity boundary condition at the change-of-phase front (Equation 38a) gives the following transcendental equation to evaluate the freezing coefficient, λ, as shown in Equations (39) and (40).

$$\frac{\sigma}{\text{EXP}\,(\lambda^2) + \sigma\,\text{EXP}\,(\lambda^2)\,\text{erf}\,(\lambda)} \cdot \frac{\sigma_m \left(\frac{T_b - T_f}{T_f - T_o}\right)}{\text{erfc}\,[\lambda\beta\,(1+\epsilon)]\,\text{EXP}[\lambda^2\beta^2\,(1+\epsilon)^2]} = \frac{\lambda\sqrt{\pi}}{\text{St}} \tag{39}$$

where

T_b	=	molten debris initial temperature	σ	=	coolant-crust thermal ratio
T_f	=	freezing temperature of the debris	σ_m	=	molten debris-crust thermal ratio
T_o	=	initial coolant temperature	St	=	Stefan number for freezing.

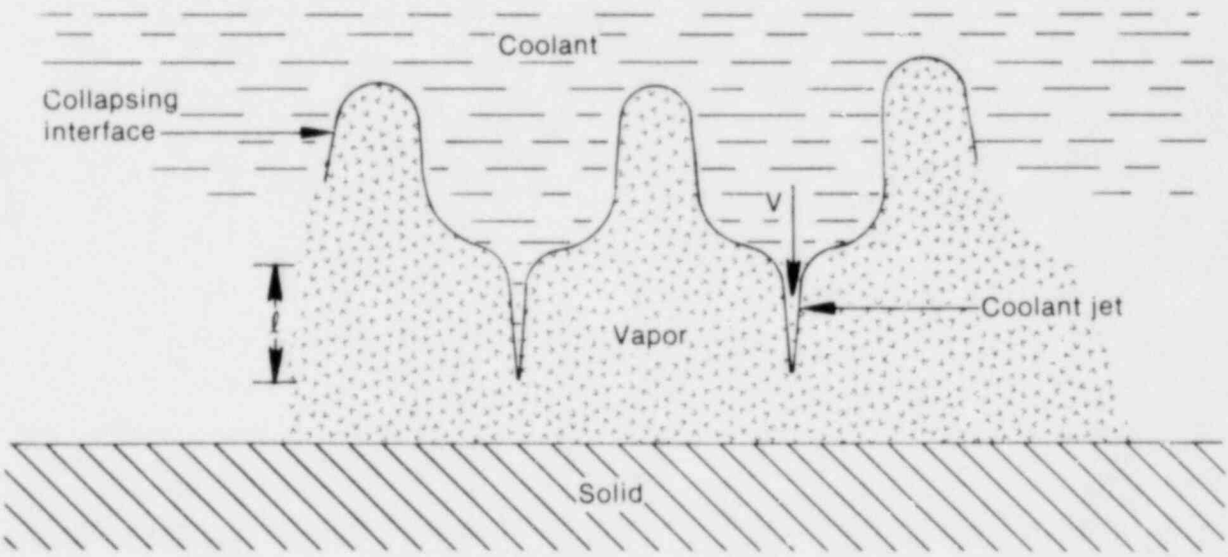

(a) Coolant jets formation

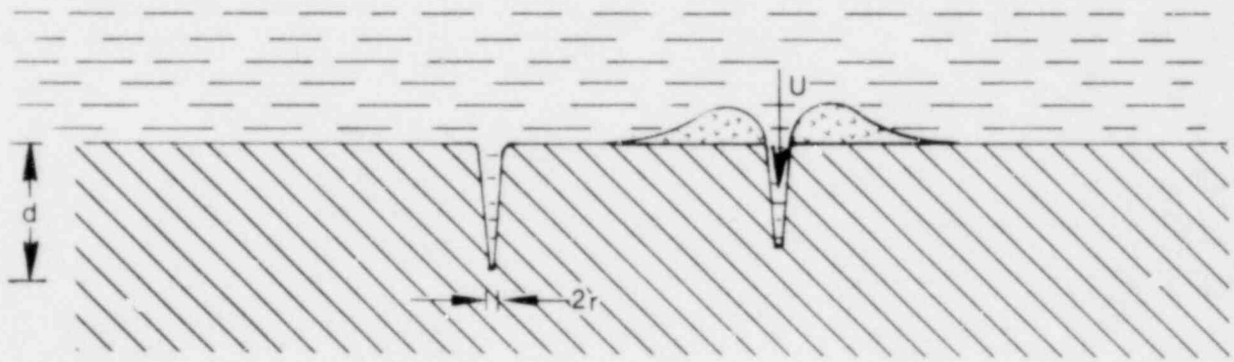

(b) Coolant jets penetrating solid surface

INEL-A-17 148

Figure 25. Illustration of the characteristics of coolant jets penetrating a solid target.

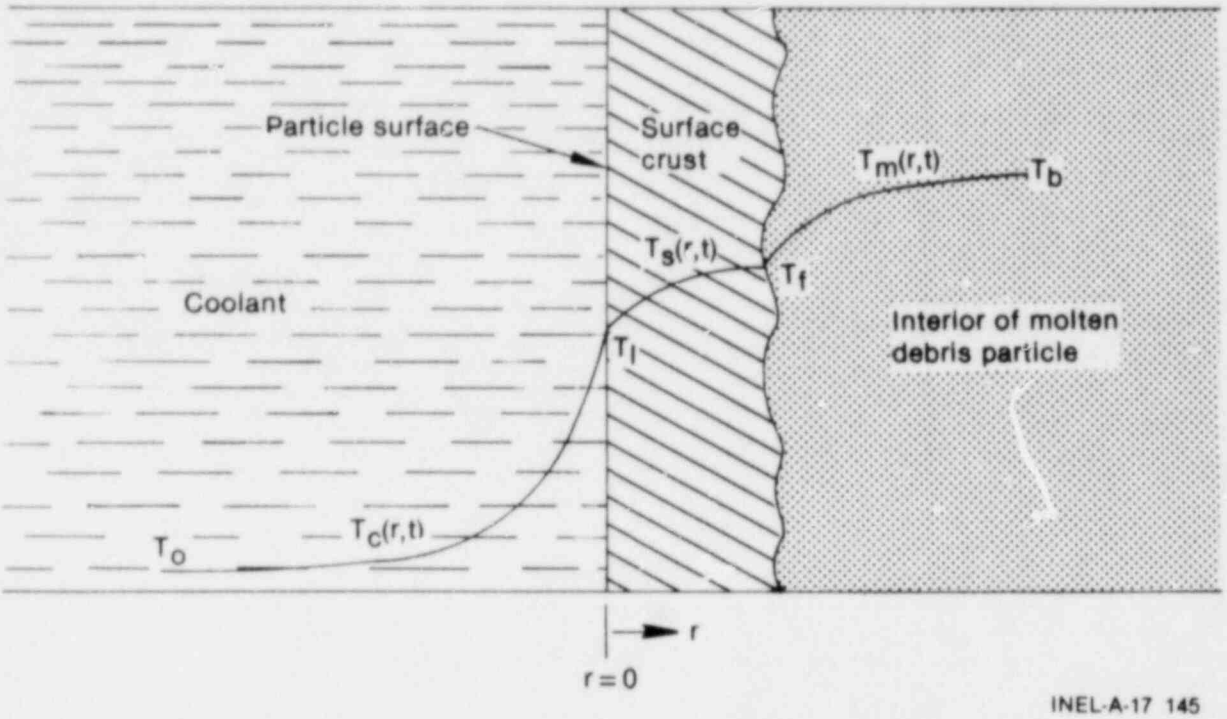

Figure 26. Physical model for the freezing of the surface of a debris particle.

$$\sigma = \left(\frac{k_c C_c \rho_c}{k_s C_s \rho_s}\right)^{1/2}, \sigma_m = \left(\frac{k_m C_m \rho_m}{K_s C_s \rho_s}\right)^{1/2},$$

$$St = \frac{C_s (T_f - T_c)}{L_s}. \quad (40)$$

The coefficients β and ϵ are

$$\beta = (\alpha_s/\alpha_m)^{1/2}$$

and

$$\epsilon = [(\rho_s/\rho_m) - 1]. \quad (41)$$

In Equations (40) and (41)

α = thermal diffusivity

k = thermal conductivity

C = specific heat

ρ = density

c = coolant

m = molten debris

s = frozen crust

L_s = latent heat of fusion of molten debris.

Equations (13) and (33) may be compared to determine whether the jet would partially penetrate or perforate the surface crust. As demonstrated in Figure 27, only partial penetration of the crust would occur if

$$\delta(t_j) > d \quad (42)$$

where t_j is the time for the coolant jet to reach its maximum penetration [Equation (32)]. Otherwise, the jet ultimately perforates the crust, where the perforation time, t_p, is given by

$$t_p = \frac{4 \lambda^2 \alpha_s}{U^2}$$

where $(t_p < t_j)$. (43)

To evaluate the freezing velocity of the surface crust, the thermophysical properties of the debris (primarily a mixture of UO_2 and zircaloy cladding) must be assessed. For simplicity, it is

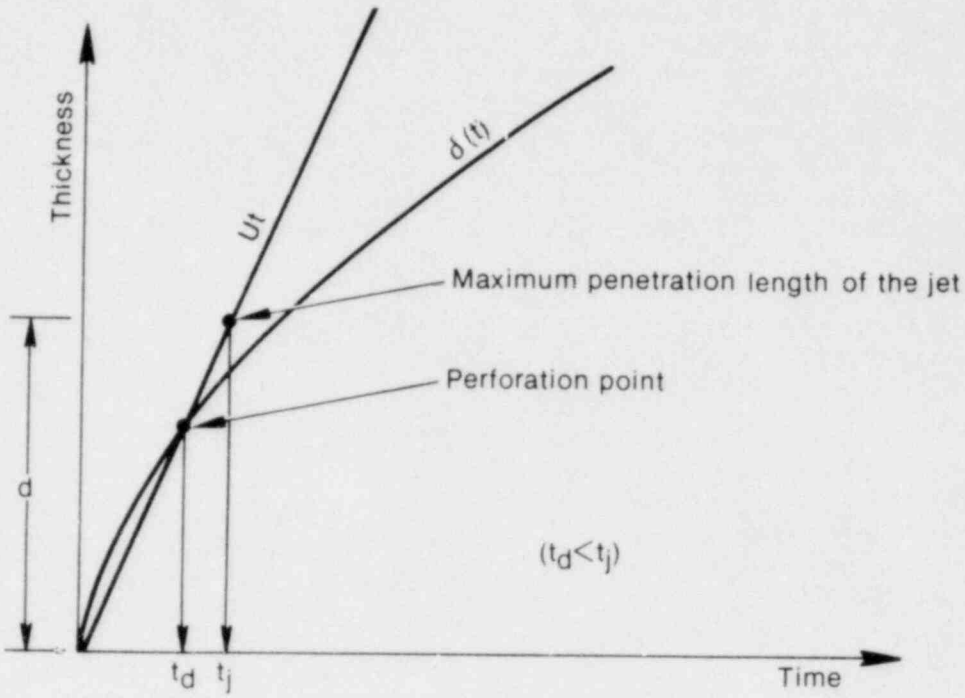

(a) Coolant jet perforation of surface crust

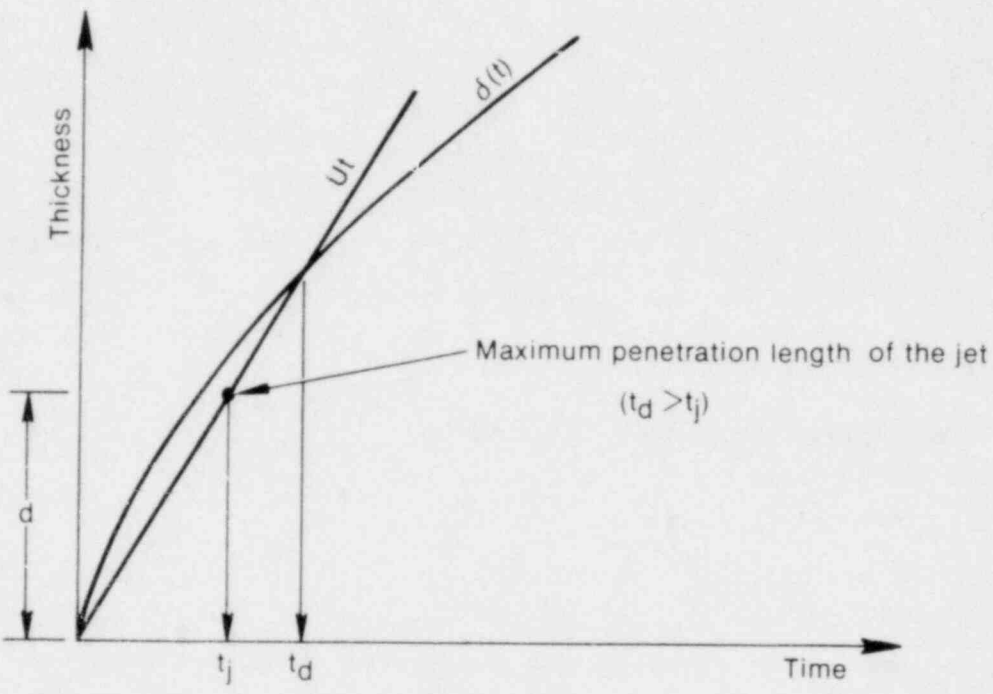

(b) Coolant jet penetration of surface crust

INEL-A-17 134

Figure 27. Conditions for perforating and penetrating the surface crust by a coolant jet.

assumed that the debris freezes as a homogeneous mixture of UO_2 and zircaloy and the properties can be estimated in terms of those of the constituents. The weight fraction of zircaloy in the debris is taken to be 22%, which is equal to that in the RIA-ST-4 experiment test fuel rod. The validity of these assumptions was examined in Reference 14 and was found to be reasonable. The examination of the debris indicated that the UO_2 and zircaloy were randomly mixed, with weight ratios that vary both below and above those used in the present investigation (22 wt% zircaloy and 78 wt% UO_2).

The thermophysical properties of the debris, calculated as detailed in Reference 14, are listed in Table 3 along with those of the coolant. In the calculations, the properties of the coolant and those of the molten and solid debris are taken to be constant but different.

The conditions for the reference case are

Initial temperature of the coolant, T_o	538 K
Initial temperature of the molten debris, T_b	2800 K
Freezing temperature of the debris, T_f	2640 K
Collapsing pressure difference, ΔP	5 and 10 MPa.

Equations (31), (33), and (39) are solved simultaneously to calculate the penetration length of the jet into the crust, d, and the instantaneous thickness of the surface crusts, $\delta(t)$. The results are plotted versus time in Figure 28. Zero time corresponds to the time at which intimate contact occurred between the coolant and the molten debris upon collapse of the vapor film. Two collapsing pressure differences, ΔP, of 5 and 10 MPa are considered. As shown in the figure, perforation of the surface crust by coolant jets is inevitable, even with coolant jets having a length as short as 150 nm (~0.15 μm). The perforation of the crust depends on the density of the crust, freezing characteristics of the debris, and the collapsing pressure difference. Increasing the ΔP induces perforation of the crust sooner and decreases the crust thickness at the point of perforation. The perforation time of the surface crust is about 0.0066 and 0.0135 ns, for ΔP equal to 5 and 10 MPa, respectively, at which times the thickness of the surface crust is ~2.25 and 3.20 nm, respectively.

These results suggest that coolant injection (if rapid evaporation of the coolant could be avoided) beneath the surface crust could occur as the coolant jets rapidly perforate the crust shortly following the collapse of the vapor film. The injected liquid coolant droplets would be overheated and may rupture the crust (causing blisters, craters, or cones) or form gaseous voids in the crust (see Section 3). Also, the evaporation of coolant jets as they penetrate the crustal surface enhances the heat flux at the surface of the particles. If the initial temperature of the debris is sufficiently high ($\geq$ 3340 K) that instantaneous freezing of the surface (based on transient heat conduction at the interface) is inhibited, coolant entrapment by molten debris might occur due to the hydrodynamic instability of the interface. In this case, the penetration of the molten surface by coolant jets would cause effective mixing of the coolant with the molten debris and might result in the formation of tiny voids close to the surface of the particle without any posttest evidence of jet penetration to the surface.

Table 3. Thermophysical properties

Property	Coolant	Solid Debris	Molten Debris
Density (kg/m^3) x 10^3	0.785	8.728	8.05
Heat capacity (J/kg•K) x 10^3	4.95	0.45	0.5354
Thermal conductivity (W/m•K)	0.611	4.80	4.7581
Latent heat of fusion (J/kg) x 10^5	—	1.923	—

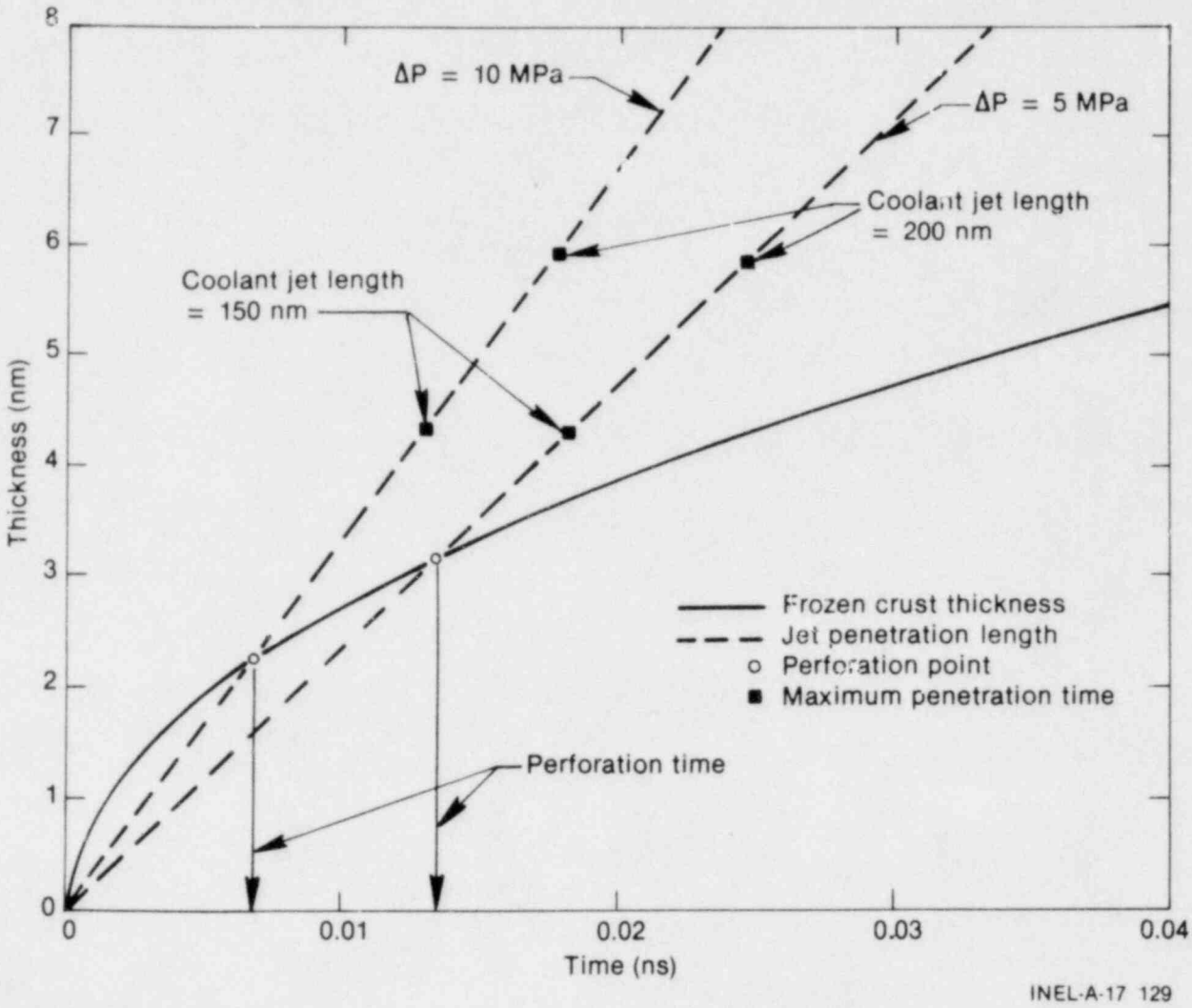

Figure 28. Effect of collapsing pressure and coolant jet length on the perforation time of the surface debris crust.

Apparently, this was the case in the RIA-ST-4 experiment in which the molten debris average temperature could have been as high as 3500 K, at which temperature instantaneous freezing at the surface of the particles upon contact with water is unlikley [interface temperature is greater than the freezing temperature of the debris (2640 K)].[15] However, freezing of the debris would begin as soon as the temperature at the surface of the debris particles dropped below the thermodynamic freezing temperature of the debris. These mechanisms (that is, coolant jet penetration and coolant entrapment) might have contributed to the formation of the large number of tiny voids observed close to the surface of debris particles (see Figure 13). As demonstrated in Section 5.3, the surface heat flux could have been ten times higher than that estimated by transient heat conduction. This supports Bankoff's[61] hypothesis concerning the enhancement of the heat flux at the interface following the collapse of film boiling, even at contact temperatures above the thermodynamic critical temperature of the coolant.

The maximum penetration time of a coolant jet into a thick debris crust depends on the jet length, ℓ, the density of the jet, and that of the crust [Equation (31)]. As shown in Figure 29, increasing the length of the jet before striking the surface crust (that is, thicker vapor film) increases the penetration time of the jet, t_j. Given a jet length (that is, a penetration depth in the crust), increasing the collapsing pressure, ΔP, decreases the maximum time of penetration, since it induces high penetration velocity for the jet [Equation (32)]. Unlike t_j, the perforation time of the crust, t_p, is governed by the initial temperature

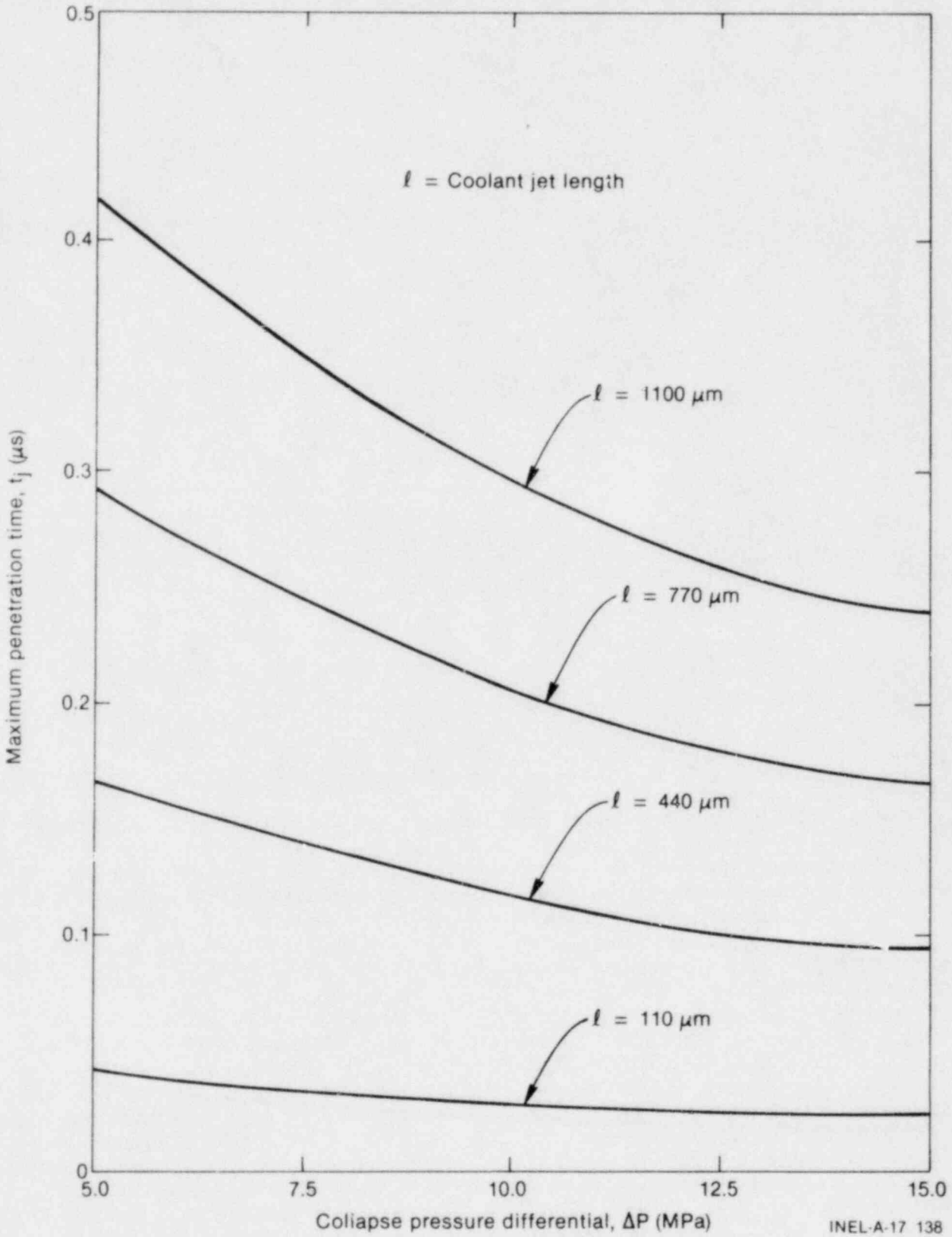

Figure 29. Effect of collapsing pressure and jet length of the maximum penetration time of the jet into a solidified debris crust.

of the molten debris ($\Delta T_{sup} = T_b - T_f$), in addition to the jet length and the collapsing pressure difference. As illustrated in Figure 30, given a ΔP and a penetration depth for the jet (that is, jet length), increasing the initial debris temperature slows down the freezing process of the crust, thus reducing the perforation time of the crust. For example, if ΔP is equal to 10 MPa, increasing ΔT_{sup} from zero to 500 K reduces the perforation time from 0.14 to 0.0061 ns. Also, increasing ΔP increases the penetration velocity of the jet and, in turn, shortens the perforation time of the crust.

The effects of the coolant properties on the perforation characteristics of the coolant jets are assessed in Figure 31. The relative perforation time (that is, the perforation time divided by the maximum penetration time of the jet) is plotted versus the initial UO_2 temperature (freezing point of pure UO_2 is ~3100 K) in both water and liquid sodium coolants. It appears from the results shown in Figure 31 that perforation of the surface crust by jets of coolant is possible in sodium as well as in water. In sodium (e.g., in a liquid-metal-cooled reactor), the perforation time of the crust is relatively longer and less sensitive to the initial temperature of the molten fuel than it is in water. This result follows from the greater thermal conductivity of sodium, which induces rapid freezing of the debris crust and delays the time at which a coolant jet may perforate the surface crust. The initial temperature of molten fuel more strongly influences the perforation time upon quenching in water than it does in sodium because of the poor thermal properties of water. In general, increasing the molten UO_2 temperature (that is, increasing ΔT_{sup}) reduces the freezing velocity of the crust and, in turn, results in a rapid decline in the perforation time of the jets.

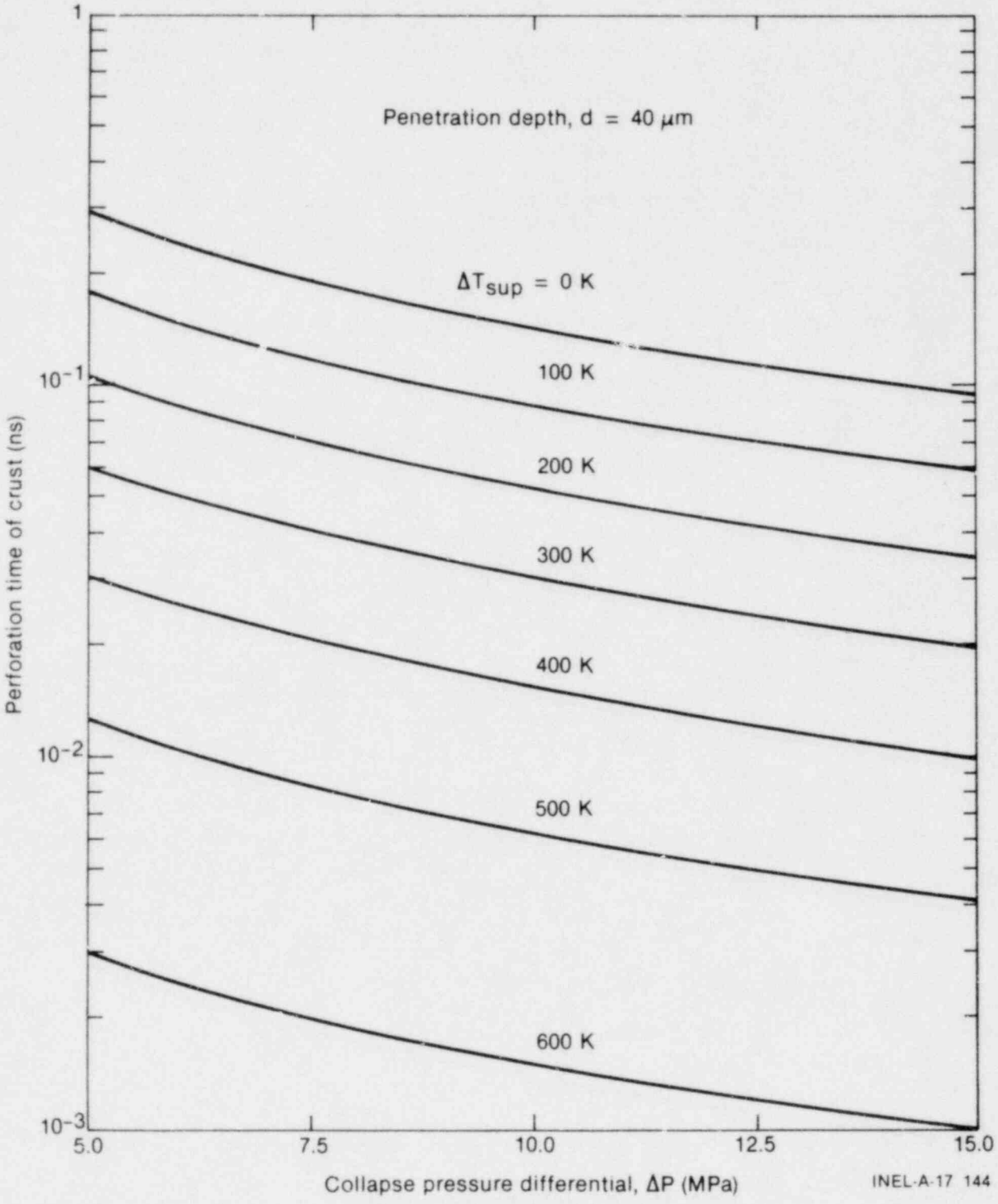

Figure 30. Effect of collapsing pressure and molten debris temperature on the perforation time of the surface debris crust.

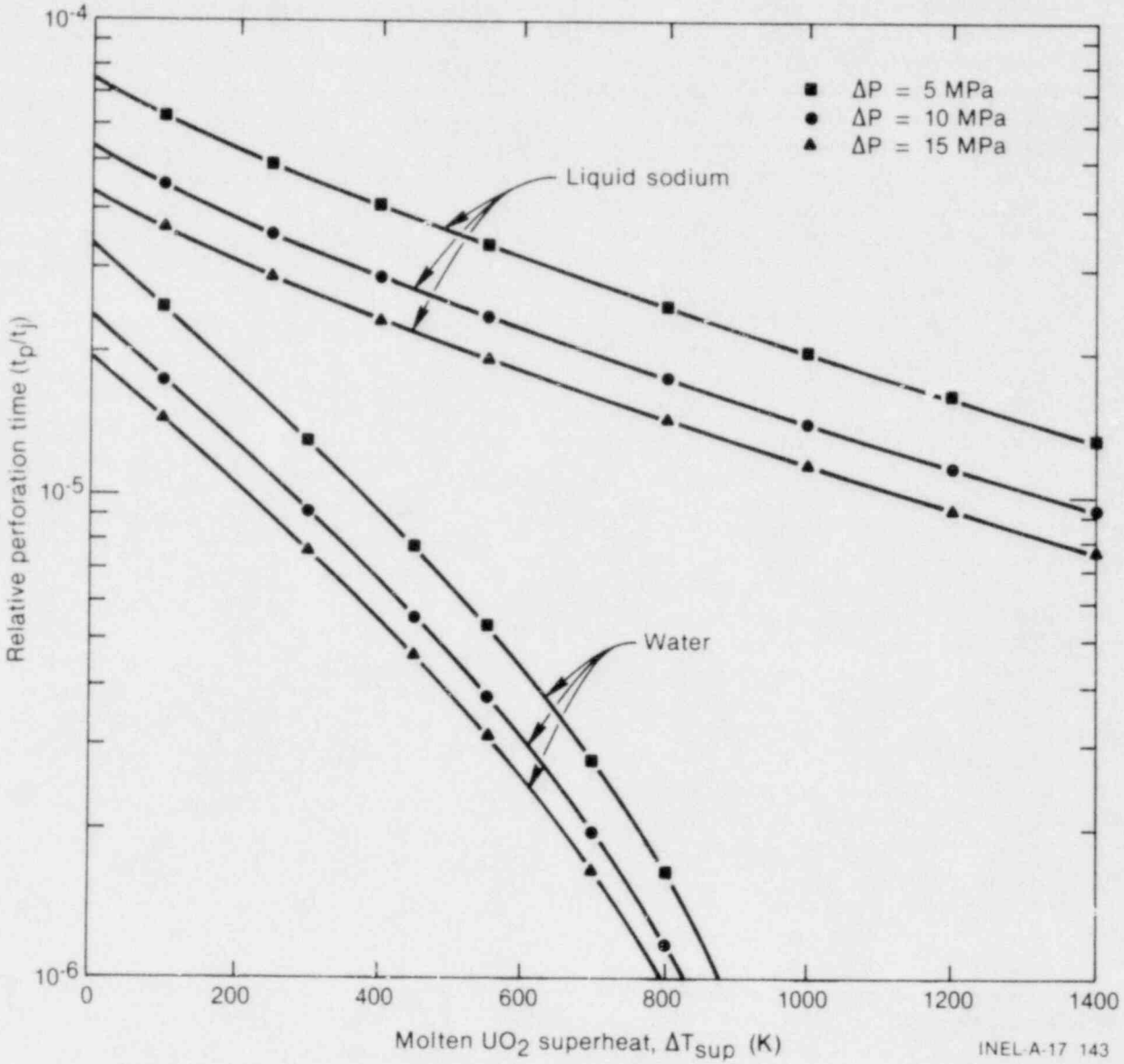

Figure 31. Comparison of perforation time in a molten UO_2-liquid sodium system with that in a molten UO_2-water system.

5. EFFECTS OF COOLANT CONDITION ON CORE COOLANT PRESSURIZATION DURING AN MFCI IN LWRs, WITH APPLICATION TO THE RIA-ST-4 EXPERIMENT

The peak pressurization and the mechanical work potential during an energetic molten fuel-coolant interaction depends in part on the system constraints; geometrical, inertial, and acoustical.[30-32] The latter two types of constraints are influenced by whether or not a coolant free surface might exist above the reactor core during the accident. This determines the acoustic relief time[a] of the system and the mass of water column to be accelerated by the pressure produced within the reaction zone (probably at the middle of the core) and, in turn, the destructive potential (that is, the thermal-to-mechanical conversion ratio) of the interaction.

If shock pressurization of the core coolant is to occur during an MFCI event, thermal energy must be transferred rapidly from the molten debris particles to the coolant within a time less than the acoustic relief time of the system. The rate of energy transfer to the coolant is primarily governed by (a) the increase in the heat transfer area, that is, the fragmentation of the molten debris; (b) the mode of heat transfer from the surface of the debris particles to the coolant; and (c) the efficiency of intermixing of the fragmented particles with the coolant. However, the maximum coolant pressure induced depends on the system constraints and the initial core coolant conditions[29] (initial phase and pressure) in addition to the rapid energy transfer to the coolant. In the following section, the effects of initial core coolant conditions on coolant pressurization during a hypothetical MFCI event are analyzed and the results applied to the coolant conditions in the RIA-ST-4 experiment.

5.1 Effects of Initial Coolant Phase

The core coolant phase (that is, liquid or two-phase mixture) at the time of contact with the molten core debris particles is important. It influences the core coolant peak pressure achieved during an MFCI and the eventual status of the working fluid (that is, a two-phase mixture or a superheated steam). To assess the effect of initial coolant phase, the pressure-enthalpy (P-h) phase diagram of water and steam was used, in which the coolant initial and peak pressures were arbitrarily chosen to be 6.58 and 35 MPa, respectively, as shown in Figure 32. For conservative considerations, let us assume an isochoric (constant volume) pressurization of the coolant (energy transfer process), followed by an adiabatic expansion back to the initial coolant pressure (inertial relief process). The contribution to the working fluid by fuel vapor or fission gases in the coolant is neglected.

During a hypothetical core meltdown accident in a light water reactor the coolant in the reactor core might be any of the following: (a) subcooled or saturated water; (b) a saturated water and steam mixture with a specific volume, v_m, less than the critical specific volume of water, v_c [in a boiling water reactor under operational conditions ($P \cong 6.5$ MPa), this corresponds to a steam quality, x, of about 7%, and in a pressurized water reactor ($P \cong 15.5$ MPa) it corresponds to a value of x of about 20%]; or (c) a mixture of saturated water and steam with $v_m > v_c$. In the latter two cases, the specific volume of the two-phase coolant, v_m, can be given in terms of the steam quality, x, as

$$v_m = v_f + x(v_g - v_f) \tag{44}$$

and in terms of the steam void fraction, α (assuming unit slip), as

$$v_m = \frac{v_f}{1 - \alpha[1 - (v_f/v_g)]} \tag{45}$$

where v_f and v_g are the specific volumes of saturated water and saturated steam, corresponding to the initial system pressure, respectively. Eliminating v_m between Equations (44) and (45) gives the following relation between x and α:

a. Acoustic relief time is the time required for a pressure wave to travel to the nearest free reflecting surface and back to the reaction zone. Simply, the acoustic relief time $t = 2L/c$, where L is the distance from the reaction zone to the core coolant free surface, and c is the sonic velocity in the coolant under accident conditions.

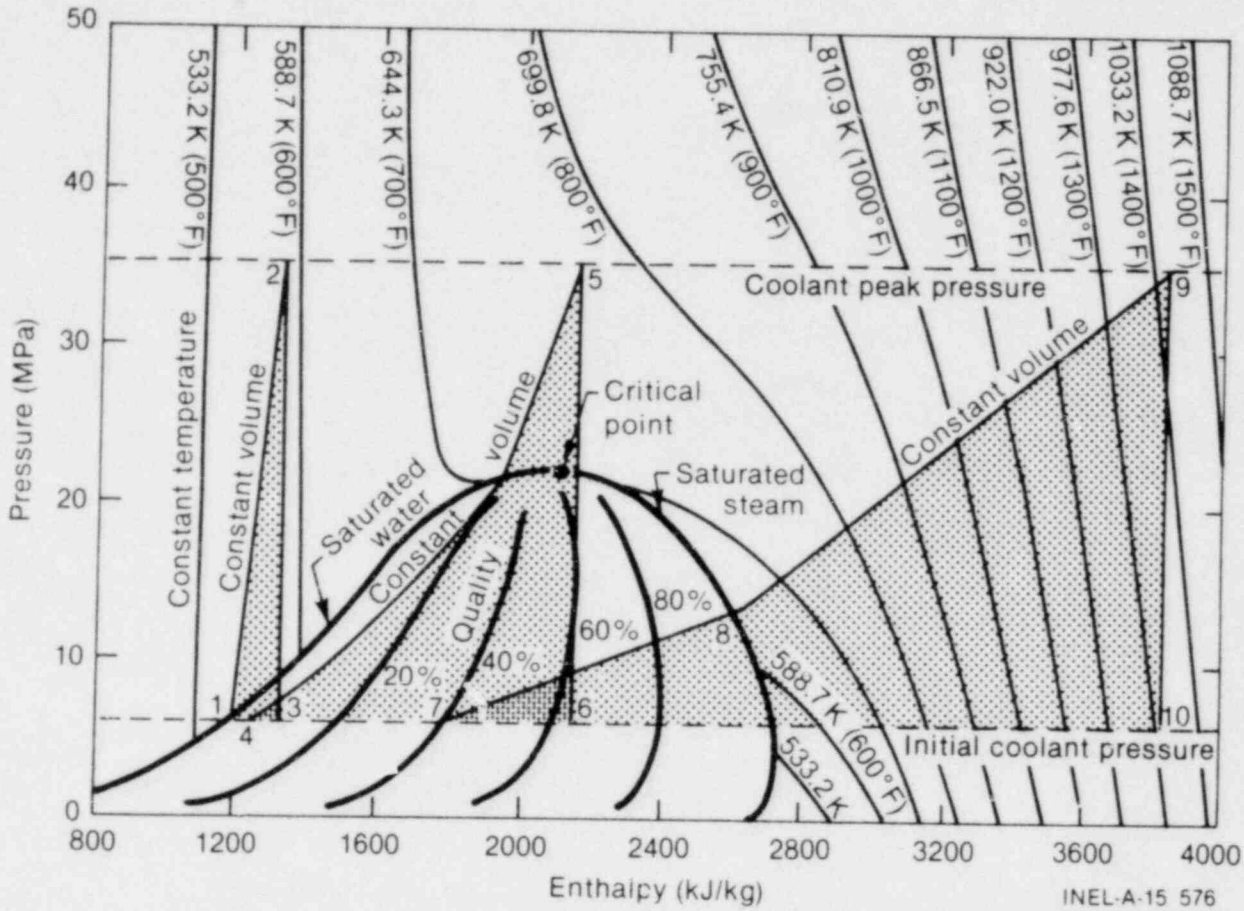

Figure 32. Effect of initial coolant phase on coolant pressurization.

$$x = \frac{\alpha\,(v_f/v_g)}{1 - \alpha\,[1 - (v_f/v_g)]}. \qquad (46)$$

Equation (46) is plotted in Figure 33 in terms of the initial coolant pressure, and it will be referred to in the following subsection.

5.1.1 Saturated Liquid. When the core coolant is initially a saturated liquid, the isochoric pressurization of the coolant to a peak pressure of 35 MPa results in the formation of a supercritical liquid (illustrated in Figure 32 by the processes 1-2-3). This requires an energy transfer of about 143 kJ/kg H_2O from the molten core debris to the coolant. Following that, the supercritical liquid (point 2) expands adiabatically back to the initial system pressure (6.58 MPa), forming a two-phase mixture of saturated water and steam (steam quality ~ 0.05) at the end of the expansion process (point 3). The final steam quality in the mixture depends on the initial system pressure and the coolant peak pressure achieved during the pressurization process. Decreasing the initial core coolant pressure[a] or increasing the peak pressure achieved would increase the steam quality of the coolant at the end of the inertial relief (expansion) process.

5.1.2 Two-Phase Mixture. Practically, film boiling commences at the outer cladding surface before fuel rod failure occurs as a result of either reactor power increase, core coolant flow reduction, or core depressurization during a hypothetical core meltdown accident. The vapor film attached to the cladding surface prior to fuel failure might mix with the coolant present in the fuel assembly, forming a two-phase mixture (if the

a. As a result of possible depressurization of the core during a hypothetical core meltdown accident, the coolant pressure at the time of interaction with molten core debris could be expected to be less than that during normal reactor operation [that is, less than 6.5 MPa in a boiling water reactor (BWR) and less than 15.5 MPa in a pressurized water reactor (PWR)].

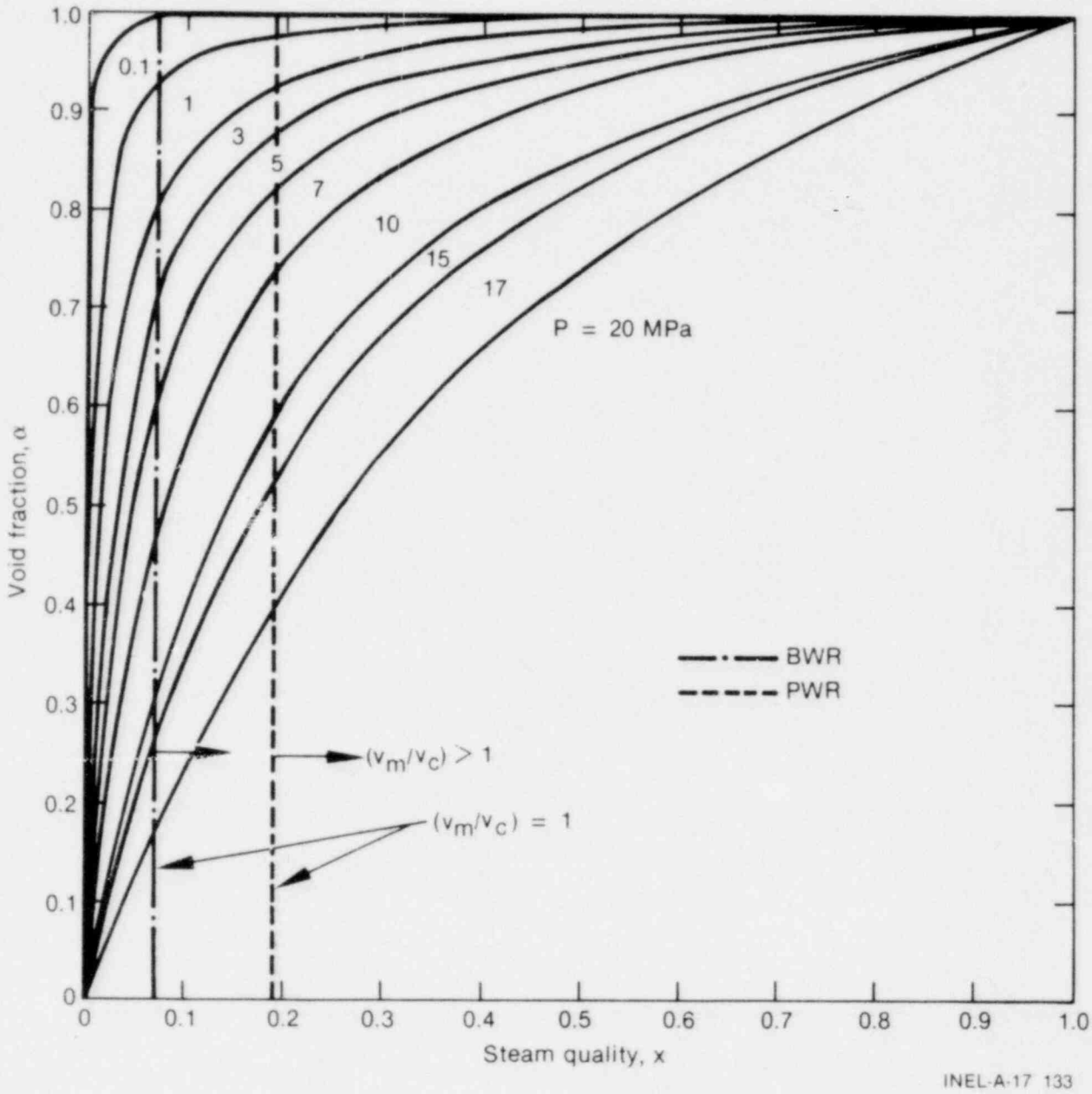

Figure 33. Effect of pressure on the coolant steam quality and the corresponding void fraction with a slip ratio of unity.

vapor film does not condense completely upon mixing with the liquid coolant) upon failure of the fuel rods. This two-phase mixture is the working fluid in a potential thermal interaction with the molten core debris. However, the behavior of the coolant during the pressurization process would depend, in this case, on the initial specific volume of the coolant, v_m, and its relation to the critical specific volume of water, v_c (that is, v_m/v_c).

5.1.2.1 Two-Phase Mixture with $v_m < v_c$—When the specific volume of the core coolant v_m (as a two-phase mixture) is initially less than the critical specific volume of water, v_c, the process 4-5-6 in Figure 32 is followed. The energy transfer to the coolant causes initial evaporation, followed by condensation of the water vapor present in the coolant. Eventually, complete condensation of the water vapor occurs when the coolant pressure reaches the saturated water line during the constant volume pressurization process. After that, the pressurization of the coolant, as a single phase, continues up to the peak pressure (point 5), forming a supercritical liquid. As shown in Figure 32, the energy required to pressurize the core coolant during this process (process 4-5) is about 950 kJ/kg of the coolant (much larger than it was with initially saturated water coolant −143 kJ/kg). This indicates that a greater energy transfer to the coolant would be necessary (that is, fine fragmentation and more efficient intermixing of the debris particles with the coolant) to pressurize a two-phase mixture. Also, the steam quality at the end of the inertial expansion back to system pressure (point 6, Figure 32) will be larger (~0.64) than it is with saturated water as an initial core coolant.

When the core coolant is initially a two-phase mixture, the preexistence of water vapor in the reaction zone influences both the fragmentation[52,53] and the intermixing[66,67] processes of the debris particles with the coolant. For example, the passage of a shock wave through a dense dispersion of the molten debris particles and two-phase coolant may accelerate the interface and produce a large velocity differential [see Figure 34(a)] between the coolant and molten particles because of the large difference in densities (density ratio greater than 10). Thus, hydrodynamic fragmentation of the molten debris particles[a] might occur, for example, due to boundary layer stripping [see Figure 34(b)]. In addition, the presence of compressible water vapor in the reaction zone reduces the mass to be accelerated,[66,67] and, in turn, may result in a much finer localized intermixing process.[b]

The change of vapor quality during an isochoric (constant volume) pressurization of the coolant is illustrated in Figure 35. The results plotted in this figure were obtained through use of the standard steam tables. When the specific volume of the coolant is initially less than the critical volume of water (that is, $v_m < v_c$), pressurization of the coolant (at constant volume) due to a rapid overheating increases the coolant steam quality until it reaches a maximum value. At such a point, further coolant overheating initiates condensation of the vapor phase. Ultimately, complete condensation of the water vapor present in the coolant occurs as the pressure reaches the saturated water line, at which point the coolant pressure is less than the thermodynamic critical pressure of water (22.1 MPa). As indicated, increasing the initial steam quality of the coolant (that is, increasing the ratio v_m/v_c) increases the coolant peak quality and the pressure at which the maximum quality occurs during the pressurization process. If the initial specific volume of the coolant is greater than the critical volume of water (that is, $v_m/v_c > 1$), continuous evaporation of the liquid coolant occurs as the coolant is pressurized.

---

a. Accelerating the interface between the interacting fluids causes Rayleigh-Taylor type instabilities, forming "tongues" of the two fluids to interpenetrate each other (that is, liquid coolant entrapment in molten debris). Rayleigh-Taylor instability takes place at the interface between two fluids of differing density when the lighter fluid accelerates the heavier one. On the other hand, the velocity differential between the two liquids initiates hydrodynamic instabilities of the Helmholtz type, causing the growth of waves in the interface to the point of breaking in a manner similar to ocean waves driven by a strong wind, but without gravity to hold the waves "down." Helmholtz instability occurs due to a differential shearing motion between the two fluids. The combination of these types of instabilities occurs when the interpenetrating tongues of Rayleigh-Taylor instability are eroded by Helmholtz instability.

b. For a coarse mixture of molten debris particles and liquid coolant, intermixing of the two fluids cannot begin until the disturbing forces are relieved at the end of melt-coolant column. However, the presence of a compressible phase of vapor in the interaction zone reduces the effective mass to be accelerated and initiates mixing of the two fluids immediately after the relief of the disturbance in the vapor region. Thus, mixing begins much sooner, resulting in a finer localized intermixing of the two fluids.[66,67]

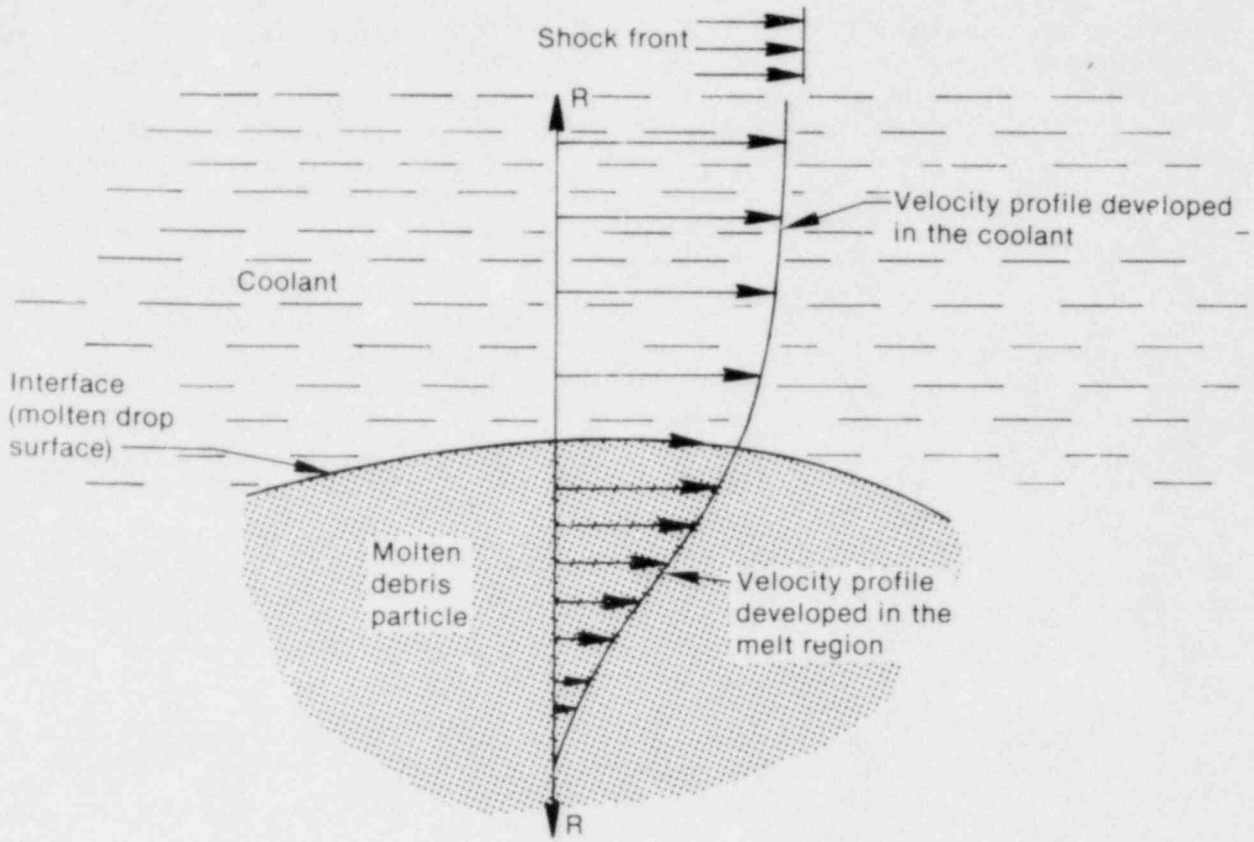

(a) Boundary layer developing at the equator of a molten debris particle

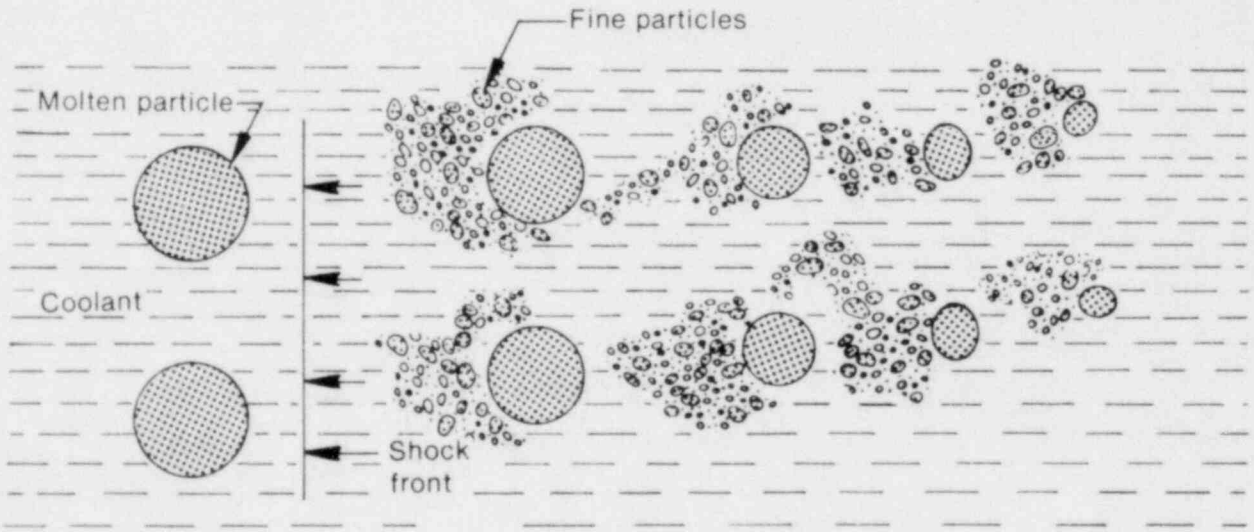

(b) Fragmentation of a debris particle due to stripping of its equator

INEL-A-17 146

Figure 34. Illustration of the hydrodynamic fragmentation of a debris particle due to boundary layer stripping.

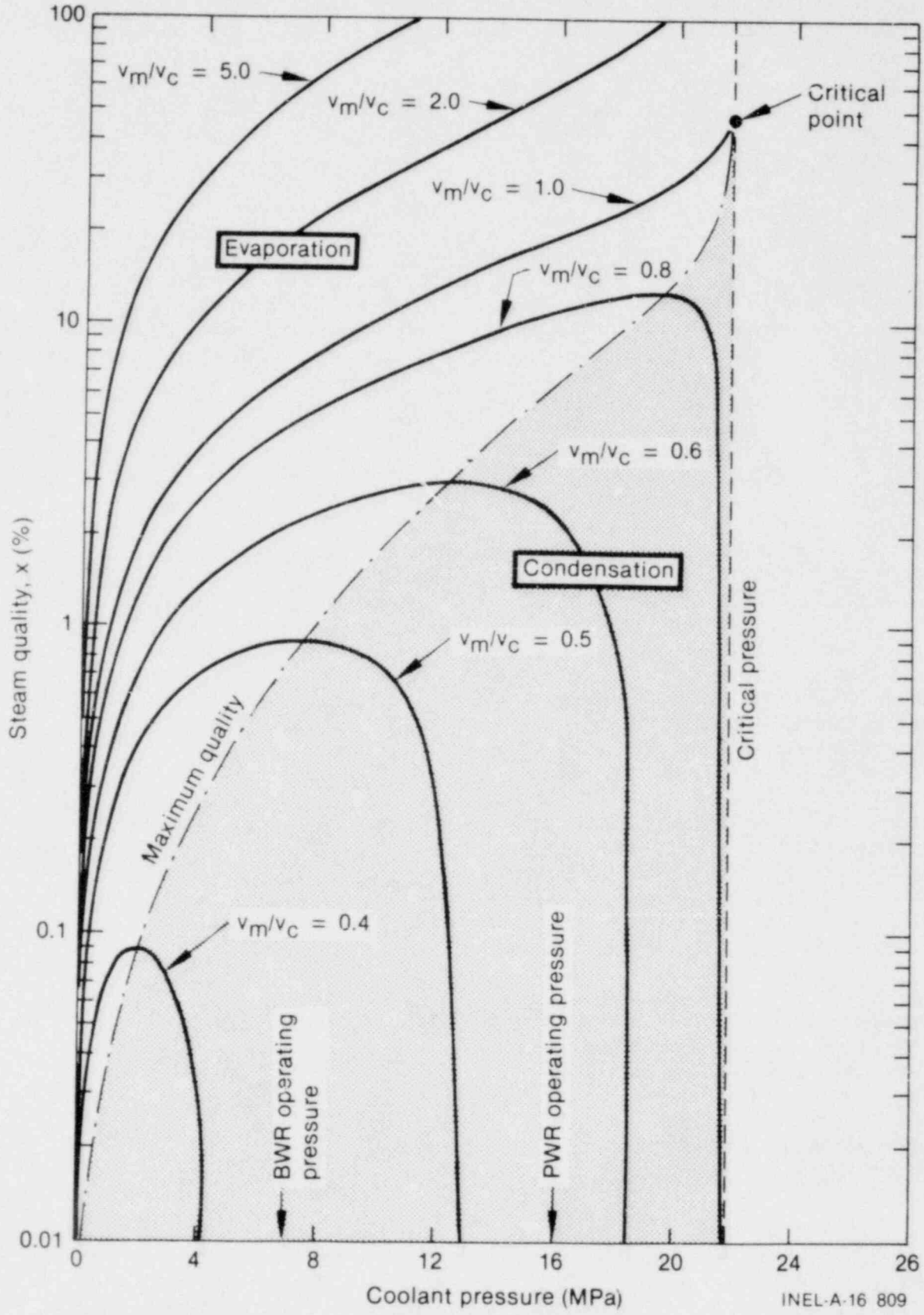

Figure 35. Change of coolant steam quality with pressure during an MFCI.

Given the initial coolant conditions (pressure, specific volume, and specific enthalpy) the amount of energy transfer per unit weight of coolant, ΔQ, required to induce a certain pressurization, ΔP, during an MFCI event (assuming constant volume pressurization) can be given from the first law of thermodynamics as

$$\Delta Q = \Delta h - v\,\Delta P \qquad (47)$$

where Δh is the increase in coolant enthalpy per kg of coolant . The second term in the right side of Equation (47) represents the energy acquired as a flow energy; v is the initial specific volume of the coolant and ΔP is the difference between the coolant peak pressure and the initial system pressure. Then, the coolant steam quality at the peak pressure, prior to the inertial relief of the working fluid, can be determined from Figure 35.

5.1.2.2 Two-Phase Mixture with $v_m > v_c$—Should the initial steam quality, x, in the core under accident conditions be sufficiently high that the coolant specific volume as a two-phase mixture, v_m, is greater than the critical volume of the water [that is, $(v_m / v_c) > 1$], then overheating the coolant produces continuous evaporation of the liquid phase initially present in the coolant (see Figures 32 and 35). Eventually, the coolant becomes a single-phase vapor when the coolant pressure reaches the saturation steam line (point 8 in Figure 32) at a pressure less than the critical pressure of the coolant. At the end of the pressurization process (point 9 in Figure 32), the working fluid becomes a supercritical gas and the total amount of energy transferred to the coolant totals ~ 2100 kJ/kg. This energy is very much greater than that in either of the previous two processes [that is, saturated liquid coolant (~143 kJ/kg) and a two-phase mixture with $(v_m/v_c) < 1$ (~950 kJ/kg)]. The adiabatic expansion of the working fluid back to the initial system pressure causes a slight decrease in temperature, and the working fluid becomes a superheated steam (point 10 in Figure 32). The effects of initial coolant pressure on the maximum coolant pressurization are assessed in the following section.

5.2 Effects of Initial Coolant Pressure

Initial core coolant pressure is an important parameter during an MFCI in a light water reactor, since it may influence the potential for core coolant pressurization. The effect of initial core coolant pressure is investigated in terms of the total energy transfer to the coolant (kJ/kg of the coolant) and the initial core coolant phase (that is, a single liquid or a two-phase mixture). The results of calculations using the standard steam tables are graphed in Figure 36, in which the increase of coolant pressure above the initial coolant pressure is plotted versus the total energy transfer to the coolant, ΔQ, during a constant volume pressurization process. As shown in Figure 36, two system pressures are considered for comparison; 6.58 MPa (representative of BWR operating pressure) and 15.8 MPa (representative of PWR operating pressure).

The interaction between molten core fragments and a core coolant that is initially saturated water induces rapid, high coolant pressurization with a relatively small amount of overheating. The hotter the coolant at the beginning of the interaction (that is, high system pressure), the more compressible the coolant will be during the pressurization process. Further explanation can be given through consideration of the liquid equation of state identified earlier in Equation 21,

$$dv = -\beta_T\, v\, dP + \alpha_p\, v\, dT$$

where β_T and α_p are the coefficients of isothermal compressibility and thermal expansion of water, respectively. These coefficients are defined as

$$\beta_T = \frac{-1}{v}\left(\frac{\partial v}{\partial P}\right)_T$$

and

$$\alpha_p = \frac{1}{v}\left(\frac{\partial v}{\partial T}\right)_p . \qquad (48)$$

For constant volume pressurization of a saturated water coolant, Equation (21) becomes

$$\frac{dp}{dT} = (\alpha_p/\beta_T). \qquad (49)$$

The right side of Equation (49) is positive, but decreases with temperature, which indicates that increasing the initial coolant pressure (thus increasing the saturation temperature of the coolant at the beginning of the interaction)

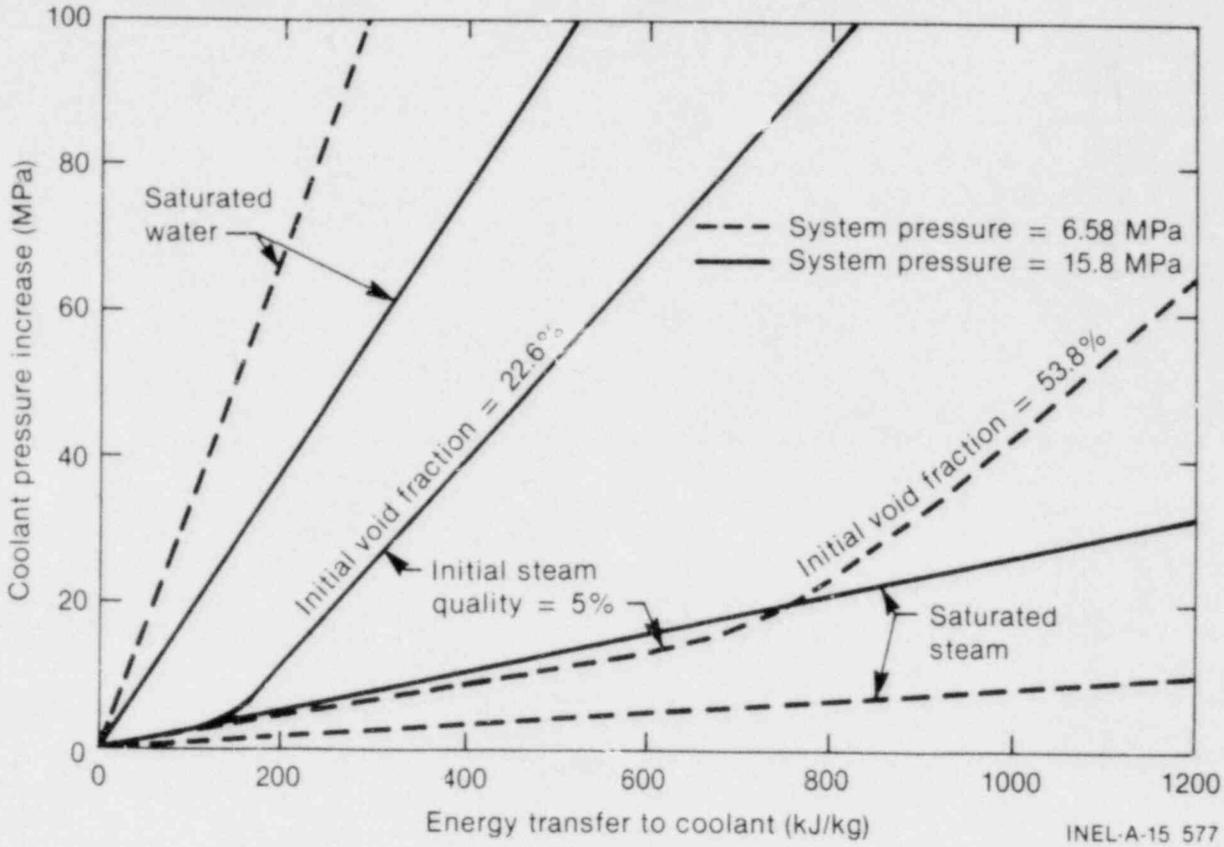

Figure 36. Effect of initial coolant pressure on core coolant pressurization.

decreases the rate of coolant pressurization (dP/dT) due to overheating. Therefore, more overheating would be required to pressurize a saturated water coolant in a high pressure system than in a low pressure system (e.g., a PWR versus a BWR).

When the core coolant is initially a two-phase mixture, shock pressurization of the coolant will require a larger amount of energy than in the previous case (core coolant is initially saturated water). Given an initial steam quality, increasing the initial coolant pressure increases the coolant peak pressure induced by a certain amount of energy transfer (see Figure 36). This is explainable, since increasing the initial coolant pressure decreases the volume of the compressible vapor phase initially present in the coolant, thus enhancing the pressurization of the coolant. As demonstrated in Figure 33, increasing the initial coolant pressure decreases the vapor void fraction, α, associated with a certain vapor quality, x, thus resulting in a high coolant peak pressure due to a given amount of energy transfer to the coolant.

In summary, the initial core coolant phase (that is, a liquid or a two-phase mixture) and pressure strongly influence the behavior of the core coolant during an MFCI event. During an interaction between the molten core debris and saturated water (that is, liquid-liquid system), rapid energy transfer to the coolant could result in a shock pressurization of the core with a relatively small amount of energy transfer (that is, less fragmentation and intermixing of core debris particles and coolant). Increasing the initial coolant system pressure under such conditions would decrease the coolant peak pressure induced by a certain amount of energy transfer.

During a hypothetical core meltdown accident in a commercial LWR, however, the initial core coolant would probably be a two-phase mixture because of the onset of film boiling on the cladding outer surface before fuel rod failure and the potential of voiding the fuel subassemblies. A large coolant overheating would be necessary in this case to induce core coolant shock pressurization (that is, fine fragmentation and more efficient intermixing of molten debris particles with

coolant). Also, for a given initial steam quality, increasing the initial coolant pressure (PWR versus BWR) would tend to increase the coolant peak pressure associated with a given amount of energy transfer.

5.3 Application to the RIA-ST-4 Experiment

It may be concluded from the foregoing discussion and Figure 32 that the coolant in the RIA-ST-4 experiment flow shroud at the time of test fuel rod failure was probably a two-phase mixture. This explains the high coolant pressure (35 MPa) and coolant temperature (in excess of 940 K) recorded during the experiment. Actually, the pressurization of the coolant was not isochoric (constant volume), and the expansion of the working fluid was not adiabatic. This implies that the thermal energy transferred to the coolant during its pressurization to the peak pressure of 35 MPa differs from that identified in Figure 32. Also, the maximum superheating of the steam might be higher than that predicted (980 K) at the end of the adiabatic expansion process (process 9-10 in Figure 32).

The generation of vapor in the flow shroud before rod failure was caused by the onset of film boiling on the cladding outer surface shortly after the initiation of the power burst [as soon as the cladding surface temperature exceeded the minimum film boiling temperature or the thermodynamic critical temperature of the coolant ($T_c \cong 647$ K)]. Upon failure, extensive amounts of molten debris were expelled from the failed rod into a mixture of vapor and liquid coolant in the shroud. The rapid energy transfer from the debris particles to the two-phase mixture, together with the geometrical, inertial, and acoustical constraints imposed by the test loop, induced the coolant peak pressure (35 MPa) recorded ~2.0 ms after test rod failure. At this time, the working fluid in the shroud was a supercritical gas. The expansion of this gas by inertial relief against the system produced a superheated steam (process 7-8-9-10 in Figure 32). The high coolant temperature (in excess of 940 K) recorded 500 ms after rod failure at the exit of the flow shroud supports this conclusion. Cooling of the superheated steam within the shroud was relatively slow, as indicated by the length of time (~5 seconds) the thermocouples were at temperatures above 940 K (Figure 8).

As shown in Figure 32, a total energy of about 2100 kJ/kg of the coolant (assuming an initial steam quality of 7%) could transfer from the molten debris to the coolant during the 2-ms rise time of the pressure pulses (assuming constant volume pressurization and adiabatic expansion). In reality, the total energy transferred might have been less than or in excess of 2100 kJ/kg H_2O, depending on the initial steam quality of the coolant. The total weight of the two-phase coolant in the active region of the flow shroud (length of ~0.92 cm, cross-sectional area of 2.02 cm^2, and coolant density of ~0.350 kg/m^3) is about 64 g (see Table 1). Thus, the total amount of energy transferred to the shroud coolant is approximately 134 kJ (which is about 12% of the total energy deposition in the test rod at failure). Such an estimate of the energy transfer is equal to the specific energy (2100 kJ/kg H_2O) required to isochorically pressurize the two-phase coolant (assuming initial quality of 7%), times the mass of the coolant (64 g) present in the active length of the shroud at the time of rod failure.

The average heat transfer area between the debris particles and the coolant is

$$A = \frac{6\ m}{\rho_s D_{av}} \tag{50}$$

where

- m = total mass of debris particles (~155 g; see Table 1)
- ρ_s = density of solid debris (~9600 kg/m^3)
- D_{av} = average diameter of debris particles (~1300 μm; see Figure 12).

This gives a total heat transfer area of approximately 720 cm^2 and an average heat flux at the surface of the debris particles (during the rise time of the recorded pressure pulse) of about 9.3×10^5 $kJ/m^2 \cdot s$. It should be noted that this estimate of the surface heat flux is conservative. This follows from the fact that a majority of the debris particles were hollow (see Section 3), thus producing a larger heat transfer area per unit mass of debris.

If the collapse of the vapor film around the debris particles occurs, molten debris-liquid coolant contact might induce freezing of the sur-

face of the debris particles. The surface heat flux is then given by transient heat conduction as

$$q(t) = \frac{k_c}{\sqrt{\pi \alpha_c t}} \left[\frac{T_f - T_o}{1 + \sigma \, \mathrm{erf}\,(\lambda)} \right] \qquad (51)$$

where

k_c = coolant thermal conductivity

α_c = coolant thermal diffusivity

T_o = initial coolant temperature

T_f = freezing temperature of debris

λ = freezing coefficient [calculated through use of Equation (39); see Section 4 for details]

σ = coolant/frozen crust thermal ratio (defined in Section 4).

The average heat flux, q_{av}, at the surface of the particles during the heat transfer time, t_{HT}, is calculated through use of Equation (51) in the form

$$q_{av} = \frac{\int_0^{t_{HT}} q(t)dt}{\int_0^{t_{HT}} dt} \qquad (52)$$

which gives

$$q_{av} = \frac{2k_c}{\sqrt{\pi \alpha_c \, t_{HT}}} \left[\frac{T_f - T_o}{1 + \sigma \, \mathrm{erf}\,(\lambda)} \right]. \qquad (53)$$

Should the interface temperature between the molten debris and the coolant be higher than the freezing temperature of the debris, no freezing of the surface occurs, and Equation (53) becomes

$$q_{av} = \frac{2k_c}{\sqrt{\pi \alpha_c \, t_{HT}}} \left(\frac{T_m - T_o}{1 + \sigma} \right). \qquad (54)$$

where T_m is the bulk temperature of the molten debris.

Equations (53) and (54) are compared in Figure 37 in terms of the initial superheat of the molten debris ($T_m - T_f$). The coolant temperature, T_o, is assumed to be equal to the saturation temperature of the coolant in the RIA-ST-4 experiment (~553 K), and the heat transfer time, t_{HT}, is assumed to be equal to the recorded rise time of the pressure pulse (~2 ms). As shown, Equation (53) gives slightly higher values than those given by Equation (54), because the freezing of the debris involves the latent heat of freezing, which increases the surface heat flux. On the other hand, both Equations (53) and (54) give values that are very much less (~10 times less) than the surface heat flux estimate of 9.3×10^5 kJ/m^2•s to induce the recorded pressurization in the RIA-ST-4 experiment.

These results suggest that the collapse of the vapor film by a shock wave may produce a larger heat flux than that predicted by transient heat conduction assuming intimate contact between the coolant and the debris particles. Local entrapment of liquid coolant by molten debris due to Rayleigh-Taylor hydrodynamic instability of the interface and the evaporation and local mixing by coolant jets as they penetrate the surface of the debris particles[13,23-25] might be responsible for the very rapid energy transfer to the coolant. The enhancement of the heat flux at the surface of the debris particles by such mechanisms should occur immediately following the collapse of film boiling and before the formation of a relatively thick debris crust at the particle surface. Once a thick crust is formed, the heat loss from the surface is, by and large, governed by the thermal properties of the crust, not by the rate of heat exchange at the surface, resulting in a relatively low rate of heat transfer.

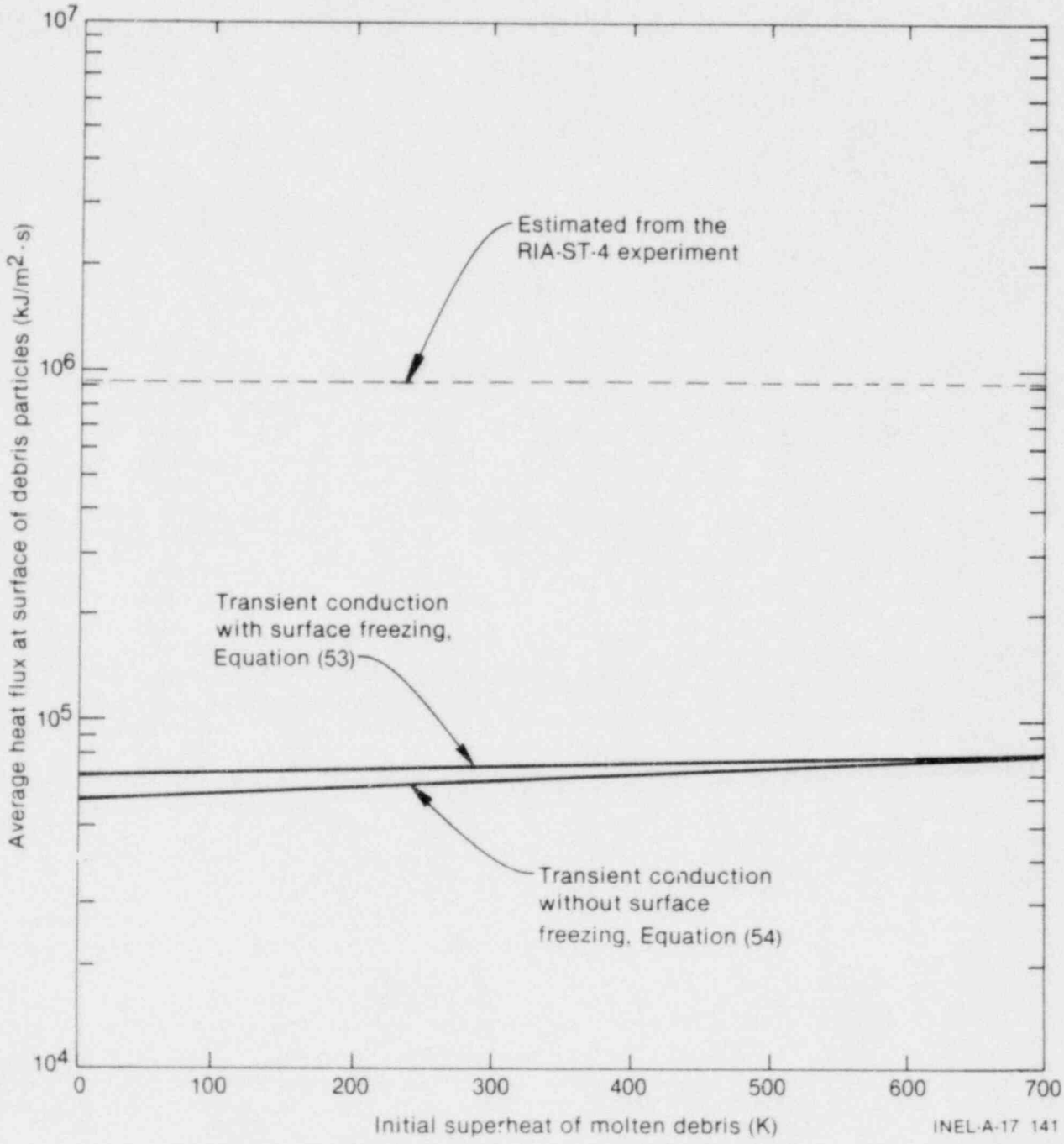

Figure 37. Comparison of calculated heat flux at the surface of a debris particle in the RIA-ST-4 experiment with that due transient conduction.

6. DISCUSSION AND CONCLUSIONS

The results of a severe reactivity initiated accident experiment, designated RIA-ST-4, were presented, discussed, and analyzed with respect to molten fuel-coolant interaction (MFCI). Extensive fuel melting and fragmentation occurred during this experiment, and a coolant peak pressure of 35 MPa and a coolant temperature in excess of 940 K were achieved. Because the RIA-ST-4 experiment was conducted at a coolant pressure of 6.45 MPa, a coolant temperature of 538 K, and a coolant flow rate of 0.085 L/s, similar to those in a boiling water reactor during a hot startup the results are of particular interest in the current effort to understand the basic phenomena involved in an MFCI occurring at high coolant pressure and temperature.

The fragmentation characteristics of molten debris in the RIA-ST-4 experiment were investigated. Three mechanisms were proposed to have contributed to the fragmentation of the debris particles: (a) fragmentation due to impact of the molten debris on the shroud wall and on the coolant, (b) rupture of the frozen crust at the surface of the particle due to pressure-induced stresses in the crust caused by overheating liquid coolant droplets entrained in the molten debris, and (c) perforation of the surface crust by coolant jets. Phenomenological modeling of the latter two mechanisms were presented. Incipient fragmentation of the particles by the second mechanism is calculated to occur within a very short time (a fraction to a few nanoseconds). Experimental evidence shows that a majority of the particles had craters and ruptures in the surface crust. Some of the particles consisted of empty, frozen shells, with numerous small voids of different sizes present in the crust. The rupture of the surface crust was dominant for both larger (few mm in diameter) and smaller (few μm in diameter) particles. This suggests that the breakup of large particles could have resulted in subsequent entrainment of coolant droplets in smaller particles produced in the breakup of the larger ones and, in turn, their fragmentation.

The results of calculations relative to the fragmentation by coolant jets show that perforation of the surface crust by jets of coolant is possible in both systems of molten UO_2-Na coolant and molten UO_2-water coolant. As jets penetrate the surface of the particles, finely fragmented particles might be produced. Also, the penetration of the jets might effectively enhance the surface heat flux and cause effective mixing at the surface of the particles. The metallographic and scanning electron microscope analysis of the debris particles show that part of the surface crust of some particles gave the appearance of swiss cheese. The holes could have been caused by coolant jets that may have developed during the collapse of void-like regions of film boiling on the surface of the particles.

The effects of core coolant conditions (initial coolant phase and coolant pressure) on the coolant peak pressurization during a hypothetical MFCI in an LWR are also analyzed. The analysis shows that in a molten debris-liquid coolant interaction (a liquid-liquid system), shock pressurization of the coolant can be induced with a small amount of energy transfer (that is, mild fragmentation and intermixing of the debris particles with coolant). Under such conditions, increasing the initial system pressure reduces the coolant peak pressure induced due to a certain amount of energy transfer. On the other hand, shock pressurization of a two-phase coolant would require a large amount of energy transfer (that is, fine fragmentation and more efficient intermixing of debris particles with coolant). Given an initial steam quality of the coolant, increasing the initial coolant pressure induces a higher peak coolant pressure associated with the same energy transfer. Application to the coolant conditions in the RIA-ST-4 experiment revealed that the coolant in the shroud at the time of rod failure was a two-phase mixture. Analysis indicated that the recorded high coolant temperature (in excess of 940 K) was due to the formation of superheated steam in the flow shroud upon the expansion of the working fluid back to the initial coolant pressure. The thermal-to-mechanical energy conversion ratio is estimated to have been about 0.3%.

From the analysis of the RIA-ST-4 experiment, the following conclusions can be drawn:

1. The coolant peak pressure recorded during the experiment was caused by an energetic molten debris-coolant interaction that may

be viewed in the light of the pressure detonation model (Appendix A). The contribution to the recorded pressure due to fill gas release from the test rod at failure and to UO_2 fuel vapor is negligibly small.

2. The destabilization and collapse of the vapor film on the surface of the debris particles by a shock wave developed in the shroud after rod failure apparently triggered the fine fragmentation of the particles and initiated a rapid, coherent thermal interaction between the particles and the coolant.

3. To induce the coolant peak pressure (~35 MPa) and the high coolant temperature (>940 K) recorded during the experiment, the thermal energy was transferred from the debris particles to the coolant at a rate calculated to be much higher than that due to transient heat conduction. This enhancement of the heat flux of the surface of the particles could be due to liquid coolant entrapment by molten debris at the interface and the penetration at the particle surfaces by coolant jets.

4. The dynamics of film boiling destabilization and collapse by a shock wave requires further investigation. An in-pile experimental program to quantify the effects of core coolant conditions, mode of fuel failure, and system constraints on core coolant pressurization during a thermal interaction between molten debris (primarily molten UO_2) and water under typical accident conditions in an LWR would be beneficial.

7. REFERENCES

1. G. Long, "Explosion of Molten Aluminum in Water—Cause and Prevention," *Metal Progress, 71*, 1957.

2. S. G. Lipsett, "Explosions from Molten Materials and Water," *Fire Technology, 2*, 1966, pp. 118-126.

3. L. C. Witte, J. E. Cox, J. E. Bauvier, "The Vapor Explosion," *Journal of Metals*, 1970, pp. 39-46.

4. D. L. Katz and C. M. Sliepcevick, "LNG Water Explosions Cause and Effects," *Hydrocarbon Processing*, November 1971, pp. 240-244.

5. T. Enger and D. Hartman,"Rapid Phase Transformation During LNG Spillage on Water," *Proceedings of the 3rd Conference on Liquified Natural Gas, Washington D.C., September 1972.*

6. L. D. Buxton and L. S. Nelson, *Steam Explosions*, SAND 74-0382, Chapter 6, 1975.

7. R. H. Bradley and L. C. Witte, "Explosive Interaction of Molten Metals Injected into Water," *Nuclear Science and Engineering, 48*, 1972, pp. 387-396.

8. L. C. Witte and J. E. Cox, "The Vapor Explosion—A Second Look," *Journal of Metals*, 1978, pp. 29-35.

9. J. R. Dietrich, *Experimental Investigation of the Self-Limitation of Power Driving Reactivity Transients in a Subcooled, Water-Moderator Reactor*, ANL-5323, 1954.

10. R. W. Miller, A. Sola, R. K. McCardell, *Report of the SPERT-1 Destructive Test Program on an Aluminum Plate Type Water Moderated Reactor*, ID-16883, 1964.

11. T. J. Thompson and J. G. Beckerly, *The Technology of Nuclear Reactor Safety 1*, Cambridge, MA.: MIT Press, 1964, p. 672.

12. M. S. El-Genk, "On a Vapor Explosion in the RIA-ST-4 Experiment," *Transactions of the American Nuclear Society, 34*, 1980, p. 972.

13. M. S. El-Genk, "Fragmentation Mechanisms Occurring During an Energetic Fuel-Coolant Interaction," *Transactions of the American Nuclear Society, 35*, 1980, p. 348.

14. R. S. Semken et al., *Reactivity Initiated Accident Test Series RIA Scoping Test Fuel Behavior Report*, NUREG/CR-1360, EGG-2024, April 1980.

15. M. S. El-Genk and R. L. Moore, *A Study of Molten Debris Freezing and Wall Erosion in the RIA-ST-4 Experiment*, NUREG/CR-1072, EGG-2030, April 1980.

16. C. Zimmermann et al., *Experiment Data Report for Test RIA-ST (Reactivity Initiated Accident Test Series)*, NUREG/CR-0473, TREE-1235, March 1979.

17. T. Fujishiro et al., *Light Water Reactor Fuel Response During Reactivity Initiated Accident Experiments*, NUREG/CR-0269, TREE-1237, August 1978.

18. A. Inoue and S. G. Bankoff, "Destabilization of Film Boiling due to Arrival of a Pressure Shock: I. Experimental," *Topics in Two-Phase Flow and Heat Transfer* (edited by S. G. Bankoff), New York: American Society of Mechanical Engineers, 1978.

19. *LWR Safety Research Program, Quarterly Report, April-June 1979*, SAND79-2057, July 1979.

20. L. S. Nelson, L. D. Buxton, W. Benedict, *Steam Explosion Triggering Phenomena, Part II, Corium A, Corium E, Simulants and Oxides of Iron and Cobalt Studied with a Floodable Arc Melting Apparatus*, NUREG/CR-0633, SAND79-0260, 1979.

21. D. S. Drumheller, "The Initiation of Melt Fragmentation in Fuel-Coolant Interactions," *Nuclear Science and Engineering, 72*, 1979, pp. 347-356.

22. S. J. Board and R. W. Hall, "Propagation of Thermal Explosions: 1-Tin/Water Experiments," *Second Specialist Meeting on Fuel-Coolant Interaction, Ispra, Italy, November 1973.*

23. D. Jakeman and R. Potter, "Fuel Coolant Interaction" *Proceedings of the Int. Eng. Fast Reactor for Safe and Reliable Operation, Karlsruhe, W. Germany, October 1, 1972*, pp. 884-897.

24. S. J. Board, C. L. Farmer, D. H. Poole, "Fragmentation in Thermal Explosions," *International Journal of Heat Mass Transfer, 17*, 1974, pp. 331-339.

25. D. J. Buchanan and T. A. Dullforce, "Mechanisms for Vapor Explosions," *Nature, 245*, 1973, pp. 32-34.

26. M. L. Corradini, "Phenomenological Modeling of Steam Explosions," *The 19th National Heat Transfer Conference, Orlando, Florida, July 27-30,1980.*

27. S. J. Board and L. Caldarola, "Fuel-Coolant Interaction in Fast Reactors," *Thermal and Hydraulic Aspects of Nuclear Reactor Safety, 11*, New York: American Society of Mechanical Engineers, 1977, pp. 195-222 (edited by O. C. Jones, Jr. and S. G. Bankoff).

28. J. A. McClure, *Particle Size Distributions from Fuel Rods Fragmented During Power Burst Test in the Capsule Driver Core*, IN-1428, October 1970.

29. M. S. El-Genk, "Effects of Coolant Conditions on Core Pressurization During an Energetic MFCI in LWRs," *Transactions of the American Nuclear Society, 35*, 1980, p. 309.

30. D. H. Cho et al., *A Rate-Limited Model of Molten-Fuel/Coolant Interactions: Model Development and Preliminary Calculations*, ANL-7919, March 1972.

31. W. L. Chen et al., *Recent Additions to the Parametric Model of Fuel-Coolant Interactions*, ANL-8130, September 1974.

32. W. L. Chen and D. H. Cho, *Heat Loss to Cold Structures During a Fuel-Coolant Interaction*, ANL-8129, September 1974.

33. M. G. Chasanov, L. Leibowitz, S. D. Gabelnick, "High Temperature Physical Properties of Fast Reactor Materials," *Journal of Nuclear Materials, 49*, 1973-74, pp. 129-135.

34. *Quarterly Progress Report on the NSRR Experiments (4), January-June 1977*, JAERI M7304, August 1977.

35. *Quarterly Progress Report on NSRR Experiments, January-June 1978*, JAERI M7977.

36. T. Fujishiro et al., "A Study on Pressure Generation Caused By Actual Fuel Failure in the NSRR Experiment," *4th CSNI Specialist Meeting on FCI in Nuclear Reactor Safety, Bournemouth, UK, April 2-5, 1979.*

37. M. Ishikawa and S. Shiozawa, "A Study of Fuel Behavior Under Reactivity Initiated Accident Conditions-Review," *Journal of Nuclear Materials, 95*, 1980, pp. 1-30.

38. M. S. Plesset and R. B. Chapman, "Collapse of an Initially Spherical Vapor Cavity in the Neighborhood of a Solid Boundary" *Journal of Fluid Mechanics, 47*, 1971, pp. 283-290.

39. A. W. Cronenberg and T. Yackle, "Interannular Fracture of Unrestricted UO_2 Fuel During Film Boiling Operation," *Journal of Nuclear Materials, 84*, 1979, pp. 295-318.

40. R. F. Cannon, J. T. A. Roberts, R. J. Beals, "Deformation of UO_2 at High Temperatures," *Journal of the American Ceramic Society, 54*, 1971, p. 105.

41. D. P. Birkhoff et al., "Explosives with Lined Cavities," *Journal of Applied Physics, 19*, 1948, pp. 563-582.

42. F. P. Bowden, "The Formation of Microjets in Liquid Under the Influence of Impact or Shock," *Royal Society Philosophical Transactions, A-260*, 1966, p. 94.

43. T. B. Benjamin and A. T. Ellis, "The Collapse of Cavitation Bubbles and the Pressures Thereby Produced Against Solid Boundaries," *Royal Society Philosophical Transactions, A-260*, 1966, pp. 221-240.

44. A. W. Cronenberg and M. A. Grolmes, "Fragmentation Modeling Relative to the Breakup of Molten UO_2 in Sodium," *Journal of Nuclear Safety, 16*, 1975, pp. 683-699.

45. W. Zyszkowski, "Thermal Explosion Hazard in (Fast) Nuclear Reactors," *Atomic Energy Review, 161*, 1978.

46. L. Caldarola and W. E. Kastenberg, "On the Mechanism of Fragmentation During Molten Fuel/Coolant Thermal Interactions," *Proceedings of the Fast Reactor Safety Meeting, Beverly Hills, CA., April 2-4, 1974.*

47. M. S. Kazimi, *Theoretical Studies of Some Aspects of Molten Fuel-Coolant Thermal Interactions*, Ph.D Thesis, MIT, Cambridge, MA, MITNE-155, May 1973.

48. H. Mizuta, "Fragmentation of Uranium Dioxide After Molten Uranium Dioxide-Sodium Interaction," *Journal of Nuclear Science and Technology, 11*, 1974, pp. 480-487.

49. T. G. Theofanous et al., "The Role of Hydrodynamic Fragmentation in Fuel Coolant Interaction," *Fourth CSNI Specialist Meeting on Fuel-Coolant Interaction in Nuclear Reactor Safety, Bournemouth, UK, April 2-5,1979.*

50. P. Patel, *Hydrodynamic Fragmentation of Drops*, Ph.D Thesis, Purdue University, December 1978.

51. A. Sharon and S. G. Bankoff, "Propagation of Shock Waves through a Fuel Coolant Mixture, Part I Boundary Layer Stripping Mechanism," *Topics in Two-Phase Flow and Heat Transfer*, (edited by S. G. Bankoff) New York: ASME, 1978.

52. M. Baines, "Hydrodynamic Fragmentation in Fuel-Coolant Interactions," *4th CSNI Specialist Meeting on FCI in Nuclear Reactor Safety, Bournemouth, UK, April 2-5, 1979.*

53. P. G. Simpkins and E. L. Bales, "Water-Drop Response to Sudden Acceleration," *Journal of Fluid Mechanics, 55*, 4, 1972, pp. 629-639.

54. F. Cooper, "Heat Transfer from a Sphere to an Inifinite Medium," *International Journal of Heat Mass Transfer*, 1977, pp. 991-993.

55. A. W. Cronenberg et al., "A Thermal Stress Mechanism for the Fragmentation of Molten UO_2 Upon Contact with Sodium Coolant," *Nuclear Engineering and Design, 30*, 1976, pp. 434-443.

56. R. B. Knapp and N. E. Todreas, "Thermal Stress Initiated Fracture as a Fragmentation Mechanism in the UO_2-Sodium Fuel-Coolant Interaction," *Nuclear Engineering and Design, 35*, 1975, pp. 69-85.

57. K. Flory et al., "Molten Metal-Water Explosion," *Chemical Engineering Progress, 65*, 1969, pp. 50-54.

58. K. H. Hsiao et al., "Pressurization of a Solidifying Sphere," *Journal of Applied Mechanics, 94*, 1972, pp. 71-77.

59. J. M. Forgac et al., "Solidification of a Sphere: The Effects of Thermal Contraction and Density Change Upon Freezing," *Journal of Applied Mechanics, 46*, 1979, pp. 83-89.

60. I. S. Habib, "Pressurization of a Solidifying Semi-Transparent Spherical Medium by Conduction and Radiation," *Journal of Applied Mechanics*, March 1973, pp. 307-309.

61. S. G. Bankoff, "Destabilization of Film Boiling," *Physicochemical Hydrodynamics, 1*, 1980, pp. 69-76.

62. M. Kornfield and L. Suvorov, "On the Destructive Action of Cavitations," *Journal of Applied Physics, 15*, 1944, p. 495.

63. M. Rattray, *Perturbation Effects in Bubble Dynamics*, Ph.D Thesis, California Institute of Technology, 1951.

64. D. C. Pack and W. M. Evans, *Proceedings of Physic Society, B64*, 1951, pp. 298-302 and 303-310.

65. H. S. Carslaw and J. C. Jaeger, *Conduction of Heat in Solids*, 2nd edition, Oxford University Press, 1959.

66. D. H. Cho et al., "Mixing Requirements for Energetic Fuel - Coolant Interaction," *Transactions of the American Nuclear Society, 23*, 1976, pp. 369-370.

67. D. H. Cho et al.,"Some Aspects of Mixing in Large-Mass, Energetic Fuel-Coolant Interactions," *Proceedings of the International Meeting on Fast Reactor Safety and Related Physics, Chicago, Illinois, October 5-8, 1976.*

APPENDIX A

ASPECTS OF MOLTEN FUEL-COOLANT INTERACTIONS RELEVANT TO THE RIA-ST-4 EXPERIMENT

APPENDIX A

ASPECTS OF MOLTEN FUEL-COOLANT INTERACTIONS RELEVANT TO THE RIA-ST-4 EXPERIMENT

Several mechanistic models[A-1—A-10] have been proposed to describe the conditions under which explosive thermal interaction may occur and to explain the physical phenomena involved. However, most of the effort has been focused on two main concepts: the spontaneous nucleation of Fauske[A-4,A-5] and the pressure-induced detonation of Board, Hall, and Hall.[A-7,A-8]

1. SPONTANEOUS NUCLEATION MODEL

The spontaneous nucleation model introduced by Fauske proposes that for an energetic thermal interaction to occur, liquid-liquid contact must be established[a] such that the temperature of the interface at the time of contact is above a certain threshold temperature. This temperature should be equal to or exceed the spontaneous nucleation temperature of the cold liquid. When a sufficient heat transfer area is readily available through the fine fragmentation of the hot liquid, a rapid coolant overheating, together with appropriate system constraints, might cause shock pressurization of the coolant.

Yet, there has not been an exact definition of the spontaneous nucleation temperature threshold except in two extremes; a well-wetted system and when no wetting occurs. In the former system, the spontaneous nucleation temperature approaches the homogeneous nucleation temperature[b] of the coolant. This follows from the fact that when a volatile liquid readily spreads over the surface of a hot liquid, the tensile strength at the interface is greater than it is inside the volatile liquid. Thus, the spontaneous nucleation in the bulk of the liquid will be easier and the spontaneous nucleation temperature of the system, T_{SN}, becomes equal to the homogeneous nucleation temperature, T_{HN}, of the volatile liquid. When no wetting occurs between the interacting liquid pair, however, the tensile strength is lower at the interface than in the interior of the volatile liquid mass, resulting in a lower energy requirement for surface nucleation. Surface nucleation of the liquid will preferentially occur at some temperature, T_{SN}, which could be as low as the saturation temperature of the coolant, T_{sat}, at system pressure. The criterion of the interface temperature, T_{int}, for the spontaneous nucleation concept can be expressed as

$$T_{int} \geq T_{SN}$$

where

$$T_{sat} \leq T_{SN} \leq T_{HN}. \qquad \text{(A-1)}$$

For light water reactor materials (that is, molten UO_2 fuel and water coolant), the possibility of an energetic molten fuel-coolant interaction (MFCI) is ruled out by the spontaneous nucleation model a priori because the interface temperature between molten UO_2 (melting point ~3100 K) and water (300-600 K) upon contact would be about three to four times higher than the thermodynamic critical temperature of water (647 K). At such an interface temperature, formation of a stable vapor film is assured on the surface of the molten particles,

---

a. An initial period of film boiling, separating the interacting liquids, is considered, in most models, as a necessary condition to ensure efficient mixing.

b. The spontaneous nucleation temperature (T_{SN}) is the maximum limit of liquid superheat when foreign matter and/or possible interfacial vapor exist. At such a temperature, spontaneous vapor bubble nucleation within the liquid becomes significant. For vapor nucleation in the bulk of a pure liquid, this temperature limit is known as the homogeneous nucleation temperature (T_{HN}) and can be approximated by 90% of the thermodynamic critical temperature of the liquid (e.g., T_{HN} is about 582 K and 2313 K for water and liquid sodium, respectively). The homogeneous nucleation temperature can also be defined as the maximum liquid superheat in the absence of foreign matter, where random molecule grouping supplies boiling nucleation sites within a boiling liquid.

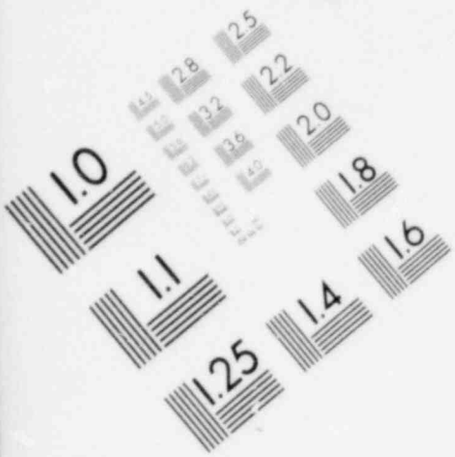

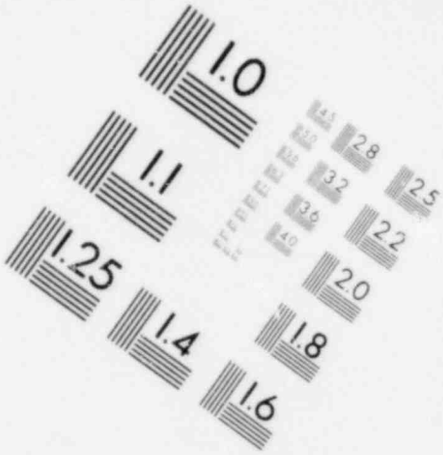

IMAGE EVALUATION TEST TARGET (MT-3)

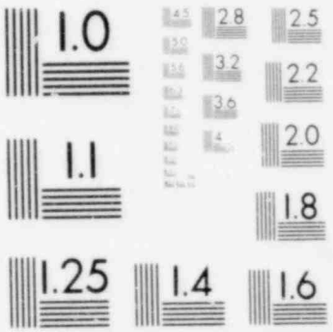

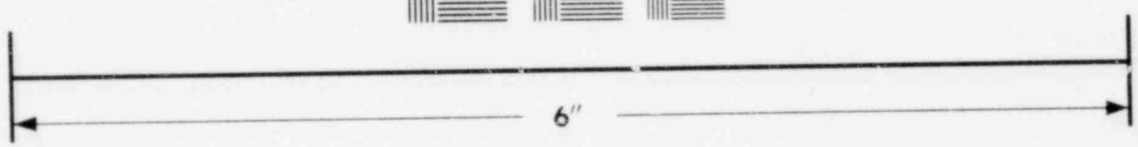

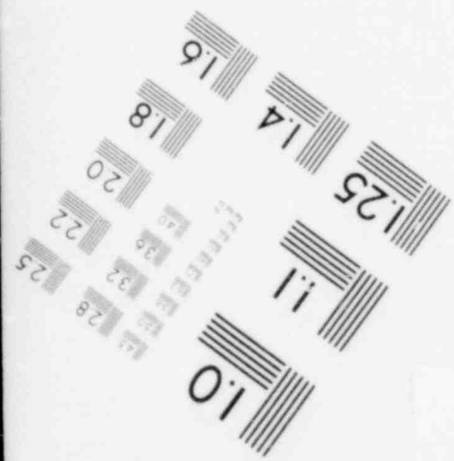

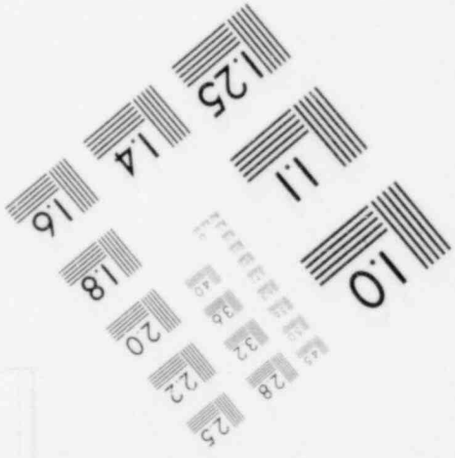

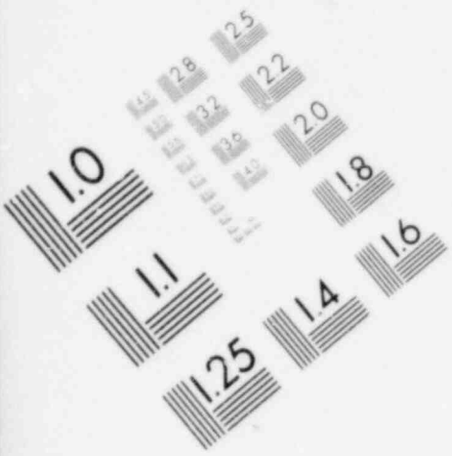

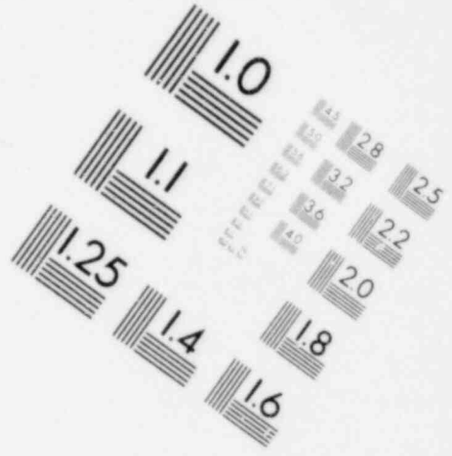

IMAGE EVALUATION
TEST TARGET (MT-3)

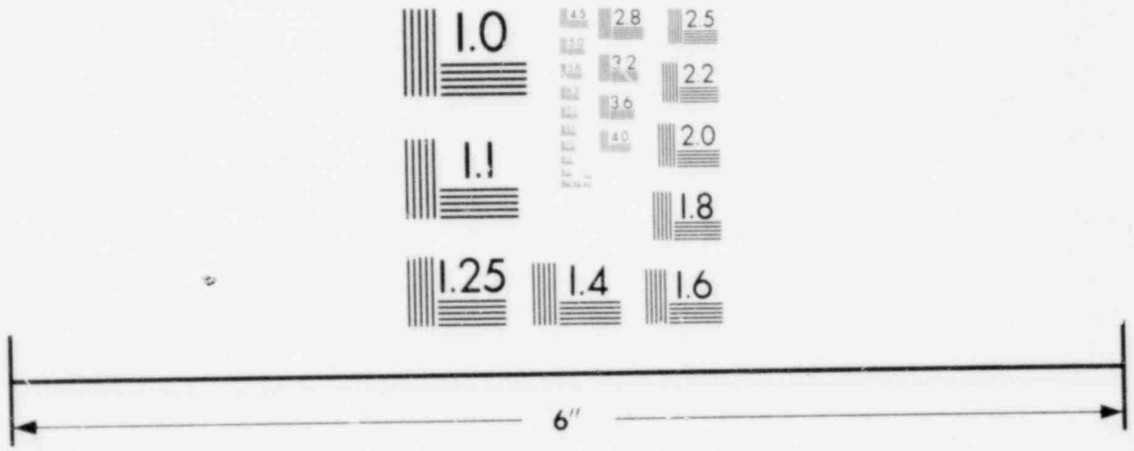

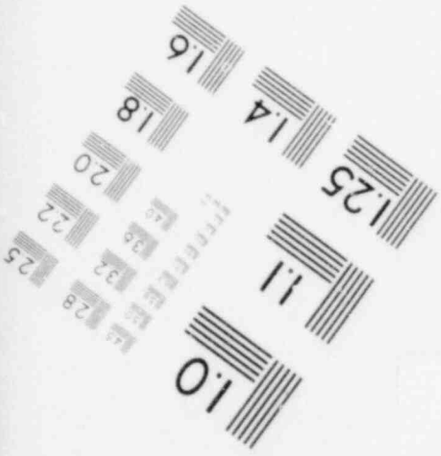

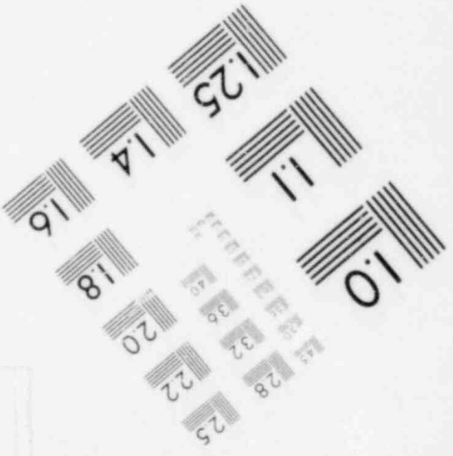

which may suppress further interaction between the two liquids. However, the spontaneous nucleation concept has been challenged on the basis of results obtained from both in-pile and out-of-pile experiments.

In the Nelson and Buxton experiment,[A-11] violent explosions occurred when molten Corium-E (a mixture of UO_2 and iron) at 2000 K was released into water at 300 K and ambient pressure. The temperature of the interface[a] between the melt and the water upon contact was calculated to be about 1650 K, which is well above the thermodynamic critical temperature of water. Also, in the RIA-ST-4 experiment,[A-12,A-13] the interface temperature between molten debris (primarily UO_2 fuel and zircaloy cladding) and coolant (water initially at 538 K) could have been higher than 2000 K; however, an energetic molten fuel-coolant interaction occurred.

Although the initial coolant pressure in the RIA-ST-4 experiment[A-12,A-13] was 6.45 MPa, which is well above the 1.3-MPa cutoff limit of bubble nucleation in water suggested by Henry,[A-15—A-17] coolant pressurization up to 35 MPa occurred. Henry[A-15—A-17] illustrated that at high coolant pressure, the thermally limited growth of vapor bubbles is predominant, which precludes the initiation of an explosive interaction because vapor bubbles cannot grow at a sufficiently rapid rate. On the basis of this analysis, the potential for an energetic MFCI in an LWR was ruled out during postulated accidents in which the coolant pressure is much higher than the 1.3-MPa pressure limit proposed by Henry. However, it may be argued that during an energetic MFCI in LWRs, vapor bubble nucleation and growth might not be the governing mechanisms, since the potential exists for core coolant pressurization beyond the thermodynamic critical pressure of water (22.1 MPa).[A-13] At such a high pressure, the vapor phase is no longer present, regardless of the initial phase of the core coolant (that is, liquid or a two-phase mixture).

It appears from the previous discussion that the experimental findings are at variance with spontaneous nucleation[A-4,A-6] and pressure suppression[A-15—A-17] concepts, relative to the potential for a thermal interaction between molten UO_2 and water. The disagreement also appears to exist for other materials in cases in which the interface temperature is less than the spontaneous nucleation temperature of the cooler liquid. This was pointed out in molten UO_2-liquid sodium[A-18,A-19] and the R-22-water experiments.[A-9,A-20] In those experiments,[A-9,A-18,A-20] vapor explosions occurred despite the fact that the interface temperature was believed to be below the spontaneous nucleation temperature of the cold liquid.[b]

---

a. The interface temperature, T_{int}, is calculated using the following expression:[A-14]

$$T_{int} = \frac{T_b + \beta T_o \, \mathrm{erf}(\lambda)}{1 + \beta \, \mathrm{erf}(\lambda)}$$

and

$$\beta = [(\rho Ck)_c/(\rho Ck)_{\text{solid fuel}}]^{1/2} \qquad \text{(A-2)}$$

where

ρ = density

C = specific heat

k = thermal conductivity

λ = freezing coefficient of molten fuel at a bulk temperature T_b in contact with water at a bulk temperature T_o.

The above expression for T_{int} is obtained (assuming constant thermophysical properties) by solving the transient temperature distribution due to conduction during the freezing of a stagnant liquid onto a semi-infinite slab suddenly brought into intimate contact.[A-14]

b. The spontaneous nucleation temperature of R-22 was expected to be near the homogeneous nucleation temperature of R-22 (~336), since R-22 has been shown to spread easily on cold water.

2. PRESSURE-INDUCED DETONATION MODEL

Another major contribution to the theory of vapor explosions was the pressure detonation-propagation model introduced by Board et al.[A-7,A-8] They suggested that in an energetic MFCI (vapor explosion), the rapid energy transfer from the molten fuel particles to the coolant (water or liquid sodium) is initiated by a shock front in a manner similar to a chemical detonation. The passage of a shock front through a coarse mixture of the two interacting liquids, with a stable vapor film surrounding the fuel particles, triggers the fragmentation process by collapsing the vapor film and forcing liquid-liquid contact. The intermixing of the fragmented fuel particles with the coolant may induce rapid overheating and subsequent shock pressurization of the coolant. The expansion of the pressurized coolant would sustain the shock front propagation through the entire region of the interaction zone. They suggested[A-8,A-21] that thermal interaction will only propagate in a highly constrained geometry and that all steadily propagating thermal explosions have structures analogous to chemical detonations, that is, a steadily propagating zone headed by a shock and terminated by the sonic Chapman-Jouguet (C-J) plane.[a]

The triggering mechanism(s) (e.g., a shock front) needed to initiate the explosive interaction may develop due to several causes, such as rapid vaporization of the cold liquid, mechanical disturbance of the interacting liquids, and, in some instances, the chemical interactions between the liquid pair. Additional causes may be the release of hot, pressurized gas from fuel rods upon failure, the impact of molten masses on core structures and on the coolant, and the travel of molten particles at high velocity through the coolant. Also, the precipitous collapse of a vapor layer or bubbles in the coolant adjacent to the interaction zone can mechanically produce pressure disturbances that may lead to a large-scale explosive growth. Anderson and Armstrong have observed in their R-22 water experiment[A-9] that random turbulent fluctuations in the interaction liquid and the vapor layer, which separates the two liquids, caused localized liquid-liquid contacts, with a resultant pressure pulse that grew and propagated along the vapor film until it generated a stable shock wave. However, such a mechanism for developing a shock wave seems unlikely to occur in a high pressure system, because the vapor film will be more pressurized and the turbulent fluctuations, if any, might be suppressed.

Board and Hall[A-22] have investigated the effect of vapor blanket collapse on triggering an explosive thermal interaction by pouring about 50 g of molten tin (melting point ≅ 505 K) at 1073 K into a shallow crucible under water at an ambient pressure of about 0.0133 MPa. A vapor blanket surrounded the tin mass upon contact with water because the interface temperature of water (~900 K) was higher than both the melting point of tin and the thermodynamic critical temperature of water (~647 K). The vapor blanket collapsed when it was subjected to a rapid increase in ambient pressure (~0.1 MPa with a rise time of about 0.5 ms) by rupturing a diaphragm connecting the apparatus to the atmosphere. The collapse of the vapor blanket occurred within 1 ms after rupturing the diaphragm, and expolsive interaction followed within 250 μs. The experiment was repeated using molten aluminum (melting point ≅933 K), and a less vigorous explosion occurred.[b] The results of this experiment support the idea that an explosive thermal interation can be triggered through a pressure-driven blanket collapse if sufficient constraints are provided by the surrounding medium. Also, it indicated that propagation of an energetic explosion through blanket collapse is likely.

Nelson's arc-melter apparatus and single-drop experiments,[A-23—A-25] and those of Armstrong et al.,[A-26] have also demonstrated the importance of an external trigger to initiate vapor explosions. Vapor explosions were only observed when

---

a. At some distance behind the shock front there is a surface wave over which the particle flow velocity is equal to the local sound velocity in the medium. This surface separates the subsonic regime from the supersonic flow of the detonation product, and is termed the Chapman-Jouguet (C-J) plane or surface.

b. The interface temperature upon contact with water is about 1000 K, which is close to the freezing temperature of aluminum, but is higher than the thermodynamic critical temperature of water.

a pressure transient was applied (using a bridgewire or a minidetonator) in the coolant. Nelson used Corium-E (a mixture of UO_2 and iron) and iron oxide melts to simulate molten fuel. In the Armstrong et al., experiment,[A-26] molten aluminum was used, and different experimental techniques were introduced to force the contact of molten aluminum with water. Nelson and Armstrong et al., indicated that a definite trigger threshold (that is, peak pressure and impulse) for the initiation of a small-scale vapor explosion does exist. However, the explosion energy (thermal-to-mechanical conversion ratio) appeared to be independent of the energy of the trigger.[A-26]

The effect of the ambient pressure of the coolant on suppressing the interaction (that is, the destabilization and collapse of the vapor blanket around the melt particles) has been observed in several experiment.[A-15,A-16,A-25—A-33] In Nelson's experiments,[A-23—A-25] interactions were suppressed when the ambient pressure was increased. The triggers used to initiate explosions in water at an ambient pressure up to 0.5 MPa were unable to initiate any explosive interactions when the water pressure was increased to 0.75 MPa. Kottowski et al.,[A-27] in their stock tube experiments using molten steel and water at an ambient pressure of 2.6 MPa, have triggered vapor explosions only when the impact pressure was increased from 4 to 20 MPa.

On the basis of the foregoing discussion, Figure A-1 presents a suggested chain of events for the interaction between molten core debris and coolant under postulated accident conditions in LWRs. For an energetic interaction to occur, sufficient thermal energy should be available in the molten debris mass(es). As illustrated in Figure A-1, an energetic thermal interaction is characterized by four, main successive processes: (a) pre-trigger or coarse premixing; (b) trigger; (c) post-trigger, or propagation phase; (d) expansion or destruction phase. In the first phase, initial breakup of large molten masses and coarse intermixing with the coolant is necessary. Because the interface temperature is well above the thermodynamic critical temperature of water, a stable vapor film may form on the surface of molten fuel particles and suppresses any further interaction (a period of stable film boiling).

The triggering phase of the interaction is initiated by the destabilization and collapse of the vapor film on the surface of the particles, forcing liquid-liquid contact. Vapor film collapse triggers the fine fragmentation and intermixing of the molten particles with the coolant. Because the interface temperature between molten UO_2 and water upon contact might be less than both the freezing temerature (~ 3100 K) and homogeneous crystallization temperature of UO_2 fuel[A-34] (~ 2373 K), surface solidification of molten fuel particles[a] may occur almost instantaneously upon contact following vapor film collapse. Should surface freezing of molten particles occur upon contact, the hydrodynamic fragmentation of fuel particles becomes difficult, and fragmentation due to thermal effects would be dominant. By contrast, if the interface temperature between the interacting liquids upon contact is higher than the thermodynamic freezing is inhibited and hydrodynamic fragmentation could be important.

The trigger magnitude (that is, energy and impulse) sufficient to cause film boiling collapse depends on the core coolant pressure. At elevated pressures, the vapor film becomes more resistant to collapse for a given trigger magnitude.[A-23—A-27] However, if the magnitude of the trigger is sufficient to overcome the effect of coolant pressure, coherent thermal interaction may be initiated. Futher investigations are needed to quantify the threshold value of the trigger in terms of the initial coolant conditions (that is, temperature and pressure).

The interaction between the fragmented fuel particles and the coolant escalates by the continuous fragmentation and intermixing of interacting liquids. Feedback processes may contribute to the propagation of the interaction, in which

---

a. The interface temperature (~ 1100 K) between molten UO_2 at its melting point and liquid sodium at 600 K is almost half that (~ 2100 K) for molten UO_2 and water at 600 K, because sodium has much better thermophysical properties than water. Therefore, instantanous freezing of molten fuel particles upon quenching in sodium is inevitable, even at high fuel temperatures. On the basis of transient heat conduction alone, this would not be true with water initially at 600 K, because increasing the initial fuel temperature (> 3400 K) may produce an interface temperature in excess of the UO_2 melting point. However, the surface heat flux could be much higher than that calculated by transient heat conduction, which rapidly reduces the interface temperature and may initiate freezing shortly thereafter.

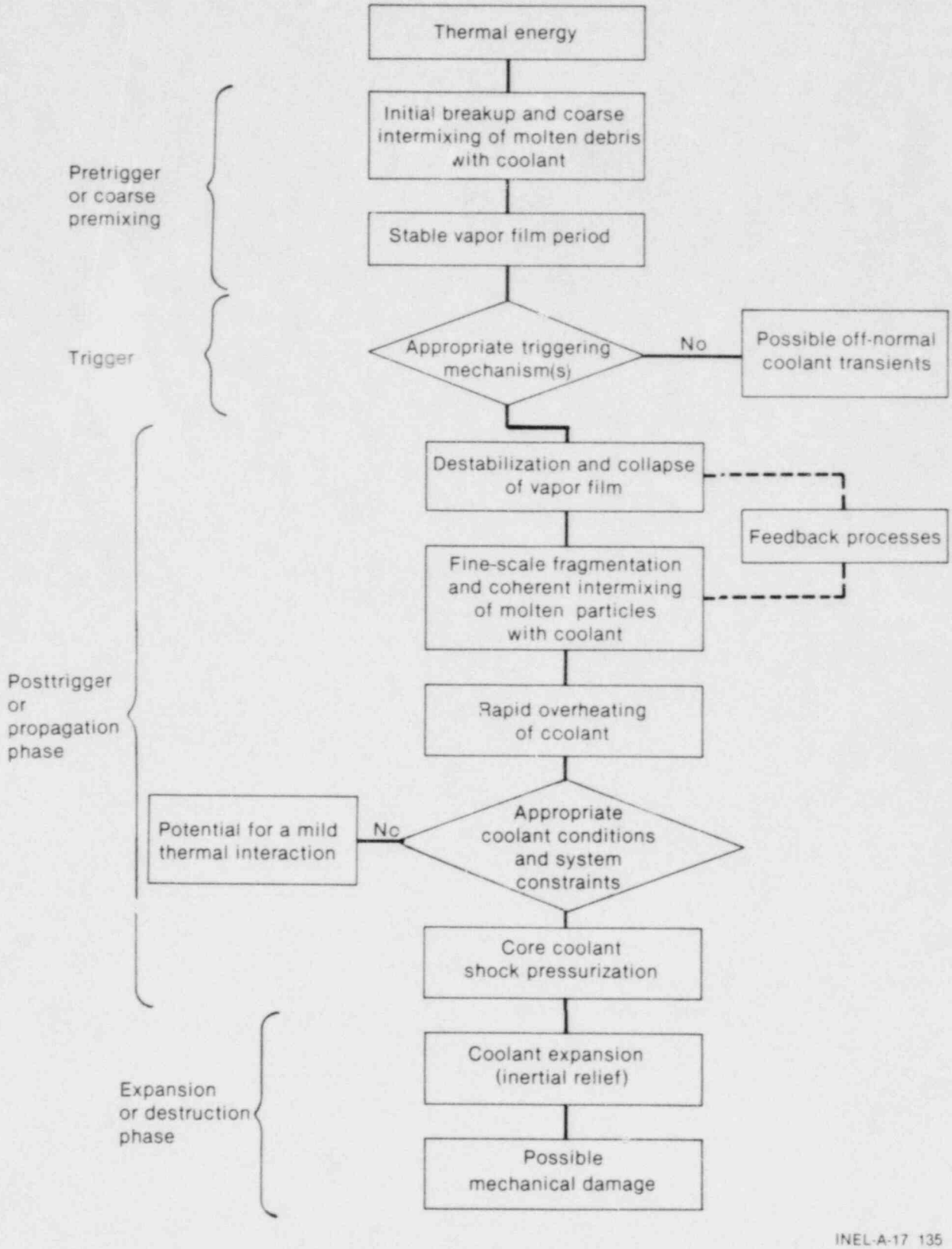

Figure A-1. A proposed chain of events leading to an energetic MFCI in a light water reactor.

initial interactions produce pressure transients to stimulate additional interactions. Finally, the expansion of the overheated, pressurized coolant against the inertial constraints of the system may cause destructive mechanical work. This depends on the efficiency of the thermal-to-mechanical energy conversion during the expansion process (that is, the mass of the water slug and the coolant peak pressure achieved during the previous phase of the interaction).

3. MFCI CONCEPT RELEVANT TO THE RIA-ST-4 EXPERIMENT

One sequence of events leading to the recorded pressure pulses (peak pressure of 35 MPa and rise time of 2 ms) in the RIA-ST-4 experiment[A-12,A-13] may be explained by the pressure detonation concept of Board et al.[A-7,A-8] During the RIA-ST-4 experiment, the fragmented debris particles coarsely intermixed with the coolant in the flow shroud upon fuel rod failure. Film boiling forms a vapor blanket around the particles upon contact with the coolant, since the interface temperature is much greater than the thermodynamic critical temperature of water. The fine-scale fragmentation and intermixing of the debris particles with the coolant is then triggered by the propagation of a shock wave through the dense dispersion in the shroud, inducing film boiling destabilization and collapse.

The fine fragmentation and efficient intermixing of molten particles with the coolant resulted in rapid coolant overheating, which together with the system constraints, caused the recorded pressurization of the coolant (coolant peak pressure of ~35 MPa). The coolant in the RIA-ST-4 test train was a two-phase mixture at the time of test rod failure because of the onset of film boiling on the surface of the zircaloy cladding before rod failure. The interaction between the two-phase coolant and the molten debris particles resulted in high coolant pressurization. Thus, the expansion of the working fluid back to the initial coolant pressure produced superheated steam. This is supported by the high coolant temperature (in excess of 940 K) measured during the experiment.

4. REFERENCES

A-1. D. H. Cho et al., "Pressure Generation by Molten Fuel-Coolant Interaction Under LMFBR Conditions," *Proceedings of the Conference on New Development in Reactor Materials and Applications*, USAEC Report No. Conf-710302, 1971, p. 25.

A-2. L. Caldarola, "A Theoretical Model for the Molten Fuel Sodium Interaction in a Nuclear Fast Reactor," *Nuclear Engineering and Design, 22*, 1972, p. 175.

A-3. A. Padilla, "Transient Analysis of Fuel Sodium Interaction," *Transactions of the American Nuclear Society, 13*, 1970, p. 375.

A-4. H. K. Fauske, "On the Mechanisms of Uranium Dioxide Sodium Explosive Interactions," *Nuclear Science and Engineering, 51*, 1973, pp. 95-101.

A-5. H. K. Fauske, "The Role of Energetic Mixed Oxide Fuel-Sodium Thermal Interactions In LMFBR Safety," *Proceedings of the 3rd CSNI Specialists Meeting on Na/Fuel Interactions in Fast Reactors, Tokyo, Japan, March 22-26, 1976.*

A-6. H. K. Fauske, "Some Aspects of Liquid-Liquid Heat Transfer and Explosive Boiling," *Proceedings of ANS Topical Meeting on Fast Reactor Safety, Beverly Hills, CA 1974*, Conf. 740401-P2, p. 992.

A-7. S. J. Board, R. W. Hall, R. S. Hall, "Detonation of Fuel Coolant Explosions," *Nature, 254*, March 1975, pp. 219-221.

A-8. S. J. Board and R. W. Hall, "Recent Advances in Understanding Large Scale Vapor Explosions," *Proceedings of 3rd CSNI Specialist Meeting on Na/Fuel Interactions In Fast Reactors, Tokyo, Japan, March 22-26, 1976.*

A-9. R. P. Anderson and D. R. Armstrong, "*R-22 Vapor Explosions, Nuclear Reactor Safety Heat Transfer*, (edited by A. D. Bishop et al.), New York: American Society of Mechanical Engineers, 1977, pp. 31-45.

A-10. G. J. Vaughan, L. Caldarola, N. E. Todreas, "A Model for Fuel Fragmentation During Molten Fuel/Coolant Thermal Interaction," *Proceedings of the International Meeting on Fast Reactor Safety and Related Physics, Chicago, IL, October 5-8, 1976.*

A-11. L. S. Nelson and L. D. Buxton, *Steam Explosion Triggering Phenomena: Stainless Steel and Corium-E Simulants Studied with a Floodable Arc Melting Apparatus*, SAND-77-0998, NUREG/CR-0122, May 1978.

A-12. M. S. El-Genk and R. L. Moore, "Transient Debris Freezing and Potential Wall Melting During a Severe RIA Experiment," *Journal of Nuclear Technology* (in print, 1981).

A-13. M. S. El-Genk, "On a Vapor Explosion in the RIA-ST-4 Experiment," *Transactions of the American Nuclear Society, 34*, 1980, p. 972.

A-14. H. S. Carslaw and J. C. Jaeger, *Conduction of Heat in Solids*, 2nd edition, Oxford University Press, 1959.

A-15. R. E. Henry and K. Miyazaki, "Effects of System Pressure on the Bubble Growth from a highly Superheated Water Droplets," *Topics in Two-Phase Heat Transfer and Flow*, (edited by S. G. Bankoff et al.), New York: American Society of Mechanical Engineers, 1978, pp. 1-10.

A-16. R. E. Henry and L. M. McUmber, "Vapor Explosive Behavior at Elevated Ambient Pressure," *Light-Water Reactor Safety Research Program Quarterly Progress Report, January-March 1977*, ANL-77-34, 1977, pp. 113-119.

A-17. R. E. Henry and H. K. Fauske, "Nucleation Processes in Large-Scale Vapor Explosions," *Journal of Heat Transfer, 101*, May 1979, pp. 280-287.

A-18. D. R. Armstrong, F. J. Testa, D. Raridon, Jr., *Interaction of Sodium with Molten UO_2 and Stainless Steel Using a Dropping Model Contact*, ANL-7890, 1971.

A-19. D. R. Armstrong, G. T. Goldfuss, R. H. Gebner, *Explosive Interaction of Molten UO_2 and Liquid Sodium*, ANL-76-74, March 1976.

A-20. R. H. Holt and A. H. MuenKer, *Flameless Vapor Explosions in LNG-Water and Other Cryogen-Hot Liquid Systems*, GRV.1, GRP.72, May 1972.

A-21. R. W. Hall and S. J. Board, "The Propagation of Large Seal Thermal Explosions," *International Journal of Heat Mass Transfer, 22*, 1979, pp. 1083-1093.

A-22 J. S. Board and R. W. Hall, Propagation of Thermal Explosions: 1. Tin/Water Experiments," *2nd CSNI Specialist Meeting on Fuel-Coolant Interactions in Nuclear Reactor Safety, Ispra, Italy, November 1973.*

A-23 *LWR Safety Research Program, Quarterly Report, April-June 1979*, SAND 79-2057, February 1979.

A-24 *LWR Safety Research Program, Quarterly Report, April-June 1980*, NUREG/CR-150912of4, SAND 80-130412of4, August 1980.

A-25. *LWR Safety Research Program, Quarterly Report, January-March 1979*, SAND-79-1542, December 1979.

A-26. D. R. Armstrong et al., *An Experimental Study of Combined Physical-Chemical Explosions in an Aluminum/Water System*, ANL/RAS/LWR 79-2, April 1979.

A-27. H. Kottowski et al., "Importance of the Coolant Impact on the Violence of the Vapor Explosion," *4th CSNI Specialist Meeting on Fuel-Coolant Interactions in Nuclear Reactor Safety, Bournemouth, UK, April 2-5, 1979.*

A-28. A. Sharon, "Studies of the Mechanism of Fuel-Coolant Interactions," Ph.D Dissertation, Northwestern University, June 1979.

A-29. A. Segev, R. E. Henry, S. G. Bankoff, "Fuel-Coolant Interactions in a Shock Tube Geometry," *Journal of Nuclear Technology, 46*, 1979 pp. 482-492,.

A-30. R. E. Henry, "Vapor Explosions of Freon-22 with an External Trigger," *6th LWR Safety Information Meeting, Gaithersburg, MD, November 1978.*

A-31. R. E. Henry et al., "The Effect of Pressure on NaCl-H_20 Explosions," *4th CSNI Specialist Meeting on Fuel-Coolant Interactions in Nuclear Reactor Safety, Bournemouth, UK, April 2-5, 1979.*

A-32. R. C. Asher et al., *The Effect of Ambient Pressure on a Vapor Explosion (Fuel-Coolant Interaction)*, AERE-M-2862, December 1976.

A-33. M. J. Bird, "Fuel-Coolant Interaction Studies with Water and Thermite-Generated Molten Uranium Dioxide," *4th CSNI Specialist Meeting on Fuel-Coolant Interaction in Nuclear Reactor Safety*, Bournemouth, UK, April 2-5, 1979.

A-34. A. W. Cronenberg and H. K. Fauske, "UO_2 Solidification Phenomena Associated with Rapid Cooling in Liquid Sodium" *Journal of Nuclear Materials, 52*, 1974, pp. 24-32.